Università degli Studi di Napoli "Federico II"

PhD Program in Earth, Environment and Resources Sciences

XXIX Cycle

PhD Thesis

Multiscale Modeling of the European aeromagnetic field

Maurizio Milano

Tutor:

Prof. Maurizio Fedi

Co-tutor:
Prof. J. Derek Fairhead

PhD Coordinator:

Prof. Maurizio Fedi

A mia Madre

Contents

Summary

In this research, the aim of the study is the interpretation of the main magnetic anomalies at the European scale. Being the field characterized by anomalies originating by sources at different depth within the crust, a multiscale approach is the most suitable method to take into account all the different components of the anomaly field. In fact, at different altitudes, say from 5 km to 350 km, the anomaly field is varies and there is no specific scale, which can be judged as the most relevant for the analysis.

The multiscale analysis of aeromagnetic data is based on a multiscale dataset, which is generated by the upward continuation of the dataset of the *European and Mediterranean Magnetic Project* up to satellite altitudes. The interpretation of the magnetic anomalies was carried out following two main steps:

a) producing the total gradient maps of the magnetic field at low and high altitudes, in order to identify the magnetic features through the whole crust. This technique has been particularly useful because of three main properties: i) the anomalies of the total gradient modulus are monopolar, so losing the dipolar aspect of the magnetic field, regardless the source and field magnetization directions; ii) the maxima of the total gradient modulus are placed above the source position, regardless of the source and field magnetization directions; iii) the areas where it reaches very low values may be safely regarded as regions with a low-magnetization crust; conversely magnetic lows of the magnetic field are not exclusively linked to low-magnetization areas, but depends mainly on the total magnetization of the sources, either normally or reversely magnetized.

   Our total gradient analysis showed that the origin of the Central European Magnetic Low (CEML) should be attributed to the strong differences in magnetization between the central European crust and the North-Eastern platform. However, due to the property i) some reversely magnetized sources were detected, in different regions of central Europe (Anglo-Brabant Massif, Bohemian Massif, Pannonian basin).

b) using specific multiscale tools for the simultaneous interpretation of the field at many scales. In particular, the Multiridge method allows the multiscale magnetic field to be interpreted in terms of source depths and shape. By this method, a model is obtained of the crustal magnetic sources beneath the TESZ, the Bohemian Massif and the Adriatic magnetic anomalies, which are key anomalies for the magnetic field in Europe, no matter the altitude. In order to estimate the deepest source depths in the TESZ region, the Multiridge method was applied to the large scales (50-100 km altitude), obtaining a set of singular points at depths ranging between 35-40 km. Considering the trend of the heat flow and the geological models around the study areas, a meaningful correspondence was found among the location of the estimated singular points and the most abrupt variations and complex morphology features of the magnetic basement and the Moho boundary. The interpreted models are largely in agreement with geological models based on seismic surveys and contribute to the whole knowledge of the areas, since refer to a wider region, if compared to that covered by seismic.

Multiscale methods contribute to a complete knowledge of the area since they refer to the wider region, when compared with that covered by the seismic models.

Introduction

Modeling potential field data of dynamic features of the global crust is a subject of great interest. Particularly in Europe, the interpretation of potential fields has been performed by many researchers (e.g. Thybo, 2001, Wonik et al., 2001; Banka et al., 2002; Williamson et al., 2002; Grabowska et al., 2011). In this work a multiscale approach is adopted, consisting of studying the source properties of the field at a set of different altitudes or, in other words, in the 3D space. By this approach, the interpretation of the field at multiple scales, is different from more usual methods of interpretation referring to a single scale (or altitude) (e.g., for satellite data: Taylor and Ravat, 1995; Pucher and Wonik, 1998; Kis et al., 2011).

In the last decade, several theoretical and application aspects of multiscale analysis of potential fields were proposed (Fedi et al., 2009; Fedi et al., 2012), including the continuous and discrete wavelet transforms (Fedi et al., 2010; Fedi and Cascone, 2011) and the Depth from EXtreme Points (DEXP, Fedi, 2007; Fedi and Pilkington, 2012; Fedi and Abbas, 2013) transformation. The rational for all these approaches is that potential fields are characterized by a scaling property, which simply means the absence of a characteristic scale. In fact, let us consider a simple case of a single source, such as a fault: at short distance the magnetic field reflects mainly the properties of its top, so that a reasonable source-model at a single (low) scale is a vertically extended source (a contact-like source); but this model could not well satisfy the data at a greater distance where the more favourable model would rather be a relatively thin source (a sill-like source). Thus, there is no a specific scale at which the source is characterized at best. Instead than studying the signal at a specific scale, it can be useful to establish a relation among the signals observed at different scales and, from that relation, retrieving the best source parameter estimation. This is the main motivation for a multiscale approach.

Potential fields can be either homogenous or inhomogeneous. Homogeneous fields are scale invariant and are characterized by a single homogeneous degree at all scales. They obey the homogeneity law (e.g., Blakely, 1996; Fedi et al., 2015):

$$f(ax, ay, az) = a^n f(x, y, z) \qquad (1)$$

where a >0 and n is the homogeneity degree. Typical source models generating a homogeneous magnetic field are the uniformly magnetized sphere (n=-3), the dipole (n=-3), an infinite line of dipoles (n=-2), the contact (n=0) and others (Reid et al., 1990). Homogeneous fields obviously enjoy the above mentioned scale invariance property, meaning that there is no a specific scale at which the source is best characterized (e.g., Fedi et al., 2015).

For inhomogeneous fields, these simple models are still useful in the asymptotic regions, which are at large-distances or very close to the sources. For example, the sphere model is usually adopted at very high altitudes, while the infinite contact or dyke models are used to study near-surface sources. So, a homogeneous field roughly is expected to occur over a quite restricted range of scales (Fedi et al., 2015; Fedi, 2016). At other scales, the more complex model of inhomogeneous field must be adopted. In fact, the inhomogeneous field's scaling properties change not only horizontally, but also vertically across the scales.

For inhomogeneous fields, which are better represented by the common behavior of real-world fields, it is worthwhile to consider, at each position, the Euler differential homogeneity equation (e.g., Blakely, 1996; Fedi et al., 2015):

$$\frac{\partial f}{\partial x}(x-x_0)+\frac{\partial f}{\partial y}(y-y_0)+\frac{\partial f}{\partial z}(z-z_0)=-nf \tag{2}$$

where x_0, y_0, and z_0 are the coordinates of the unknown homogeneous source. This equation is related to the homogeneity equation (1) by the Euler's theorem (e.g., Olmsted, 1991), provided that f is a continuously differentiable and homogeneous function of degree n in R. Thus, the Euler equation implies that the field is homogeneous, but the homogeneity property is now assessed locally; so, the Euler equation has been used, assuming that the homogeneous properties may vary continuously with position. This imposes a local homogeneity concept, which despite of being implicitly used at a single-scale with the well-known Euler Deconvolution method (e.g., Reid et al., 1990), was only recently restated in a more general multiscale framework by Fedi et al. (2015). One needs to refer to Fedi et al. (2015) for a deeper discussion about the theoretical aspects of local homogeneity and inhomogeneous fields.

The goal of this study is analyzing and interpreting the magnetic anomaly field of Europe in a multiscale framework, consisting of interpreting the field, and/or its horizontal and vertical derivatives, at various altitudes, to evaluate the source parameters (Fedi, 2007; Florio and Fedi, 2014). More specifically, this work aims at interpreting the main European magnetic anomalies at

several altitudes from the Earth's surface. The used dataset was taken from the high-resolution EMMP magnetic field compilation. The upward continuation was performed up to satellite altitudes in order to build up a three-dimensional multiscale dataset. The reliability of the upward continued anomalies was pointed out by comparing the aeromagnetic field maps with the MF7 satellite model data up to 350 km altitude.

Specifically, attention has been focused on the Trans European Suture Zone (TESZ), the most prominent geological structure of central Europe, which divides the continent into two large platforms with different features and histories (Pharaoh, 1999). Previous studies of the TESZ were based on potential field, seismic and heat flow analysis and yielded information about this structure in the upper and lower portions of the crust (e.g. Guterch et al., 1999; Pharaoh, 1999; Mushayandebvu, 2001; Banka et al., 2002; Majorowicz and Wybraniec, 2011). At high altitudes the magnetic effect of the TESZ is clearly recognized by the presence of a wide magnetic low (Central European Magnetic Low- CEML) and its relative magnetic high towards North-Eastern Europe. This suggests a strong influence of such magnetic structure down to the deeper portion of the crust. The CEML was object of debate for many authors in the past and several geological interpretations were proposed combining petrologic and geological studies with satellite magnetic anomaly maps and modeling (Taylor and Ravat, 1995; Pucher and Wonik, 1998).

The first phase of the interpretation concerns the evaluation of the total gradient of the field, because of its property of strongly attenuating the magnetic dipolar shape and so placing the signal's maxima over the source (Nabighian, 1972). This technique allows retrieving the distribution of the rock's magnetization, so providing important details about the possible presence of reversely magnetized sources. The total gradient maps is computed at different altitudes (or scales), in order to recognize the magnetic contribution of the main geological structures of the whole European crust.

The second phase regards the Multiscale analysis over the main European magnetic regions, thanks to which the characterization and modelling of the sources occurring at different depths in the crust, without separating the field into different components by band-pass or similar filtering. This follows from being multiscale algorithms entirely built with physically-based tools, such as upward continuation and differentiation. The source depth and shape are extracted by the simultaneous analysis of the field at multiple scales. The Multiridge method (Fedi et al., 2009; Florio and Fedi, 2014) is then applied to obtain information about the source depth. Further the

scaling function method (Florio and Fedi, 2006; Fedi et al., 2009) is applied, in order to estimate the homogeneity degree and, consequently, retrieve information about the kind of source.

1

Earth's Magnetic Field

Our planet is surrounded by a magnetic field, which, similarly to the gravity field, admits a scalar potential and can be measured by magnetic instrumentation. The geomagnetic field is approximately dipolar with a dipole axis inclination of about 10.3° from the Earth's rotation axis. However, the signal obtained from magnetic field measurements is a sum of different source contributions which may be summarized in three main categories:

- The main field, generated in the Earth's fluid core by a geodynamo mechanism;
- The lithospheric field, generated by magnetized rocks in the Earth's lithosphere;
- The external field, produced by electric currents in the ionosphere and in the magnetosphere, due to the interaction of the solar electromagnetic radiation and the solar wind with the Earth's magnetic field.

Moreover, the Earth's magnetic field structure varies not only in a spatial scale but is also subject to continuous long-term and short-term time variations. The long-term variations (*secular variations*) have deep origin and may be detected by the use of datasets covering large periods of time (at least 5-10 years), while the short-term variations have external origin and generally cover very short range of time (from second to few years) (Lanza and Meloni, 2006).

In this study we aim at retrieving the properties of the magnetic sources in the Earth's crust, and so only the lithospheric component of the magnetic field is considered. Note that we refer to a *lithospheric* and not to *crustal* component, since magnetic contribution has been inferred by many authors also in the uppermost mantle, at least in in specific geological environments (e.g. Arkani-Hamed and Strangway, 1987; Bostock et al., 2002; Blakely et al., 2005; Chiozzi et al., 2005; Ferré et al., 2013).

In the next section we describe briefly the main mathematical expression of the lithospheric magnetic field and the concept of magnetic anomaly.

1.1 The Lithospheric magnetic field

In the space exterior to the Earth's surface, assuming the absence of magnetic material, Maxwell's equations are expressed in SI units as:

$$\nabla \bullet \mathbf{B} = 0 \tag{3}$$

$$\nabla \times \mathbf{B} = \mu_0 \mathbf{J} \tag{4}$$

Where **B** is called *magnetic induction* or flux density. It is measured in teslas (T) or nanoteslas (nT), more conveniently in the geomagnetic field studies; **J** is the current density in amperes per square meter (A/m^2), and μ_0, known as the *permeability of free space*, is a constant equal to $4\pi \times 10^{-7}$ henrys per meter (H/m) (Blakely, 1996).

Then, if $\nabla \times \mathbf{B} = \mathbf{0}$, we have that:

$$\boldsymbol{B} = -\nabla \Psi. \tag{5}$$

Where Ψ is the magnetic potential,

So, substituting (5) in (3) we have:

$$\nabla^2 \Psi = 0, \tag{6}$$

that is, the potential satisfies Laplace's equation.

So the magnetic field measured at a specific position **r** and time *t* may be defined as:

$$\mathbf{B}(\mathbf{r},t) = \mathbf{B}_m(\mathbf{r},t) + \mathbf{L}(\boldsymbol{r}) + \mathbf{D}(\mathbf{r},t) + \mathbf{e}(t), \tag{7}$$

where $\mathbf{B}_m(\mathbf{r},t)$ is the field produced by the Earth's core (main field), $\mathbf{L}(\mathbf{r})$ is the lithospheric field, $\mathbf{D}(\mathbf{r},t)$ the external field and $\mathbf{e}(t)$ the measurement error. By this, the lithospheric or external residual field may be obtained subtracting the main field to the magnetic measurement. The mathematical description of the core magnetic field is called the International Geomagnetic Reference Field (IGRF), which is updated every five years by IAGA (International Association of Geomagnetism and Aeronomy) due to time variations of the geomagnetic field.

Separating the individual contributions of the magnetic field is an active area of research and the modeling of the lithospheric component is one the main issues of geophysical investigation. To study the lithospheric component of the Earth's magnetic field, this anomaly field must be identified and isolated from the fields due to the other source categories. So, the scalar residual field is defined as:

$$\Delta B(\mathbf{r},t) = |\mathbf{B}(\mathbf{r},t)| - |\underline{\mathbf{B}}_m(\mathbf{r},t)|, \quad (8)$$

where $\underline{\mathbf{B}}_m(\mathbf{r},t)$ is an estimate of $\mathbf{B}_m(\mathbf{r},t)$.

The main strategy to separate such magnetic field contributions is considering whether the source lies above or below the region in which measurements are made, and at which scale they are calculated. So, the standard hypothesis is to consider the measurement region as being free of magnetic field sources (equation 6).

The solution of Laplace's equation expressed in a spherical harmonic representation provides a formal separation of the internal ($\mathbf{B}_m$+ **L)** and external (**D**) field components. In fact, each source region is defined by specific spherical harmonic terms (degree *l* and order *m*), which determine the spatial scale of such contribution. Generally, low degrees correspond to the largest spatial scales, or to the deepest source contributions, and vice-versa. This representation was used by Gauss in the 19th century to fit the magnetic observatory data and show that the largest part of the geomagnetic field is by far of internal origin.

1.2 Magnetic properties of the rocks

The origin of the lithospheric fields is strictly related to the magnetic properties of the rocks within the crust, which vary for different geographical regions, mineral composition and temperature. The magnetic effect on materials allows identifying three different categories (Reynolds, 1977):

- Diamagnetic materials have a weak, negative susceptibility to magnetic fields.

- Paramagnetic materials have a small, positive susceptibility to magnetic fields. These materials are slightly attracted by a magnetic field and the material does not retain the magnetic properties when the external field is removed.

- Ferromagnetic materials have a large, positive susceptibility to an external magnetic field. They exhibit a strong attraction to magnetic fields and are able to retain their magnetic properties after the external field has been removed.

For understanding the behavior of rock materials in a magnetic field environment, we may start defining **m** as the magnetic moment of a simple dipole, expressed in [A · m^2], which may be defined as *magnetization* (**M**) in the case of a larger volume (*V*) composed of several single dipoles:

$$\mathbf{M} = \frac{\sum_i \mathbf{m}_i}{\mathrm{V}} \tag{9}$$

where **M** is measured in A/m.

Then, we may rewrite the Maxwell's equation to obtain the *magnetization current* $\mathbf{J}_m$:

$$\nabla \times (\mathbf{B} - \mu_0 \mathbf{M}) = \mu_0 \mathbf{J} \tag{10}$$

and we define the *magnetic field intensity* **H** as:

$$\mathbf{H} = \frac{\mathbf{B} - \mu_0 \mathbf{M}}{\mu_0} \tag{11}$$

M and **H** are related by a specific term called *magnetic susceptibility* (χ), which determines the ease with which a material is magnetized:

$$\mathbf{M} = \chi \mathbf{H} \tag{12}$$

So, the magnetic field expression becomes:

$$\mathbf{B} = \mu_0(\chi + 1)\mathbf{H} = \mu \mathbf{H} \tag{13}$$

where μ is the absolute permeability.

Here we mean that the magnetization is *induced* ($\mathbf{M}_i$) by the external field **H**, but if the magnetization **M** does not go to zero when the external field is absent, there is a component of the magnetization which is called *permanent* or *remanent* ($\mathbf{M}_r$). In crustal materials, remanent magnetization is a function not only of the atomic, crystallographic, and chemical make-up of the rocks, but also of their geologic, tectonic, and thermal history (Blakely, 1996). So, the rock magnetization may be written as:

$$\mathbf{M} = \mathbf{M}_i + \mathbf{M}_r \tag{14}$$

from which we obtain the *Koenigsberger ratio* (*Q*):

$$Q = \mathbf{M}_r / \mathbf{M}_i = \mathbf{M}_r / \chi\, |\mathbf{H}|. \tag{15}$$

Both magnetizations arise from spontaneous magnetization, a complex property of the ferromagnetic minerals in the Earth's crust. The spontaneous magnetization is dependent on the temperature. As a material is heated, the spacing between neighboring atomic moments increases to a threshold point where the spontaneous magnetization falls to zero. This temperature is called the *Curie temperature*, whose definition is discussed in more detail in Chapter 3. Hence, both induced and remanent magnetizations vanish at temperatures greater than the Curie temperature. Paramagnetic and diamagnetic effects persist at these temperatures, but from the perspective of magnetic-anomaly studies we may consider rocks above the Curie temperature to be nonmagnetic. The Curie temperature differs for each mineral formation but, in magnetic field studies, the Curie temperature of Magnetite (about 580°C) is considered as the standard temperature boundary for the whole magnetic crust with magnetite as the main magnetic mineral for percentage, size, and shape (Hunt et al., 1995).

2

Multiscale Theory

In this section we will introduce the Multiscale methods which will be employed to estimate the depth position of the magnetic source. The property of such Multiscale methods is the possibility to analyze the potential field behavior simultaneously at different altitudes. However, the interpretation of the European magnetic field was carried out previously using an additional technique, namely the Total Gradient, which will be employed by observing the maps of the anomalies at different altitudes step-by-step, which differs from the Multiscale methods. For this reason the theory of the total gradient is discussed further in Chapter 5.

The way potential fields convey source information depends on the scale at which the field is analyzed. In this sense, a multiscale analysis is a useful tool to study potential fields, particularly when the field main-contributions are caused by sources with different depths and extents. The study of gravity and magnetic fields at different scales is an important part of several interpretation methods, from the Continuous Wavelet Transform (CWT) (e.g. Mallat, 1992; Hornby et al., 1999; Sailhac and Gibert, 2003; Fedi et al., 2010) to older methods (e.g. Paul et al., 1966; Paul and Goodacre, 1984; McGrath, 1991; Pedersen, 1991). Other recent methods involving a multilevel data set are the Depth from EXtreme points (DEXP) method (Fedi, 2007), the Multiridge method (Fedi et al., 2009; Florio et al., 2009) and the Euler deconvolution of vertical profiles of potential fields (Florio and Fedi, 2006).

Interpretation of potential fields by these methods is based on the fact that the magnetic anomalies $f(x)$, generated by simple ideal sources (such as dipole, line of dipoles, dyke-sill and contact) are homogeneous functions and then satisfy the homogeneity equation (equation 1). The exponent n changes with the source type and holds integer and constant values for the ideal sources, whereas it is fractional and varies within the harmonic region for complex sources (Steenland, 1968; Fedi et. al, 2015). Using multiscale methods, the depth to the source of homogeneous fields can be determined by a geometric approach: as a consequence of the dilation of potential fields

versus the scale, the maxima of the field modulus at various scales are located along straight lines which are called ‘ridges’ or WTMML lines (Wavelet Transform Modulus Maxima Lines). In the case of homogeneous potential fields, sources are located at singular points of the field, under the measurement level, and the source depth could be retrieved by simply extrapolating the ridges below the measurement surface and by identifying their intersection point (e.g., Moreau et al., 1997). The structural index is the opposite of the homogeneity degree ($N = -n$) of the magnetic field. It characterizes the shape of simple sources generating homogeneous fields. Simple sources, such as spheres, horizontal cylinders and sills, have a singular depth point corresponding to their centre; for dykes, vertical cylinders and contacts, it corresponds to the top of the source. The estimation of the source structural index is an important step in potential field interpretation (Reid et al., 1990) such as for the Euler deconvolution (ED) that has become a standard tool in rapid, semi-automated interpretation of potential fields. Its success is mainly because of providing a sound estimate of the source position if the correct parameter describing the shape of the source (structural index, N) is used. Different approaches to Euler deconvolution allow obtaining the vertical source position and N (e.g., Stavrev, 1997; Nabighian and Hansen, 2001; Hsu, 2002). However, these parameters may be recovered also through other methods, e.g., Smith et al. (1998), Salem and Ravat (2003), Fedi, (2007), including the continuous wavelet transform (e.g., Hornby et al., 1999; Sailhac and Gibert, 2003; Fedi et al., 2004; Fedi et al., 2010; Fedi and Cascone, 2011).

By using data at many altitudes, we may recover the depth to the source (z_0) with a geometric method and z_0 and N with a linear regression applied to the rescaled upward-continued data along selected ridges. This method has reduced sensitivity to noise with respect to the Euler deconvolution because the multiscale methods involve upward continuation, and so the high-wavenumber noisy components are naturally attenuated. The multiscale set will in turn depend on the depth-range of the source, which we are seeking for. For instance, if we are looking at shallow crustal sources, a reasonable multiscale set is from the measurement surface to some kilometers.

2.1 The Multiridge Method

Methods, such as those based on the Multiridge analysis (Fedi and Florio, 2013), the Euler deconvolution versus *z* (Fedi et al., 2009), and the DEXP (Fedi, 2007), explore the homogeneity properties of a field at several scales or altitudes and are typically based on analyses performed on vertical sections built considering the field at such scales. On these sections, ridges generated by isolated simple sources (point, line, sheet, and contact) are straight lines defined by the zeros of a potential field and its horizontal and vertical derivatives, at all measured or computed levels. The number of ridges depends on the order of differentiation of the potential field data, and their intersection occurs in the source region at the source position (the center of a sphere, the top of a dike, see: Fedi et al., 2009, Figure 1). The way ridges are defined may vary with the method, that is: CWT typically considers WTMML of *q*-order horizontal derivatives (Mallat and Hwang, 1992), whereas the scaling function or DEXP methods define ridges by using *q*-order vertical derivatives of the field.

Obviously, any combination of horizontal and vertical derivatives may be considered. As we said, for simple sources ridges intersect at the source position; however the Multiridge geometric method does not yield information about the source shape (i.e., the structural index). Nevertheless, by using the source-position estimates and considering that any ridge of the Multiridge set can be analyzed by Euler deconvolution, we can readily obtain the structural index. The classic implementation of Euler deconvolution implies the use of 1D or 2D moving windows along the measurement profile or plane. We use an original method in which Euler deconvolution is implemented by using 1D-moving windows along selected ridges (Fedi et al., 2009; Fedi and Florio, 2013).

The first step of the Multiridge analysis consists of using a suitable method to continue the field and computing its derivatives. We will assume a coordinate system with the depth positive downward and *x* and *y* representing north-south and east-west directions, respectively. Consider the magnetic field at *P* (*x*,*y*,*z*) generated by a simple source at *Q* (x_0,y_0,z_0), such as a uniformly magnetized sphere, or equivalently, a point dipole:

$$f_3 = C_m \mathbf{f} \cdot \nabla \left[\mathbf{t} \cdot \nabla \frac{|\mathbf{M}|}{\|\mathbf{r} - \mathbf{r}_0\|_2} \right] \tag{16}$$

where r and r_0 indicate the positions of points P and Q, respectively,

$\|\mathbf{r}-\mathbf{r}_0\|_2 = \sqrt{(x-x_0)^2+(y-y_0)^2+(z-z_0)^2}$, **M** is the sphere dipole moment, $C_m = \frac{\mu_0}{4\pi}$, μ_0 being the permeability of free space, **h** (h_x, h_y, h_z) is the unit vector parallel to the local direction of the geomagnetic field **h**, **t**(t_x, t_y, t_z) is the unit vector along the direction of **M** and ∇ is the gradient operator vector.

A first type of ridges for the magnetic field is defined by the zeros of the first-order horizontal derivative of f (equation 16). Without any loss of generality, we assume the cross section $x=x_0$ and $|\mathbf{M}| = 1$ and find:

$$\frac{\partial f_3(\mathbf{r},\mathbf{r}_0)}{\partial y} = \\ = 3\frac{\left(Y^3+YZ^2\right)t_x f_x + \left(3YZ^2-2Y^3\right)t_y f_y + \left(Z^3-4Y^2Z\right)t_z f_y + \left(Z^3-4ZY^2\right)t_y f_z + \left(Y^3-4YZ^2\right)t_z f_z}{\left[(Y^2+Z)^2\right]^{7/2}} = 0 \quad (17)$$

where $Y = y-y_0$ and $Z = z-z_0$.

From equation (17), one can see that the ridge equations are simple straight lines of the type

$$y - y_0 = g(z - z_0) \quad (18)$$

where g is the angular coefficient of the straight-line, g = tan (ϕ), where ϕ is the angle of the ridge line from the vertical z-axis (positive clockwise). Assuming for instance induced magnetization with inclination I= 90° and declination D= 0° and y-axis pointing North, we have: $h_x=t_x=\cos I \cos(D\text{-}90°)=0$; $h_y=t_y=\cos I \sin(D\text{-}90°)=0$; $h_z=t_z=\sin I =1$.

In this case the solution of equation (18) leads to the following ridge equations:

$$y = y_0, \quad (19)$$
$$y - y_0 = 2(z - z_0),$$

and

$$y - y_0 = -2(z - z_0).$$

Because the three ridges intersect at the sphere center (y_0, z_0), we can retrieve the source position by a geometrical method. A similar behavior occurs for higher-order derivatives (horizontal or vertical) of potential fields, but the number of ridges increases according to the order.

The ridge lines of different type may be automatically drawn in different ways, by algorithms searching either for the zeros or for the maxima/minima of a function. One of the most efficient algorithms for the search of extreme points is that of Canny (1986), originally developed for detecting the edges of images. Once extreme points are determined at different altitudes, ridges may be obtained by linking each of them, at a given altitude, to the nearest one computed at the altitude just above.

An example is shown in **Figure 2. 1**, for the magnetic field generated by two different spherical sources, one placed at 5 km depth and the second at 15 km depth. We see that the ridges based on the zeros of the horizontal derivative (cyan dots) and those based on the zeros of the vertical derivative (yellow dots) may be extended in the source region (dashed lines) and all converge to the singular points of the two spherical sources, i.e. at their centers.

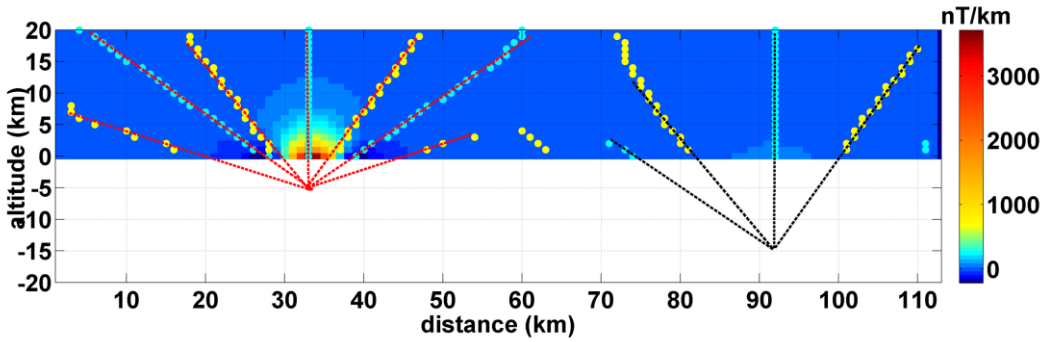

Figure 2. 1 Synthetic example of the Multiridge analysis considering the magnetic field due to two spherical sources: the first (a) is placed at 5 km depth and the second (b) is at 15 km depth. Ridges corresponding to the zeros of the horizontal field derivative are indicated by cyan dots, those corresponding to the zeros of the field vertical derivative are indicated by yellow dots. The geometric approach consists of fitting the ridges by straight lines, prolonging them into the source region (dashed lines) and identifying the sources at their intersection.

2.2 The Scaling Function method

The structural index (N) was introduced in the frame of the Euler Deconvolution method and, for most sources, reflects the fall-off rate of the potential field anomaly with distance. N can be

important in the interpretation of potential field data because it characterizes the anomaly source in terms of simple shapes, thus helping to build a starting model for a forward method of interpretation. Euler deconvolution is defined for 1D and 2D data sets, and care must be taken to circumvent effects from noise and regional field interference.

The interest for evaluating the field homogeneity degree *n* is that it may be related to a source parameter, the structural index *N*, by the equation:

$$N=-n+k \tag{20}$$

where *k* is the order of differentiation of any magnetic field derivative. By the estimation of *N* from the measurements, we may determine the right type of source. *N* is equal to 0 for a contact-like source, to 1 for dykes or sills, to 2 for vertical semi-infinite cylinders or for an infinite dipole line and to 3 for a sphere or for a dipole source (Reid et al., 1990). The technique used for estimating n is described in: Fedi (2007); Fedi and Florio (2006); Cella, Fedi and Florio (2009), and consists of forming along any ridge the scaling function, τ_k:

$$t_k = \frac{\partial \log\left(f_k(z)\right)}{\partial \log(z)} = \frac{(n+k)z}{z - z_0} \tag{21}$$

from which the homogeneity degree n may be easily computed and from that the structural index *N*.

The scaling function is a dimensionless quantity, which characterizes the scaling behavior of a given field and enjoys interesting properties. For instance, when $a >> -z_0$, $t_q(z,0) \to -N_k$. Another main property is that when ζ is equal to the depth z_0, the scale function is a constant function of the scale *a* and its value is equal to $-N_k$.

3

Geological setting of Europe

3.1 The European Crust

The European continent is constituted of a complex 'collage' of many crustal blocks originated in different geological periods and constituted by specific series of formations (Figure 3. 1). Central Europe is the result of the dismantle of the supercontinent Rodinia from the Neoproterozoic times (McCann, 2008; Vozár et al., 2010) and includes several tectonic boundaries, such as the Alps mountain system, the Carpathians chain, the Pannonian basin, the Bohemian massif and the Trans European Suture Zone (TESZ). This last geological structure is one of the most prominent crustal boundary in central Europe which is the result of the juxtaposition of the stable and ancient north-eastern East European Craton (EEC) (Baltic Shield) and the mobile and younger south-western Paleozoic platform (PP), occurred during the Caledonian and Variscan orogenic episodes (e.g. Pharaoh, 1999; Thybo, 2001; Banka, 2002). The TESZ comprises two main structural segments: the Sorgenfrei–Tornquist Zone (STZ) in the northwestern part of the TESZ and the Teisseyre–Tornquist Zone (TTZ) and extends from the Baltic Sea in the northwest to the Black Sea in the southeast (Pharaoh, 1999). On the NE of Europe, the Baltica paleocontinent evolved during several Precambrian episodes of crustal accretion and reworking and comprises the Fennoscandian and Ukrainian shields and the East European Craton. The EEC extends from Denmark to the eastern side of Russia and comprises the three segments of Sarmatia, Volgo-Uralia and Fennoscandia differing in forming dynamics and lithological and tectonic features (Bogdanova et al., 2006). Generally, the EEC is characterized by a thick and cold crust composed mainly by Precambrian rocks evolved during Archean-Paleoproterozoic episodes of accretion and reworking (Gaàl and Gorbatschev, 1987) and covered by thin series of Phanerozoic rocks (Plant et al, 1998). To the SW of the TESZ, the Avalonia microcontinent is defined by many Proterozoic-Paleozoic crustal blocks rifted from the southern Gondwana continent, subsequently accreted to the Baltica during various

orogenic episodes (Nolet and Zielhuis, 1994; Pharaoh, 1999; Winchester and the PACE TMR Network Team, 2002; Banka et al., 2002) and the closure of the Lower Palaeozoic Tornquist Sea in late Ordovician to Silurian times (Plant et al., 1998). The Rhenohercynian Zone is part of the Avalonia continent reworked as foreland thrust belt during the Variscan Orogeny (Dallmeyer et al., 1995). The Rheic Suture represents the boundary between the Rhenohercynian Zone and the Saxothuringian Zone and extends from the SW England through the Paris basin to the Northeastern Germany (Figure 3. 1). In the Armorica region, the Saxothuringian terranes belong to the late Silurian/early Carboniferous Variscan orogeny and their terranes derive from the Gondwana crust, as demonstrated by paleomagnetic and glacial facies evidences (Krs et al., 1986; Tait et al., 2000, 2000). Similar origin has the Moldanubian zone which comprises the areas of the Massif Central, Vosges, Black Forest and the Bohemian Massif (Banka et al., 2002). In Paleozoic ages many events led the accretion of the ancient terranes at high southerly palaeolatitude (Ziegler, 1990) forming the main structures of central Europe and the formation of the TESZ boundary during the closure of the Tornquist Sea and the juxtaposition between the Avalonia and Baltica (Cocks and Fortey, 1982; Trench and Torsvik, 1992). In particular, the Lysogory, Malopolska and Bruno-Silesian are constituted by part of Gondwana crust accreted to the EEC margin during the Cambrian time (Belka et al., 2000). In the northern part of the Paleozoic platform the main structural feature is the North German Basin, extended up to the northern Poland (Dallmeyer et al., 1995). The homogeneous microcontinent of Avalonia extends from the Appalachians to the North Sea and accreted to the eastern margin of Baltica during the Caledonian orogeny (Pharaoh, 1999).

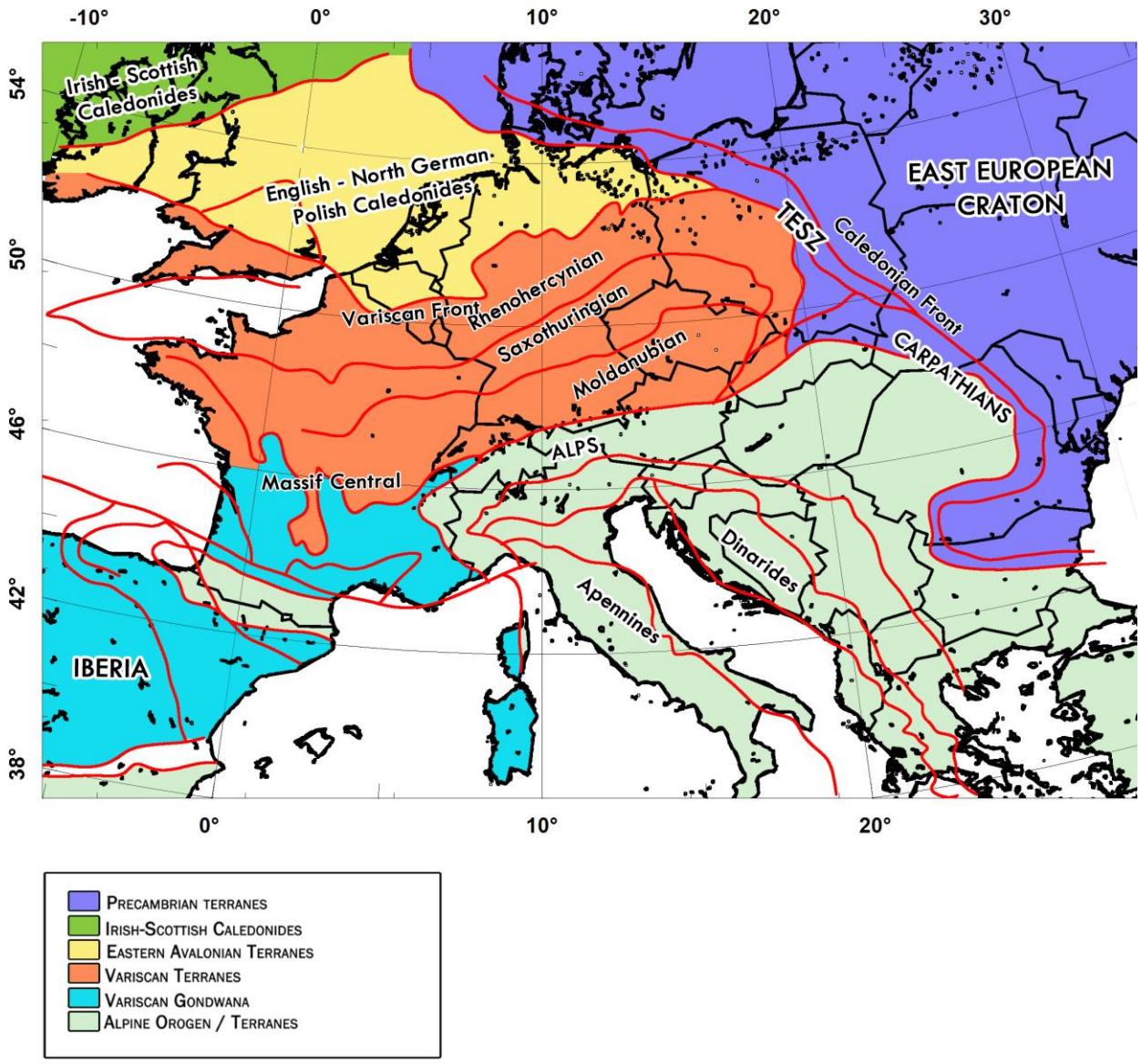

Figure 3. 1 Tectonic setting of the European continent (redrawn after Blundel et al., 1992).

3.2 Geophysical Framework

The complex geological framework of the European continent has been studied in last decades using detailed geophysical methodologies. In particular, many potential fields' analysis and seismic surveys allowed recognizing the strong differences between the different crustal blocks composing the European crust.

In the last four decades, various deep seismic reflection surveys, such as BIRPS (UK), CROP (ltaly), DEKORP (Germany), ECORS (France) and NFP 20 (Switzerland), revealed important details on the European crustal and upper-mantle structures down to 60 km of depth. The European Geotraverse (EGT) is the main project based on the study of several deep seismic experiments of the continental Europe, which aimed at developing a three-dimensional representation of the geological structures and properties of the European lithosphere (Freeman and Mueller, 1990; Freeman et al., 1990; Blundell et al., 1992). Further deep seismic sounding (DSS) studies were carried out in central Europe, such as KTB in Germany (Gajewski and Prodeh, 1987; DEKORP Research Group 1988; Gebrande et al. 1989; Schmoll et al. 1989) and the POLONAISE'97, CELEBRATION 2000, ALP 2002 and SUDETES 2003 (Guterch et al., 1998, 1999, 2001, 2003a, b; Grad et al., 2003; Brückl et al., 2003) in Poland, which allowed revealing the strong contrast between the PP and the EEC and the structural features of the TESZ area. The results have shown significant variation in thickness between central Europe and the Precambrian platform assigning a Moho depth range of 28-35 km beneath the Paleozoic crust and a range of 40-50 km depth of the Moho beneath the EEC (e.g. Pharaoh et al., 1997; Guterch et al., 1999; Guterch et al., 2004).

Potential field studies in Europe pointed out important additional information of the crustal composition and the distribution of the density and magnetization. Observation of gravity and magnetic maps revealed that the PP and EEC differ not only on structural features but even more on potential field properties. The TESZ, in fact, represents also an important boundary, separating the maps in two different potential field anomaly regions. The Bouguer anomaly map of central Europe (Grosse et al., 1990) reveals clear regional anomalies related to the tectonic structures and magmatic intrusions within the crust. Wybranic et al. (1998) published a new compiled European gravity field map which was produced by merging several datasets of different countries. Many negative anomalies are associated to the main mountain belts and diffuse positive anomalies are referred to tectonic structures and boundaries. In particular the margin between the PP and the EEC is strongly

highlighted by several gravity lineaments with the same orientation, reflecting the variation in crustal thickness and sedimentary successions. Moreover, many anomaly patterns are explained by the variation of the Moho depth in Europe and the presence of igneous intrusions. The map of the gravity field model EGM2008 (Pavlis et al., 2012) above the European continent is shown in Figure 3.2. EGM2008 global gravity model was formed by merging terrestrial, altimetry-derived, and airborne gravity data and is complete up to spherical harmonic degree and order 2159 (Pavlis et al., 2012).

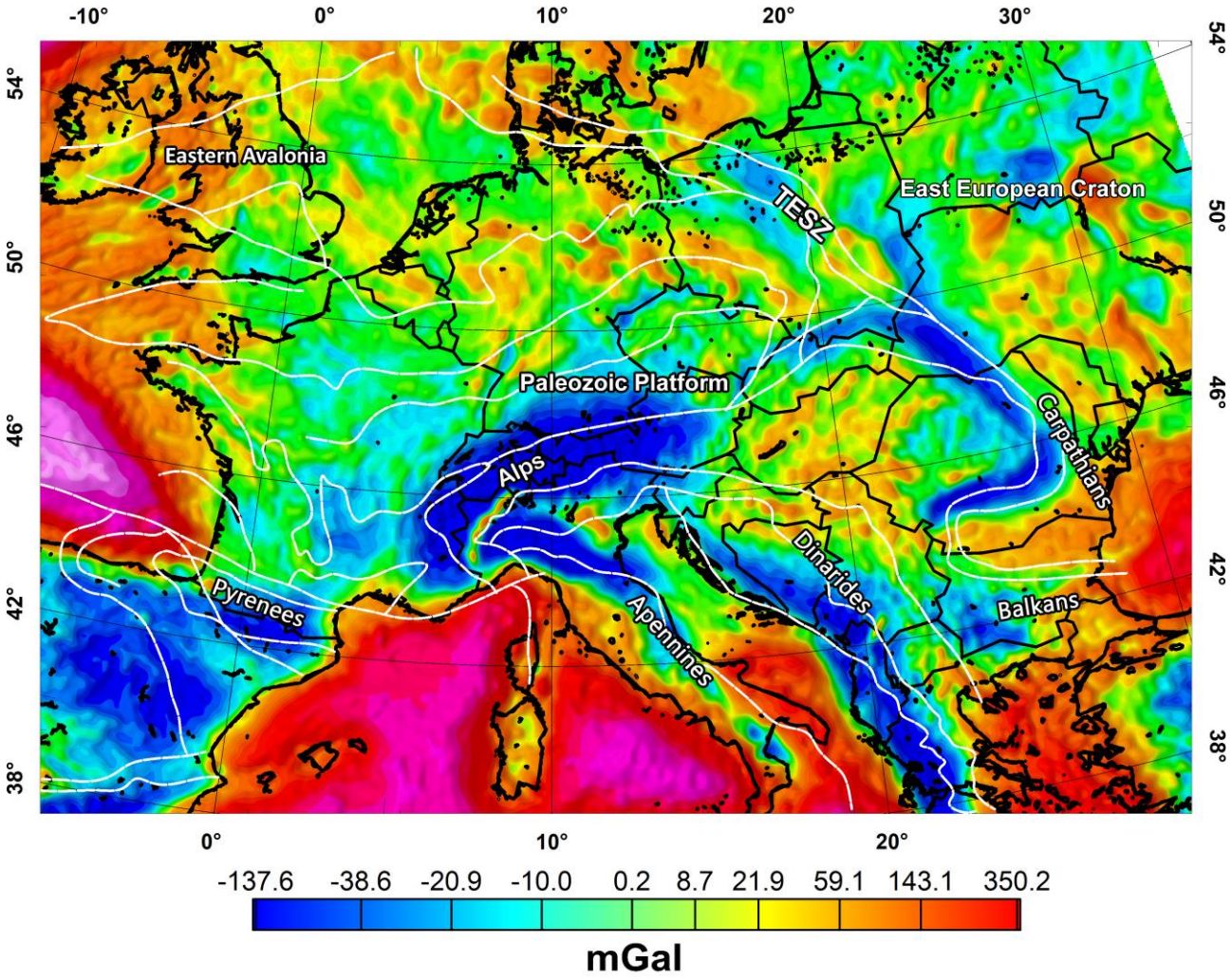

Figure 3.2 EGM2008 gravity field over the European continent compared with the geological structure lineaments.

3.3 Moho depth and crustal thickness

The Moho discontinuity is the main first-order structure within the lithosphere, between crust and upper mantle, which was discovered by Mohorovičić through the study of seismic waves propagation within the Earth. The Earth's crust was defined by the results of several geophysical and mineralogical studies which aimed to describe the change of rock parameters with depth, such as density, type of rock, chemical composition, etc.. The Moho discontinuity is studied especially by deep seismic sounding surveys, in particular by wide-angle arrivals from the Moho discontinuity, the so-called PMP phase, the waves reflected at that interface or quasi-reflected in a strong gradient zone in the transition between the lower crust and uppermost mantle. In terms of seismic waves' velocities, the 'crust' is defined as the outermost shell of the Earth where V_p is smaller than about 7.6 km s^{-1}, and V_s velocity is smaller than about 4.4 km s^{-1} (e.g., Meissner, 1986). The Moho, so, specifies the passage between two environments differing significantly in elastic parameters and rock type. Generally, crustal thickness varies strongly with tectonic setting, but the average crust was determined to be ~40 km thick (Christensen and Mooney, 1995; Rudnick and Fountain, 1995) and more recently was calculated by Huang et al. (2013) as 34.4 km thick. Thickness of the European crust is strongly influenced by the overlap of different crustal type passing from deep cratonic environment to thin and warm crustal regions. The cratonic parts of Europe are characterized by anomalous thickness, where the roots may reach the maximum depth of 55-60 km (Artmieva and Meissner, 2012), such as in the Ukrainian shield, Uralides and Baltic shield. Variscan terranes in central Europe show instead a uniform thin crust of around 28-32 km. The TESZ marks also in this case a significant change in crustal thickness passing from the thin crust of central-western Europe to a thick cratonic crust on the NE characterized by high-velocity lower crust (e.g. EUROBRIDGE SWG, 1999; Korja and Heikkinen, 2005; Pavlenkova, 1996; Guterch and Grad, 2006). Obviously, this structural feature of the European continent is observed in the maps of the Moho depth which were produced since last century by collecting a huge amount seismic data covering most of Europe. In this paragraph, only the main references of the numerous publications available in literature describing the datasets and the results have been cited. Some models were compiled in the past using the seismic surveys of the 1970s and the 1980s and covering only specific regions (e.g. Radulescu 1988; Ziegler, 1990; Luosto 1991; Ansorge et al., 1992; Scarascia and Cassinis, 1997; Chadwick and Pharaoh 1998) and essentially the continental Europe (e.g., Meissner et al., 1987; Giese and Pavlenkova, 1988; Tesauro et al., 2008). In the last

decade, thanks to the availability of new highly detailed seismic surveys and the integration of the different available models and older data, it was possible to produce new high resolution map of the p) depth to the Moho. In particular, Grad et al. (2009) compiled a complete Moho depth map covering the whole Europe, from the mid-Atlantic ridge to the west to the Ural Mountains to the east and from the Mediterranean Sea to the south to the Barents Sea and Spitsbergen in the Arctic to the north. The model was constructed using both the old seismic data and the new ones deriving from the projects POLONAISE'97, CELEBRATION 2000, ALP 2002 and SUDETES 2003 (Guterch et al., 1999; 2003). Receiver function (RF) data were also used, which provide detailed information of the distribution of *S*-wave velocity in the crust and Moho depth (Guterch et al., 2003). Moreover, modelling of gravity Bouguer anomalies were considered to study the inhomogeneities of density distribution in the crystalline crust and at the Moho. A new study of the Moho boundary and crustal structures in Europe was performed by Artemieva and Thybo (2013) compiling data of original seismic profiles and RF and excluding non-seismic data. The obtained model provided a representation of the *Vp* velocities and thickness of five crustal layers of the Europe and the outer areas.

The main geological features and structures of the European crust have their images in the Moho depth map in Figure 3. 3, produced considering the data compilation of Grad et al. (2009). On regional/continental scale the main visible feature is the strong difference in thickness between the thicker north-eastern Precambrian platform (40-60 km) and thinner south-western Paleozoic Europe (20-40 km), with the exception of the thick collisional Alpine crust. As discussed in the previous section, the thickness doesn't change gradually, but shows a sharp variation in correspondence with the TESZ margin, which is clearly identified in the map. In recent years many large-scale seismic experiments (e.g., POLONAISE'97 (Guterch et al., 1999), CELEBRATION 2000 (Guterch et al., 2003a), SUDETES 2003 (Grad et al., 2003b) and EUROBRIDGE (EUROBRIDGE Seismic Working Group, 1999; Yliniemi et al., 2001)) allowed estimating and mapping the depth to the Moho boundary and deep structures beneath the TESZ area (e.g. Thybo, 1999; Grad et al., 1999; Grad et al., 2001; Jensen et al., 2001; Guterch and Grad, 1999; Wilde-Piórko et al., 2010; Knapmeyer-Endrun et al., 2014; Janutyte et al., 2014). The results agree in describing the variable Moho topography within TESZ with undulations in the range of 10 km (Jensen et al., 2002; Thybo, 1997; Artemieva and Thybo, 2013) passing from the Paleozoic platform to the EEC, and increasing down to 50 km depth in some regions of southern Sweden, Denmark, Baltic Sea, Poland and Slovakia (BABEL Working Group, 1993a; Giese and Pavlenkova, 1988; Guterch et al., 1986; Thybo, 1990, 2001; Guterch et al., 2006). Moreover, several strong heterogeneities of crustal

structures may be observed at local scale in each European platform (Tesauro et al., 2008). Generally, the EEC is characterized of a relatively uniform Moho topography and high V_p velocities (~7 km/s) in the lower crust. In the Bohemian Massif region, (Czech Republic) (e.g. Beránek and Dudek, 1972; Enderle et al., 1998; Hrubcová et al., 2005, 2008; Grad et al., 2007) several interpretation of seismic data agree in identifying a shallow Moho in the Saxothuringian zone along the Czech-German (28-32 km) and increasing down to the central part of the Bohemian Massif (33-34 km) with a local maximum beneath the Sudetes Mountains (35 km). Hrubcová et al. (2005) studied the deep crustal structures in this region by interpreting the results of profile CEL09 of the CELEBRATION 2000 seismic project (Guterch et al., 2003a), which crosses the Saxothuringian, Barradian, Moldanubian and Moravian zones. The authors point out a complex Moho topography reaching a maximum depth of 39 km and the crust-mantle boundary is here assigned as a sharp variation of velocity contrast corresponding to the passage from 6.8 to 8.1 km s^{-1}. However, in some areas of the profile (e.g. beneath the Moravian zone) the seismic Moho boundary is not clearly visible, but a thick transition zone from the crust to the mantle is retrieved corresponding to depths of 23–40 km with V_p velocities ranging from 6.8 to 7.8 km s^{-1}. Grad et al. (2008) carried out a further seismic modeling of the Bohemian Massif lithosphere using the data of the SUDETES 2003 seismic experiment. The authors studied the seismic profile S01 which extends from the Bohemian Massif region to the Polish basin and TESZ. The Moho boundary retrieved has a relative narrow depth interval varying between 28 and 35 km, corresponding to a transition of the wave velocities to about 8.3 km s^{-1} below the Moho. Beneath England and Ireland, the Moho depth is around 30-35 km (Kelly et al., 2007) with an increase of the velocities from 6.7 to 7 km/s in the lower crust south of the Iapetus Suture Zone (Landes et al., 2005). The North German basin is characterized by a strong change in crustal thickness and composition, where the Moho boundary rises from ~35 km depth to 28-25 km from north to south and velocities decreases consistently (Scheck et al., 2002). The eastern Carpathians and Alpine Mountain systems show a common thick crust with Moho depth grater then 50 km, while beneath western Carpathians the boundary depth decreases up to 35 km (Finetti, 2005; Horváth et al., 2006). High Moho depths are also found beneath the Pyrenees and Cantabrian area (~45 km) (Tesauro et al., 2008) reflecting the subduction of the Iberian plate.

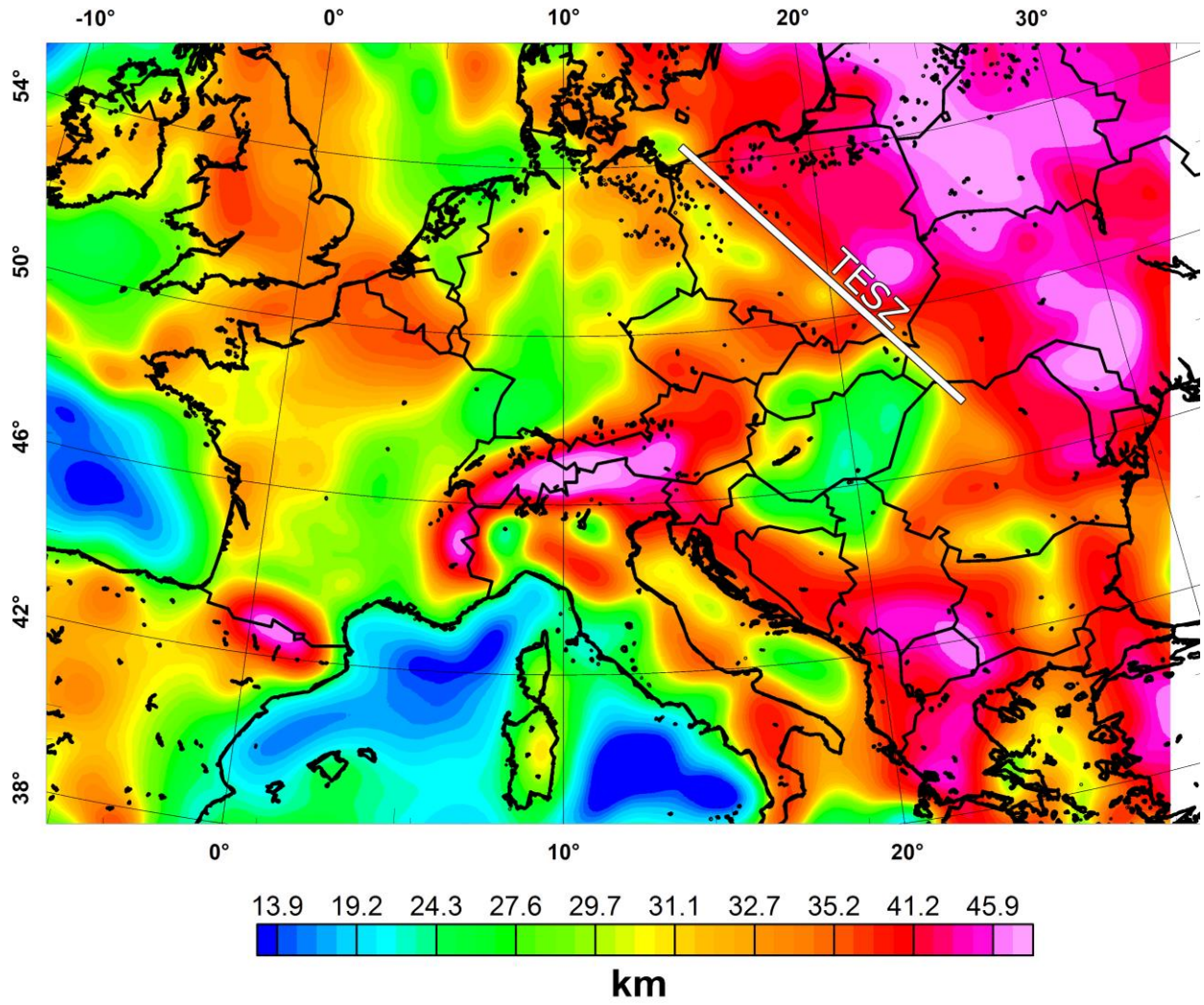

Figure 3. 3 Depth to the Moho of Europe (data from Grad et al., 2009).

3.4 Geothermal regime

Geothermal studies are the fundamental of understanding the material properties and the dynamic of the Earths' crust. The terrestrial heat flow refers to the natural heat of the Earth produced by the decay of long-lived radioactive isotopes occurring in the crust, to the heat contribution of the mantle and lower crust transmitted through the rocks and, secondary, to some convection of fluids (Čermák, 1993) that is considered as the product of the thermal gradient and the thermal conductivity of a specific interval (Beardsmore and Cull, 2001). The heat flow provides important information about the rheological behavior, the evolution of the lithosphere and past

geological events. The thermal gradient of a continental crust is affected mainly by two particular conditions: the crustal thickness and the age. Generally, the radiogenic elements of older crust are conditioned by higher natural decay and, consequently, determine a lower surface heat flow (e.g. Sass and Lachenbruchm, 1979). Likewise, thicker crust contributes more heat than thinner crust of the same age, due to a high concentration of heat-producing materials. However, the crust-mantle boundary thermal condition also affects the thermal regime of the crust. In fact, if the base of the crust is a constant temperature boundary, then the thermal gradient and heat flow decrease with the increasing of crustal thickness (Beardsmore and Cull, 2001). In any case, the thermal regime of the lithosphere changes considerably region by region due to differences in the structural features and heat-producing contributions.

In magnetic studies of the crust, the knowledge of the thermal condition in the area of interest is fundamental especially for deep source exploration. As mentioned earlier, the magnetic properties of rock mineral are strictly related to temperature and composition. The *Curie temperature* is defined as the point at which a mineral loses its ferromagnetic properties. In magnetic studies, it is common to consider the Curie temperature of Magnetite (580°C), the main magnetic mineral in the Earth's crust, as the standard thermal boundary below which the rock magnetization vanishes (*paramagnetic* rocks). The Curie depth is generally calculated by employing a Fourier analysis on aeromagnetic data of the total magnetic intensity field (Spector and Grant, 1970). However, ferromagnetic minerals within andesites and alkali-basalts generally have Curie temperatures in the range 100-300°C, and intermediate to mafic compositions are in the range 300-450°C. So, the estimation of the Curie depth may be necessarily correlated to seismic and other geophysical methods in order to determine if such temperature coincides with a specific change in velocity or density and rock composition. The mantle is generally considered to be nonmagnetic (e.g., Wasilewski, et al., 1979; Frost and Shive, 1986) and so rock magnetization may be considered down to the Moho interface or the Curie isotherm. This thermal boundary is generally located in the upper mantle, both in continental and oceanic lithosphere, but in the case of high heat flow, such as tectonically active regions, the Curie isotherm may rise up to shallower depths producing a thinner magnetic crust and, subsequently, a lower magnetic field contribution. Moreover, several studies pointed out that, in some geological regions, the upper mantle may have magnetic properties, especially in oceanic regions (e.g., Arkani-Hamed, 1989; Harrison and Carle, 1981; Counil, at al., 1989) and the crust-mantle boundary may be considered as a magnetic basement (Corrado et al., 1979; Gasparini et al., 1981).

Such geological environments may be retrieved in the European continent where an inverse correlation of the heat flow with the magnetic crustal thickness is observed in several areas (Jakoby et al., 1991). The map of the heat flow in Europe is shown in Figure 3.4 and was produced using the data of the global heat flow dataset made available by the International Heat Flow Commission (for more detail see the website 'heatflow.und.edu').

Many geothermal studies of Europe were carried out by using several existing observations and deep borehole temperature measurements, which aimed to model and map the variation of the European heat flow at regional and local scale (e.g. Lee, 1965; Chapman and Pollack, 1975b; Čermák and Rybach, 1979; Čermák, 1982; Čermák and Bodri, 1986; Čermák et al., 1989; Čermák et al., 1991; Hurting et al., 1992; Čermák, 1993; Plewa, 1998; Królikowski, 2006). In these studies, there is a general agreement in describing a main geothermal feature, a consistent NE-SW increase of the thermal activity correlated to the tectonic evolution of the lithosphere. Consequence of the straight correlation between heat flow and tectonic units are the general increase of thermal gradient in thinner crust areas and a regional variation of the Moho boundary temperature. In particular, low regional heat flow values (30-40 mW m^{-2}) were retrieved within the Baltic shield (Precambrian platform) which is typical of thick lithosphere, whereas relatively high heat flow values were observed in specific areas of depressions of the Precambrian basement (e.g. Čermák and Rybach, 1979). Then, to the south-west of the Precambrian crust, the TESZ boundary represents again a prominent geological margin dividing Europe in two distinct thermal regimes. Central Europe, in fact, is dominated mainly by extended high heat flow zones moving from east to the west. At local scale the Paleozoic platform is characterized by a complex pattern of heat flow areas due to a very intricate framework of geological structures and formations. On the other hand, heat flow in the Baltic shield is essentially defined by low and regular trends, pointing out mainly a thick and cold Precambrian crust composed of ancient geological units.

However, in central Europe local heat flow districts may have an inverse behavior respect to the regional trend. This is the case of the Bohemian Massif region where an anomaly of low heat flow corresponds to the maximum crustal thickness in the stable central part of the massif (e.g. Čermák, 1975), while two local high heat flow anomalies correspond to the fault system bordering the northern part of the area. In western Europe, the geothermal regime is characterized by diffuse high heat flow values, especially in central and southern France, and by patterns of high and low values around the British Isles. High geothermal gradients are also retrieved in the Alpine Mountains belt due to the presence of intricate structural units, and in the Carpathians front with an

increase from east to west. Italy, in this regard, is mainly divided in two distinct heat flow regions controlled by the Apennines chain, which separates a warmer crust on the west from a colder eastern crust. However, a high heat flow zone may be found in the Tyrrenian Sea correlated to a weakened crustal thickness. Low temperature was instead retrieved in the Adriatic Sea and Balkan coast (50 mW m^{-2}).

Curie depth studies pointed out the depth of the magnetic crust bottom, which fairly well matches with the Moho interface in some regions, such as in the Variscan units of central Europe. On the other hand, deeper Curie depths have been calculated in the Ligurian Sea and beneath the main collisional boundaries, allowing considering an upper-mantle contributing to the geomagnetic field. Shallower Curie depths were expected in the Alpine system, pointing out a deeper Moho with respect to the depth to bottom of the magnetic crust (Chiozzi et al., 2005).

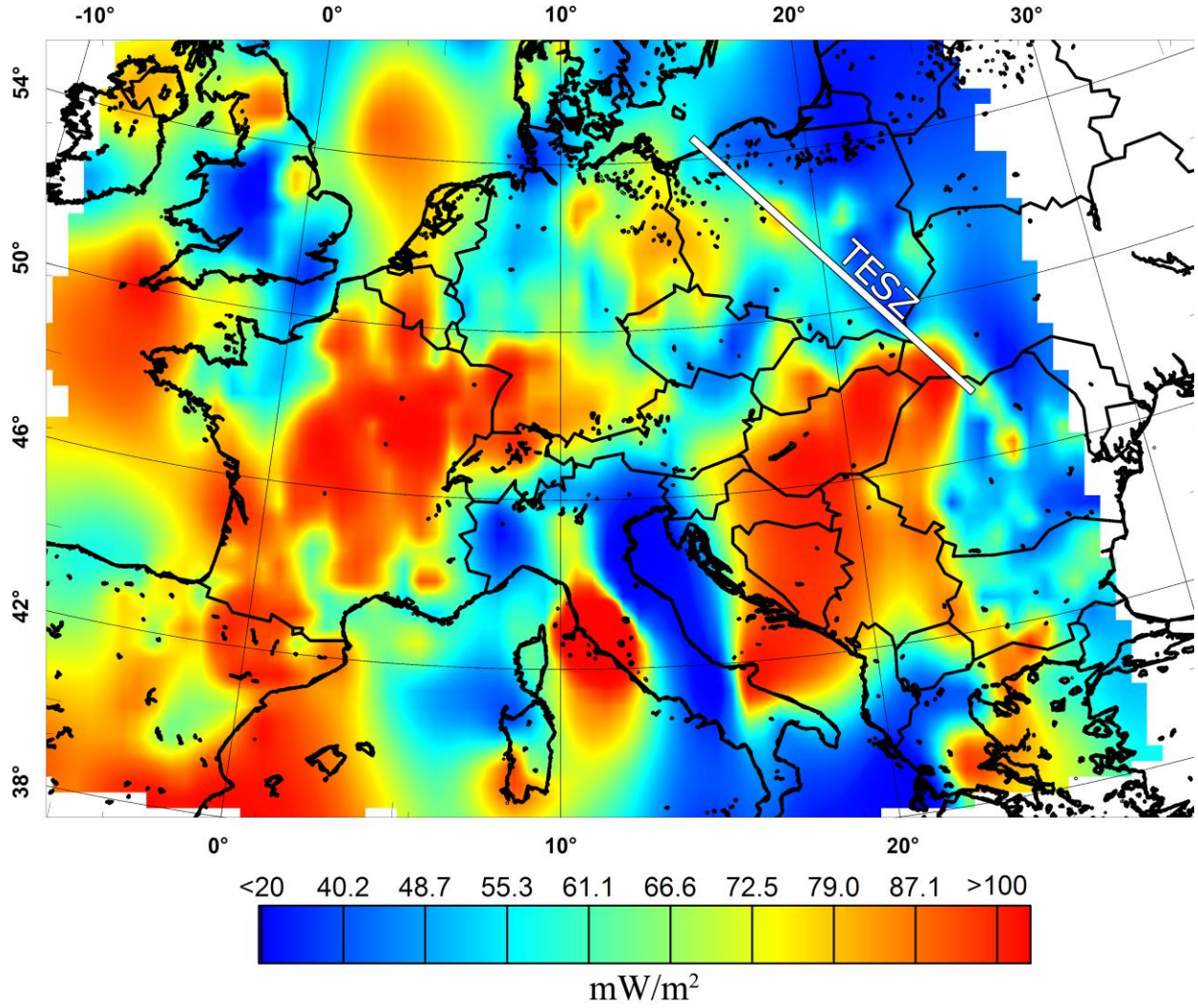

Figure 3. 4 The heat flow map of Europe (data available at http://www.heatflow.und.edu/).

3.5 Depth to the magnetic bottom

Previous magnetic studies pointed out the Moho to be a magnetic boundary marking the passage from the non-magnetic mantle to the magnetized crust (Wasilewski et al., 1979; Wasilewski and Mayhew, 1992). These authors showed that ultramafic composition of upper mantle consists mainly of non-magnetic chrome spinels and magnesian ilmenites, while titanomagnetite is the main magnetic mineral within the Earth's crust. However, in last decades several studies retrieved the bottom of the magnetic layer below the Moho interface in some specific geological environments (e.g. Ferré et al., 2013). These results were obtained from several detailed mineralogical analyses of mantle and crustal xenoliths samples. The study of aeromagnetic

anomalies in specific areas suggest that the forearc mantle may contain magnetic contribution to the long-wavelength component of the geomagnetic field (e.g. Arkani-Hamed and Strangway, 1987; Bostock et al., 2002; Blakely at al., 2005; Chiozzi et al., 2005; Ferré et al., 2013). The lower crust composition is generally estimated from exposed terrains recording lower crustal pressures, xenoliths, and from geophysical data. These rocks are mainly composed of metamorphics in granulite facies which may be retrieved as outcrop terrains or as small fragments carried up from great depths through volcanic conduits (xenoliths) (Rudnik and Fountain, 1995). For more details on the lower crust mineral composition and xenoliths, we refer to several interesting publications, such as Rudnick and Presper (1990); Rudnick and Fountain (1995); Rudnick and Gao (2003, 2014); Hacker et al. (2011); Huang et al. (2013), etc.

Generally, analyses of mantle xenoliths provide most of the information about the lithospheric mantle. The magnetic features of rocks at such depths are obviously related to the presence and properties of magnetite, which may be considered as the result of exsolution at the mantle depths in olivine and pyroxenes (Sen and Jones, 1988; Ferré et al., 2013). Despite previous author's interpretations, Ferré et al. (2013) pointed out that magnetite occurring in the mantle xenoliths carry important natural remanent magnetization (NRM) which may contribute to the long-wavelength signal of the geomagnetic field. The authors show that the lithospheric mantle is characterized by non-uniform magnetic properties in tectonic environments and the analysis of mantle xenolith samples identified a NRM intensity varying between 10^{-4} and 1 A/m, whereas other previous studies obtained values of NRM > 5 A/m (Robinson et al., 2002; McEnroe et al., 2004), which are considered contributing to the long-wavelength magnetic anomalies. Generally, the magnetization contrast in the uppermost mantle is very weak and the resulting magnetic anomaly may not be clearly identified; however, in some specific areas of low crustal magnetization, the upper-mantle magnetic effect may be significant, especially at high altitude of observation. So, the uppermost mantle may carry magnetic contribution to the long-wavelength component which could be weak in the spectrum of aeromagnetic dataset.

4

Multiscale aeromagnetic dataset of Europe

It is known that, moving away from the Earth's surface, the contribution of each source changes, according to a decay law vs. distance. In general, the anomalies related to shallow sources are mostly visible at the lowest altitudes, while the effects of the deepest sources appear more clear at high altitudes. Therefore, the aim of this study is the identification of the crustal magnetic sources by the interpretation of the anomalous field with a multiscale approach, with particular focus on the deepest magnetic structures of the lower crust. This kind of analysis is made possible as we are able to compute a multiscale dataset.

4.1 The EMMP dataset

The aeromagnetic data used in this work was made available by Getech, as part of the European and Mediterranean Magnetic Project (EMMP, Fletcher et al., 2011). EMMP aimed to bring together all available magnetic data (ground, air and marine, profiles and gridded data to yield a high-resolution total magnetic intensity field (TMI) with of 1 km grid size. In some European countries, national high-resolution aeromagnetic data are available, whereas in other countries only ground data (e.g., Serbia and Slovenia) or lower-resolution grids (e.g., France) are accessible, sometimes due to restrictions on the release of full resolution datasets (e.g., Western Germany). In Romania, the lack in availability of a high-resolution dataset was overcome using the WDMAM magnetic model, so, only regional magnetic anomalies may be observed and detailed exploration of geological structures is not feasible. Since this compilation has been derived by merging and re-gridding different small datasets of a large-scale area, the long-wavelength components have been replaced with a 15 arc minute grid of the MF7 total intensity anomaly satellite model (Maus, 2010). For doing that, a 4^{th} order Butterworth band-pass filter with cut-offs of 300 km and 500 km was

applied to both Earth and satellite grids (see Fletcher et al., 2011 for more details). Because of the presence of some gaps (Figure 4. 1A) (e.g. above Pyrenees and in central-western Spain), due to the absence of magnetic surveys covering these regions, we filled such gaps using the Maximum Entropy interpolation method (available on the Oasis Montaj© platform), which is based on the concept that for a given dataset the best representation of data distribution is the one presenting the largest entropy or uncertainty. After filling the gaps with Maximum entropy method, we obtained the map shown in Figure 4.1B.

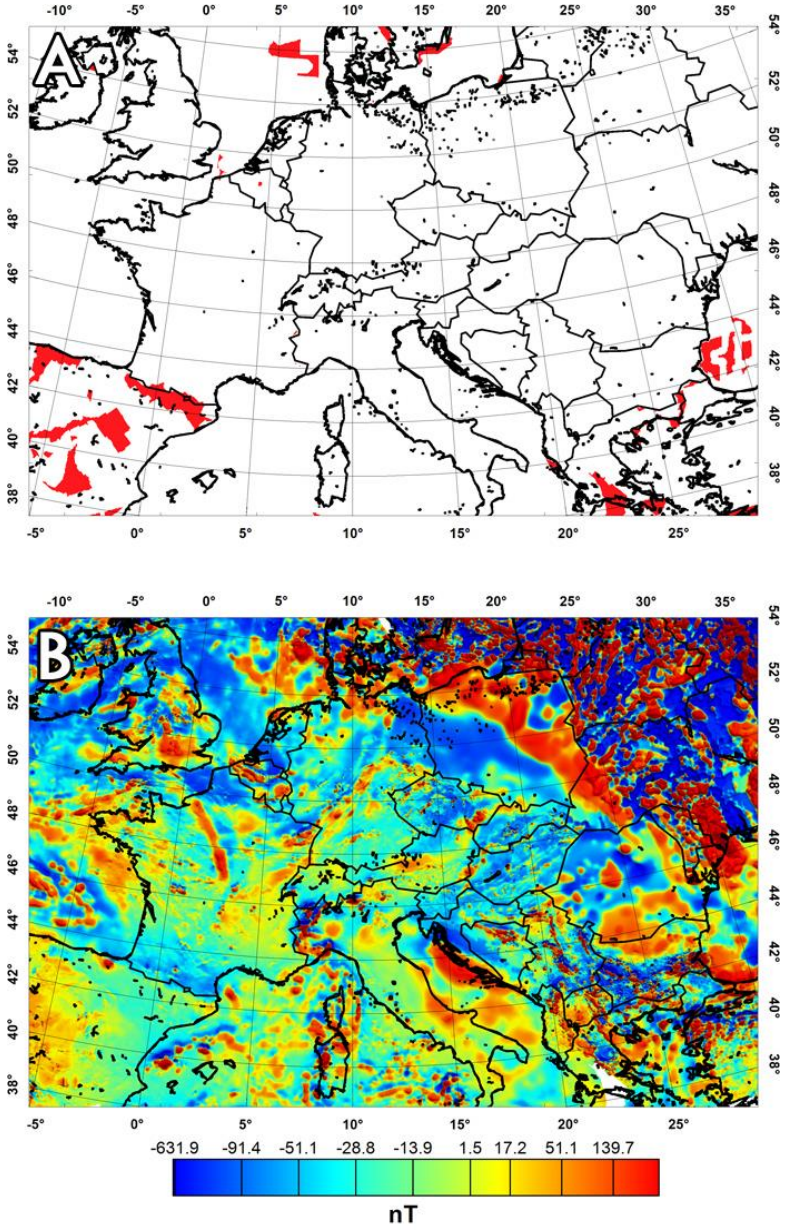

Figure 4. 1 A) Location of the dataset gaps in red; b) Original EMMP aeromagnetic dataset at 1 km altitude above the topography with gaps filled by maximum entropy interpolation.

We note now that the EMMP aeromagnetic data were gridded on a draped surface lying 1 km above the topography. So, before making a level-to-level continuation (see later, equation 22), it was first necessary performing a draped-to-level upward continuation (e.g., Mastellone et al., 2014). This is important, also because many others useful algorithms, such as reduction-to-the-pole, total gradient and others, need data at a constant altitude surface (e.g.; Mastellone et al., 2014). We so decided to draped-to-level continue the original data to a 5 km altitude level and used, to this end, the wavelet-based algorithm by Ridsdill Smith (2000) and the Digital Elevation Model SRTM30 (Farr et al., 2007).

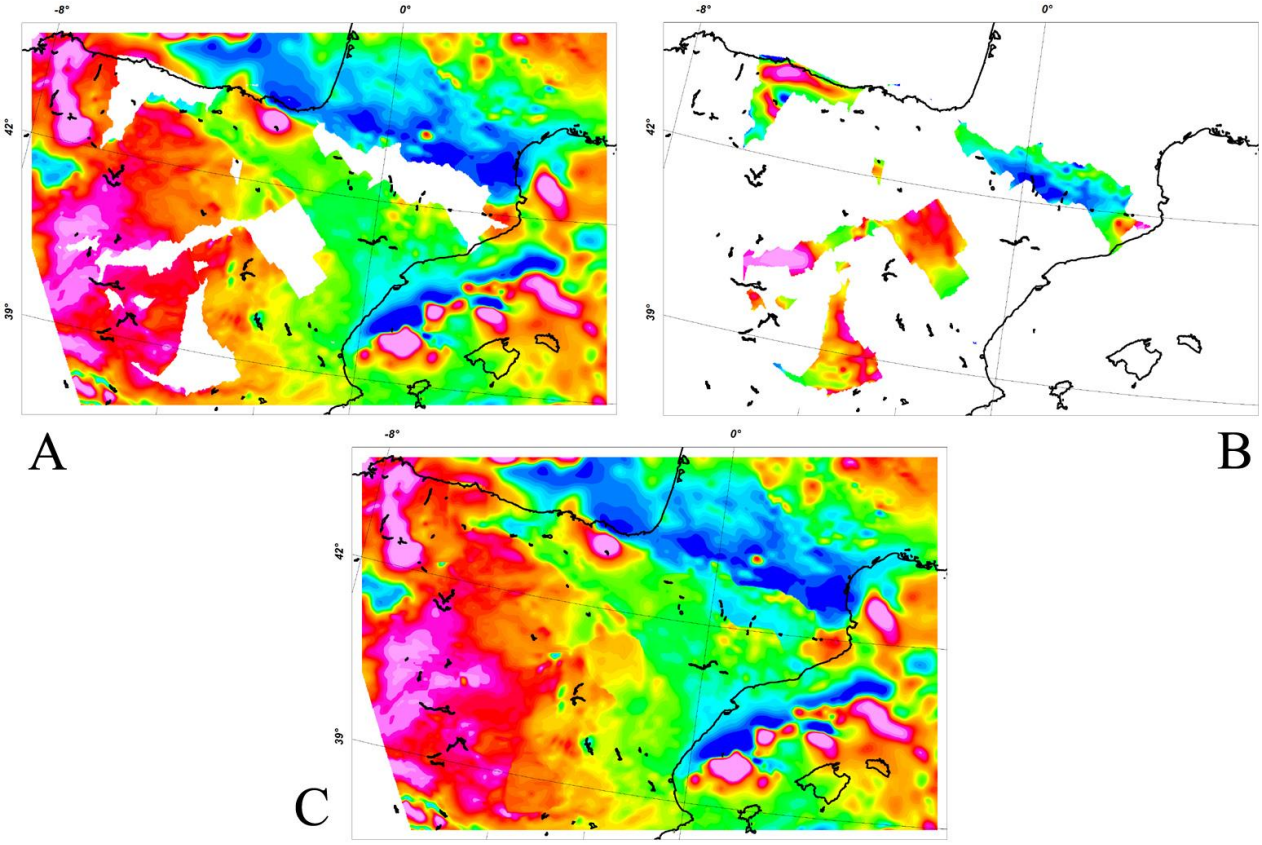

Figure 4.2. Aeromagnetic field over Spain at 5 km altitude with data gaps; B) Data extracted from the EMAG2 magnetic model upward continued at 5km altitude; C) Final magnetic map produced merging the EMAG2 data into the aeromagnetic map gaps.

With these data at a constant 5 km level, we decided to fill the above described gaps by not resorting no longer to interpolated data, but to more reliable data owning to the EMAG2 magnetic field model (Maus et al., 2009), which is the highest-resolution compilation of the lithospheric magnetic field at a global scale. The model was compiled using satellite, marine, aeromagnetic and ground magnetic surveys, in order to obtain a global 2-arc-minute resolution grid of the magnetic

intensity anomaly up to spherical harmonic degree 150 at an altitude of 4 km above geoid . In order to fill the gaps of the EMMP data with the data of the EMAG2 data, we first referred the EMAG2 data into a Cartesian coordinate system, using a Lambert conformal conic projection. Then, the EMAG2 dataset was re-gridded with a 1 km horizontal spacing and upward continued at 5 km altitude. Successively, only the data corresponding to the gaps were selected and replaced in the aeromagnetic grid using a *blend stitching method* implemented in the Oasis Montaj© software. An example of this merging knitting process is shown in Figure 4.2, where the EMAG2 data are used to fill the gaps within the aeromagnetic dataset.

We show the final map at 5 km altitude in Figure 4.3 It represents the reference dataset for our multiscale analysis.

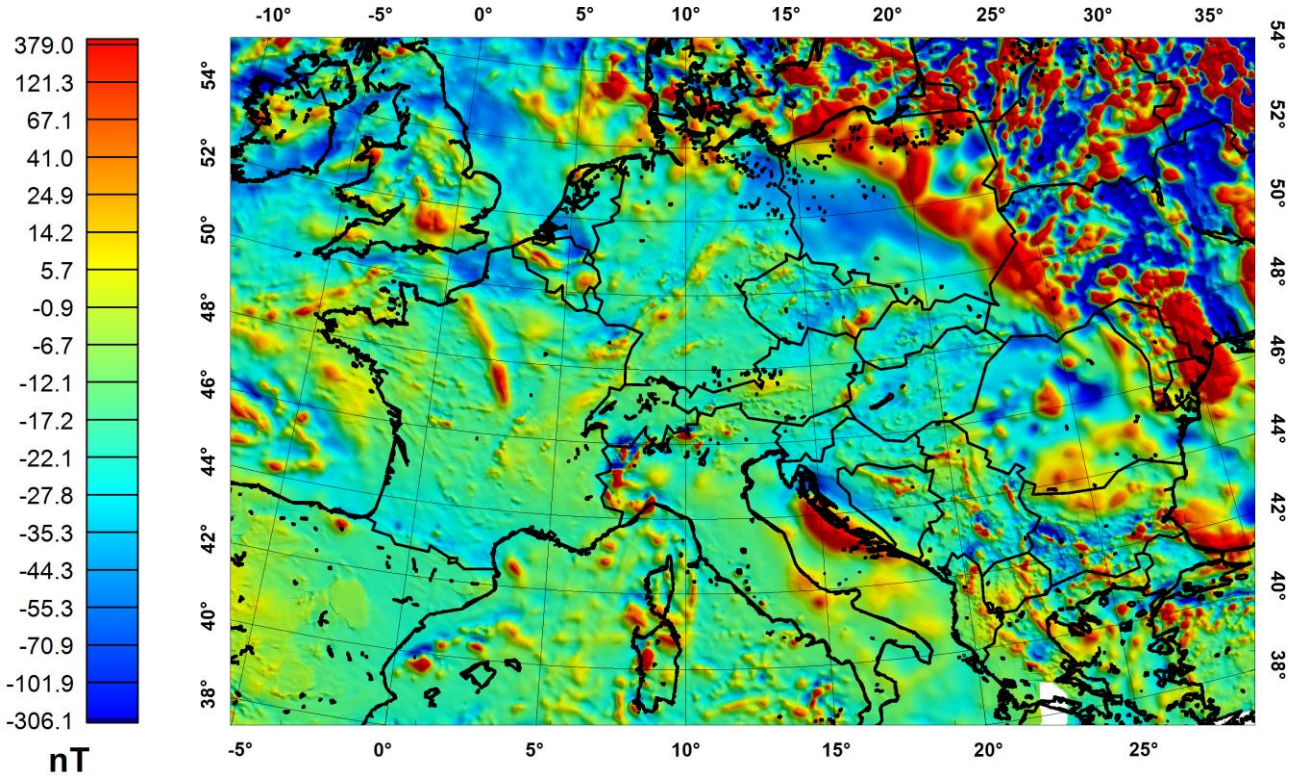

Figure 4.3 The magnetic field map of Europe at 5 km altitude

4.2 The multiscale aeromagnetic dataset

Having now available a dataset at 5 km altitude, we here describe how to form a multiscale aeromagnetic dataset. This task may be performed by using a level-to-level upward continuation algorithm (e.g., Baranov, 1976; Blakely, 1995), which is based on the following equation:

(22)

where $U(x,y,z)$ is the potential field upward continued at the scale z, $U(\xi,\eta,0)$ is the potential field at level z=0 and $z/[(x-\xi)^2+(y-\eta)^2+z^2]^{3/2}$ is the upward continuation operator.

Note that, in principle, this equation is applicable to fields known continuously on the entire flat surface. Our data, instead, are discrete datasets, containing equally-spaced data distributed on a finite surface. However, as shown in Fedi et al. (2009), accurate upward continuation may be computed if the data are known on a surface larger than the area of interest and/or by extrapolating data beyond its borders with a suitable algorithm. In fact, by upward continuing the data we may produce a border effect to the field near the grid margins and also cause some distortion of the anomaly shape (Oppenheim and Schafer, 1975; Fedi et al. 2012; Mastellone et al., 2014). Thus, before upward continuing them, the aeromagnetic data of Europe were extrapolated onto a larger area using an algorithm based on Maximum Entropy (Gibert and Galdeano, 1985).

In order to be more specific about the border error, it may be useful to calculate the extent ΔL of the upward continuation operator $z/[(x-\xi)^2+(y-\eta)^2+z^2]^{3/2}$ at different altitudes, in order to estimate the portion of the map, which may be mostly affected by the border effect. We may simply map the operator and evaluate ΔL as the horizontal half-extent. In particular, ΔL may be defined as the distance between the maximum and the maximum/e of the operator, where e is the Neper number. This is shown in Figure 4.4 where we find ΔL= 96 km at 100 km and ΔL = 347 km at 350 km altitude. Using ΔL we may so be rather confident in the upward continued field computed over most of the European continent, excluding a border defined by ΔL.

After that, we built a multiscale dataset by upward continuing the 5 km altitude aeromagnetic dataset at several altitudes, employing the level-to-level upward continuation (equation 22).

We will analyze this multiscale dataset by specifically designed multiscale tools, such as the multiridge method. We will illustrate such kind of analysis in Chapter 6.

In the following sections, we will begin to analyze the main field features at three distinct altitudes: 5 km, 100 km and 350 km.

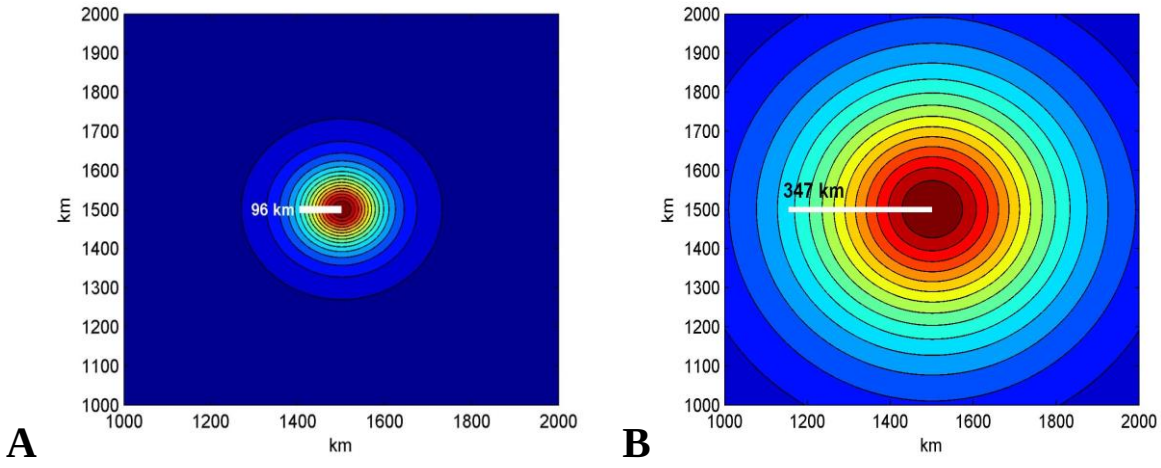

Figure 4.4 Evaluluation of the extention of the upward continuation operator ΔL at 100 km altitude (A) and 350 km altitude (B).

4.3 Low-altitude magnetic field in Europe

The magnetic field over Europe is extremely complex and defined by several anomaly patterns, correlated to the intricate structural framework of the crust and to many internal magmatic sources with strong magnetic properties.

In Figure 4.5 we show the total magnetic field map (*T*) at 5 km altitude in a Cartesian coordinate system, displayed using a Lambert conic conformal map projection with false origin at 30° and 10° and standard parallels at 43° and 62°. At low altitudes, the European magnetic field is mostly characterized of small short-wavelength anomalies, which are related to sources occurring in the middle-upper crust. The first and most important magnetic feature of the map is the visible contrast in distribution and intensity of the anomalies located above the Paleozoic and Precambrian platforms. As revealed by other geophysical studies, and as extensively described in previous sections, the TESZ is here a clear magnetic boundary, which controls the main regional trend of the magnetic field. It suggests a very sharp change in the crust's magnetic properties, in addition to geological, compositional and geothermal differences. The anomalies in the area of the TESZ define the most important magnetic anomaly zone of central Europe and are related to sources involving the whole crust. The TESZ magnetic anomaly is visible especially in Poland and Romania and it divides these countries in two opposite magnetic provinces: the *south-western area*, almost covered by magnetic lows, and the *north-eastern*, characterized by distributions of numerous magnetic highs. Actually, this anomaly trend may be extended all over the European continent, identifying the TESZ as the margin between these two opposite magnetic behaviors (Banka et al., 2002; Williamson et al., 2002).

4.3.1 Magnetic field in north-eastern Europe

The north-eastern part of Europe, including the East European Craton (EEC) and the thick crust of the Baltic shield, is mostly characterized by short-wavelength and well-defined anomalies. These magnetic anomalies are shown as linear features with SSW to NNE-trends and are interrupted to the SW by the trace of the TESZ. Such anomaly lineaments are generally correlated to the main geological structures (Wüstefeld et al., 2010) and to the shallow occurrence of the Precambrian crystalline crust (e.g. Williamson et al., 2002; Grabowska and Bojdys, 2004). In Poland, the magnetic anomalies highlight the different granitoid massifs of Pomerania, Mazovia and Dobrzyn

(Grabowska and Bojdys, 2004; McCann, 2008), which were metamorphosed in several phases and represent the oldest units of the crust. Further magnetic anomalies on the south-western part of the EEC indicate the presence of numerous faults perpendicular and parallel to the margin of the TESZ (Petecki et al., 2003). Other magnetic evidences may be found in the Polish Lithuanian terranes (Bogdanova et al., 2006), which identify the WNW–ESE trend of crustal structures, whereas the East Lithuanian belt structures may be found with a NNE trend. The magnetic anomaly pattern above the OMB (Osnitsk–Mikashevichi Igneous Belt) is constituted of round and well-defined shapes and are associated to batholiths and diorites/gabbros intrusions (Bogdanova et al., 2006), which seem to be controlled by a NE-trend of faulting zones. So, substantially, the intricate anomaly patterns of eastern Europe are the direct effects of the complex structural framework of the upper-middle Precambrian crust.

4.3.2 Magnetic field in central-western Europe

The younger and thinner crust of central-western Europe is characterized, on the other hand, by distinct magnetic anomalies, differing in shape and intensity. To the SW of the TESZ, the low-altitude anomaly map (Figure 4.5) images a complex anomaly pattern of anomalies over Germany related to the main tectonic units of the Caledonian basement to the NW, the Rheno-Hercynian zone in the central area and the Moldanubian zone and Alpine system to the SE (Gabriel et al., 2011). According to Dallmeyer et al. (1995) the origin of the magnetic anomaly distribution over central Europe may be assigned to sources occurring in the pre-Variscan basement, to Variscan and late-Variscan mafic intrusions and extrusions, or to Cenozoic volcanic activities. In northern Europe the Saxothuringian zone (ST) is interested by an extending pattern of magnetic highs whereas to the north and south intense magnetic lows characterize, respectively, the Rhenohercynian (RH) and Moldanubian (MD) zones.

A series of round magnetic anomalies may be observed above the North German basin, which are probably correlated to highly magnetized intrusions seated in the deep crust during the late-Variscan extensional episodes (Dallmayer et al., 1995). In central Germany, the most interesting feature is the magnetic high lineament with a NNE trend, correlated fairly well with the Saxothuringian zone and the Mid German Crystalline High (Gabriel et al., 2011) and almost coinciding with the Rheic suture. Spectral analysis of ST anomalies suggests that the magnetic sources are distributed in two different ranges of depth, about 2 and 11 km (Bosum and Wonik,

1991), which discriminates ST from the adjacent and weak magnetized Rhenohercynian and Moldanubian zones.

The eastern parts of Germany and the Czech Republic are characterized by the extended geologic complex of the Bohemian Massif (BM), representing the eastern side of the Variscan belt. This geological unit represents a Paleozoic chain extended from the Iberic to Bohemian complexes in Central Europe (Tomek et al., 1997) and is characterized by an anomalous crustal thickness with respect to the average thickness of the Paleozoic platform (~35 km). In the north-western sector of the Bohemian massif, the Eger Graben (EG) and its surroundings are defined by isolated magnetic anomalies probably generated by young volcanism reactivating the Saxothuringian-Moldanubian suture zone (Dallmeyer et al., 1995). To the SE, the main magnetic contributions are related to the Alpine system, due to the presence of many magnetized bodies in the upper crust. Other magnetic signatures may be retrieved above the Eger graben, where pronounced magnetic anomalies are correlated to the volcanic events of the area.

In western Europe, the main magnetic signatures are retrieved over the Brabant Massif and central France. The Brabant massif is part of the Caledonian domain located mostly above Belgium and in the southern part of the North Sea. The magnetic field of this area shows a significant difference with the close Rhenohercynian zone, suggesting a separation in two distinct units. Long wavelength component of the anomalies are correlated to deep sources of the crystalline basement, while smaller and well-defined anomalies are associated to the outcrop of the Cambro-Ordovician terranes (Bosum and Wonik, 1991).

The Paris Basin magnetic anomaly (PB) is the strongest magnetic signal of Western Europe, extending for 400 km from central France to the English Channel and characterized by a S-NE linear trend. The origin of such anomaly may be associated to amphibolites belonging to back-arc ophiolitic rocks (Cabanis and Thiéblemont, 1992).

To the south of the Alpine-Carpathians system the magnetic field is characterized by intense magnetic highs correlated to strongly magnetized rocks of the Italian, Mediterranean and Balkan territories. Magnetic anomalies over Italy reflect substantially the uplift of the magnetic basement and the complex geodynamic structures of the Apennines front belt, Adriatic-Apulian foreland areas and thinner Tyrrhenian crust. According to Speranza and Chiappini (2002), the anomalies occurring above the Apennines may be caused by a homogeneous uplift of the magnetic basement with respect to the lower depths of the surrounding foreland areas of the Adriatic Sea and Tyrrhenian margin. However, the magnetic low patterns above the Tyrrhenian Sea are associated also to the weak thickness of the crust and very high heat flow values (~200 mW/m^2) (Mongelli et al., 1989).

The anomalies of the southern Adriatic Sea may be related to the stretching of the crust with respect to the thicker continental crust of the central-northern Adriatic. Moreover, Mesozoic rifting events produced an uplift of deep magnetic rocks and, subsequently, the intrusion of magnetic material within the upper-crust (Speranza and Chiappini, 2002).

Further, strong and extended magnetic highs interest the North Adriatic Sea and the Croatia coast. The geological setting of this territory is extremely complex and dominated by the convergence between Adriatic and the European plates, started during the Late Jurassic, and by the underthrusting of Adria below Dinarides. Moreover, a similar anomaly trend may be observed also between the Adriatic coast of Italy and central Apennines, e.g., above the Conero promontory, where a strong magnetic high is probably related to the uplift of the basement or to intrusive magnetic bodies of different ages (Speranza and Chiappini, 2002). The Adriatic magnetic anomaly has not been thoroughly interpreted up to now, also due to the non-complete coverage of the area by aeromagnetic data. However, a first interpretation was carried out by Giori et al., (2007) identifying the origin of such anomaly in a progressive uplift of the magnetic basement through NE and the presence of intrasedimentary volcanic or ophiolitic bodies.

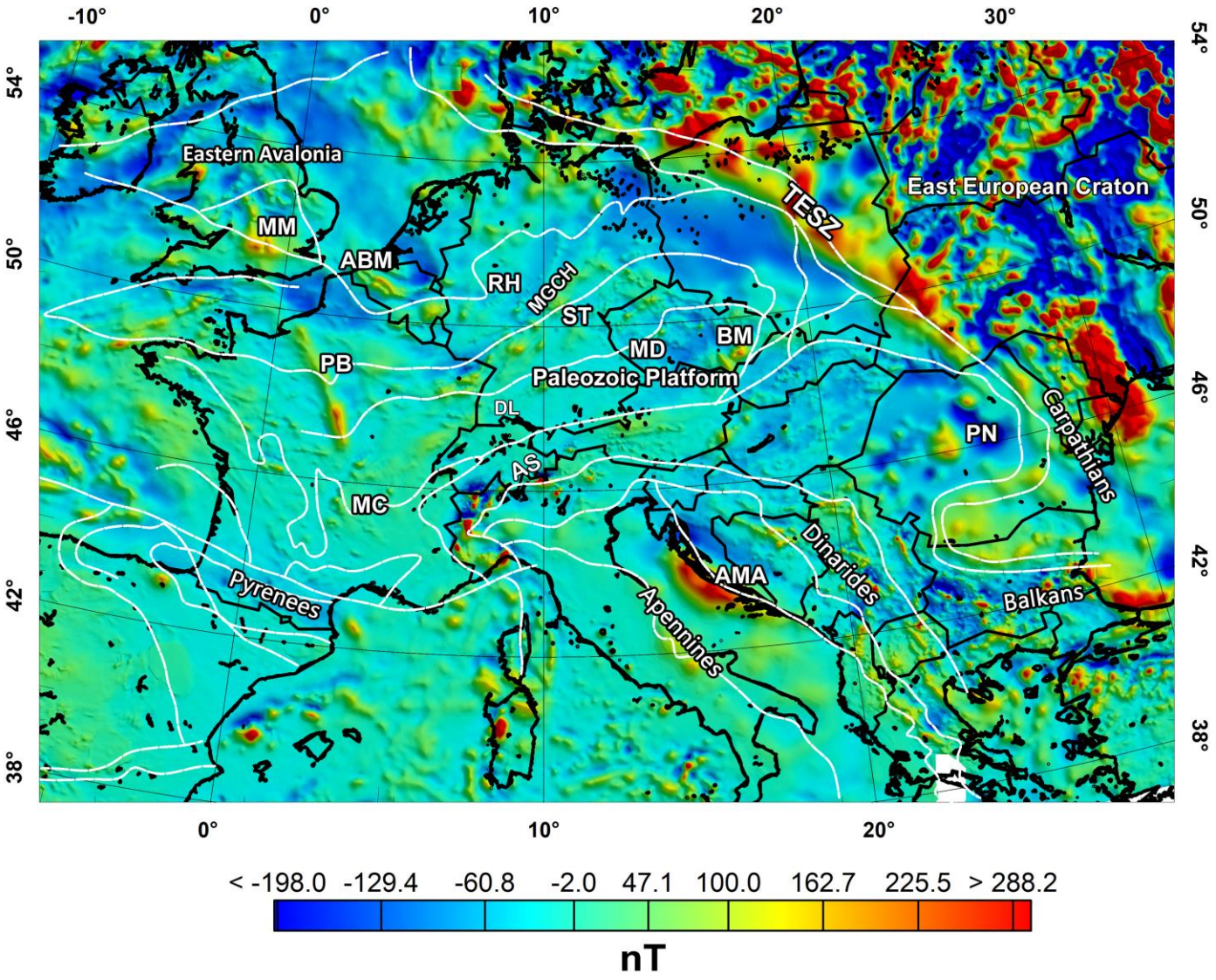

Figure 4.5 The aeromagnetic field over Europe at 5 km altitude. White lines represent the main tectonic structures (from Blundell et al., 1992). ABM: Anglo-Brabant Massif; AMA: Adriatic magnetic anomaly; AS: Alpine System; BM: Bohemian Massif; MC: Massif Central; MD: Moldanubian zone; MGCH: Mid German Crystalline High; MM: Midland Microcraton; PB: Paris Basin; PN: Pannonian basin; RH: Rhenohercynian front; ST: Saxothuringian front

4.4 Intermediate altitude magnetic field in Europe

At 100 km altitude (Figure 4.6A) the European magnetic field is considerably smooth when compared to that at 5 km. Here, the strong difference between the Precambrian and Paleozoic crusts revealed at low altitudes is even more appreciable. However, at this altitude we have to consider the border effect produced upward continuing the dataset. As we showed before, at 100 km altitude the extension of the upward continuation operator is around 96 km, so we have to exclude in our analysis the magnetic field features occurring into this extent from the grid margins.

The magnetic field above EEC is characterized by intense magnetic anomalies, whereas the Paleozoic platform to the SW is mostly covered by weaker magnetic features. In this map the TESZ margin is strongly marked by a magnetic high lineament from northern Poland down to the Carpathian-Balkan belt front of Romania and Bulgaria. Similarly, in central Europe further magnetic features almost coincide with the borders of the crustal units.

A magnetic high from eastern France to central Germany lies above the Saxothuringian units, bordered to North and South by two magnetic low trends. In other areas the anomalies have a scarce or absent correspondence with geological structures, so that their origin must be related to the properties of the magnetic basement and to the behavior of the crustal thickness. In Western Europe the magnetic effect of the Paris basin is still evident, and tends to merge with the anomalies of the Alpine front to the south. The strongest magnetic signals occur in southern Europe, where the Adriatic magnetic anomaly shows its maximum value above the Croatian coast and extends towards SW, merging with the weaker signals of the mid-Apennines (Italy). The Adriatic magnetic anomaly is strong also at high altitudes, cause it is probably related to deep sources in the lower portion of the crust. The Tyrrhenian Sea is mostly covered by patterns of weak magnetic highs with maxima values occurring above northern Sardinia (~15 nT). These magnetic features are reasonably associated to the thin crust and geologic structures formed during the extensional movements of the Tyrrhenian Sea.

All these anomalies appear as the direct effect of single magnetic sources in specific areas and surrounded by a general weak magnetic field at regional-scale. In fact, most of central Europe is covered by a wide magnetic low pattern extending from eastern France to Romania and confined to the NE by the TESZ.

These magnetic features are clearly visible also in the MF7 satellite model map calculated at the same altitude (Figure 4.6). The large-scale trends of the magnetic anomalies are mostly in agreement in the two maps, especially in the central part of Europe, where it is possible comparing the very similar magnetic low anomalies extending from eastern Germany towards central Romania. Similarly, the strong alignment of magnetic highs along the TESZ structure is very similar in extension and intensity. Moving towards south-western Europe, we may recognize a common large-scale distribution of magnetic highs covering especially the French, Tyrrhenian and Italian territories. In Western Europe, the MF7 map confirms the weak trend of relative magnetic highs corresponding to the deep roots of the crustal boundaries, even though the aeromagnetic map shows with more detail the SW-NE trending Saxothuringian unit towards central Germany and the Alps. Similarly, the magnetic effect of the Paris basin in northern France is rather evident also in the MF7 map, tending however to merge towards NW with the stronger signal of the Southern England magnetic high. To the NE of this anomaly district, a common low trend is visible in both maps over Belgium-The Netherlands and part of the North Sea. However, once again, the upward continued aeromagnetic map shows a more detailed anomaly field in this area, distinguishing two separates magnetic lows over the Anglo-Brabant massif and above The Netherlands. The higher resolution of the aeromagnetic anomalies with respect to the satellite model field is evident in southern Europe, where the Adriatic magnetic anomaly is well-defined and located over the offshore of the Croatia coast. On the contrary, the MF7 map shows a shift of such anomaly towards SW where it merges with the close magnetic high of the Conero promontory in central Italy.

In the south-western region, the magnetic field of MF7 is rather different from the aeromagnetic map. The upward continued aeromagnetic field shows a large magnetic low over the Pyrenees Mountain belt, slightly extended towards the south, whereas in the MF7, we retrieve mostly shorter and weaker magnetic N-S trending highs. These dissimilarities may be the results of the EMAG2 lower resolution data, used for filling to the gaps of the original dataset and which may produce non-reliable magnetic anomalies with the upward continuation. Otherwise, the magnetic low may represent a reliable magnetic contribution associated to the deep roots of the Pyrenean Mountains, which is not displayed in the satellite model map because of the lack in short-wavelength component of the satellite magnetic measurements. Also, we have to consider the possible border effect influencing the upward continued anomalies over Spain close to the grid margin. Nevertheless, this magnetic region will not be considered during our multiscale analysis. Further geophysical and geological studies may help to retrieve the real magnetic contribution of the deep collisional crust beneath the Pyrenean belt front.

We conclude that the upward continuation of the aeromagnetic field seems to provide a general more detailed representation of the single magnetic features at local-scale, thanks to the higher resolution of the original dataset. In the MF7 map, in fact, many singular magnetic anomalies are merged one each other, so producing a shift of the anomaly peaks and an erroneous evaluation of distinct magnetic contributions.

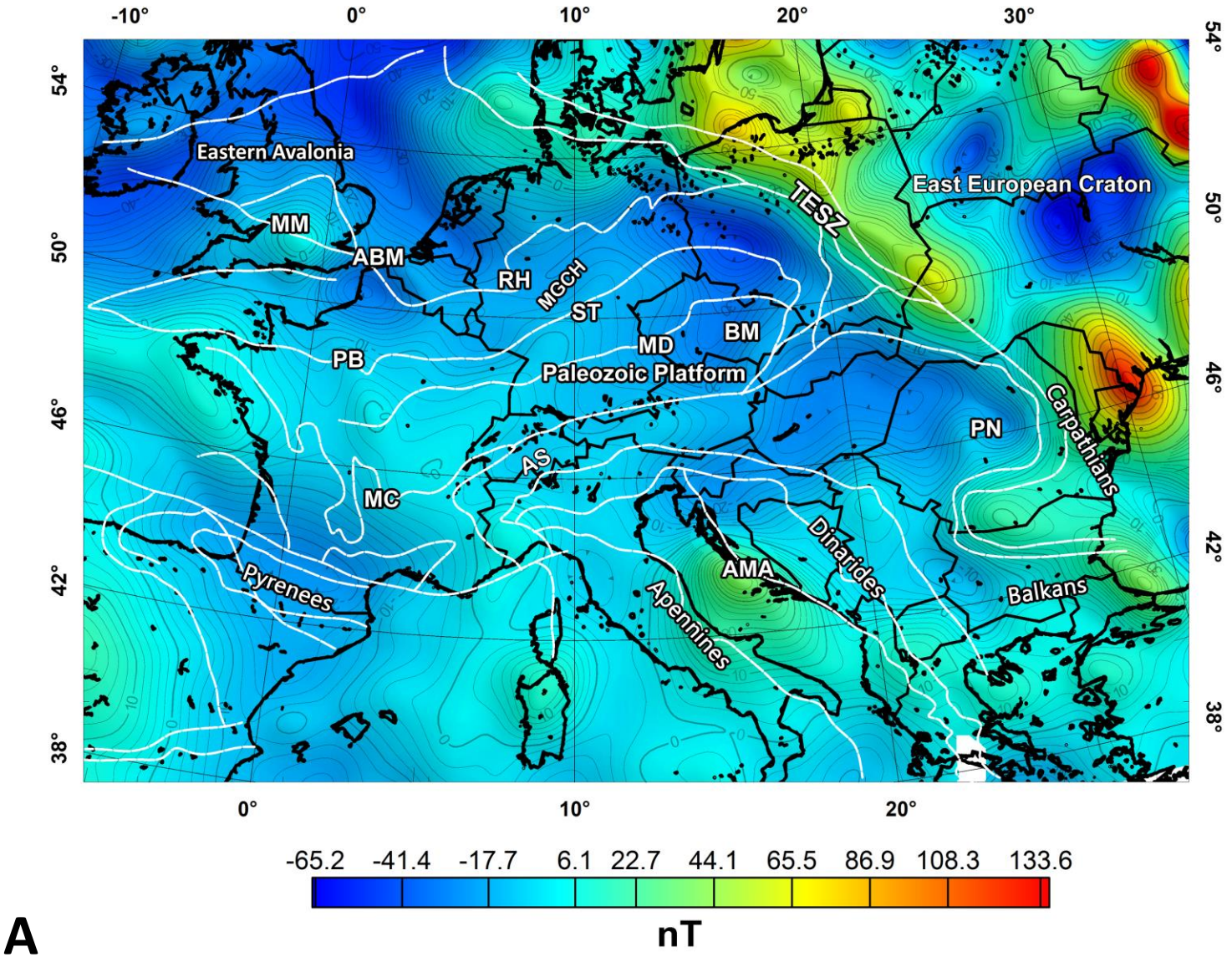
-10°
0°
10°
20°
30°
54°
50°
46°
42°
38°
Eastern Avalonia
MM
ABM
RH
MGCH
ST
MD
BM
PB
Paleozoic Platform
TESZ
East European Craton
Carpathians
PN
AS
MC
Dinarides
AMA
Balkans
Pyrenees
Apennines
-65.2
-41.4
-17.7
6.1
22.7
44.1
65.5
86.9
108.3
133.6
nT

A

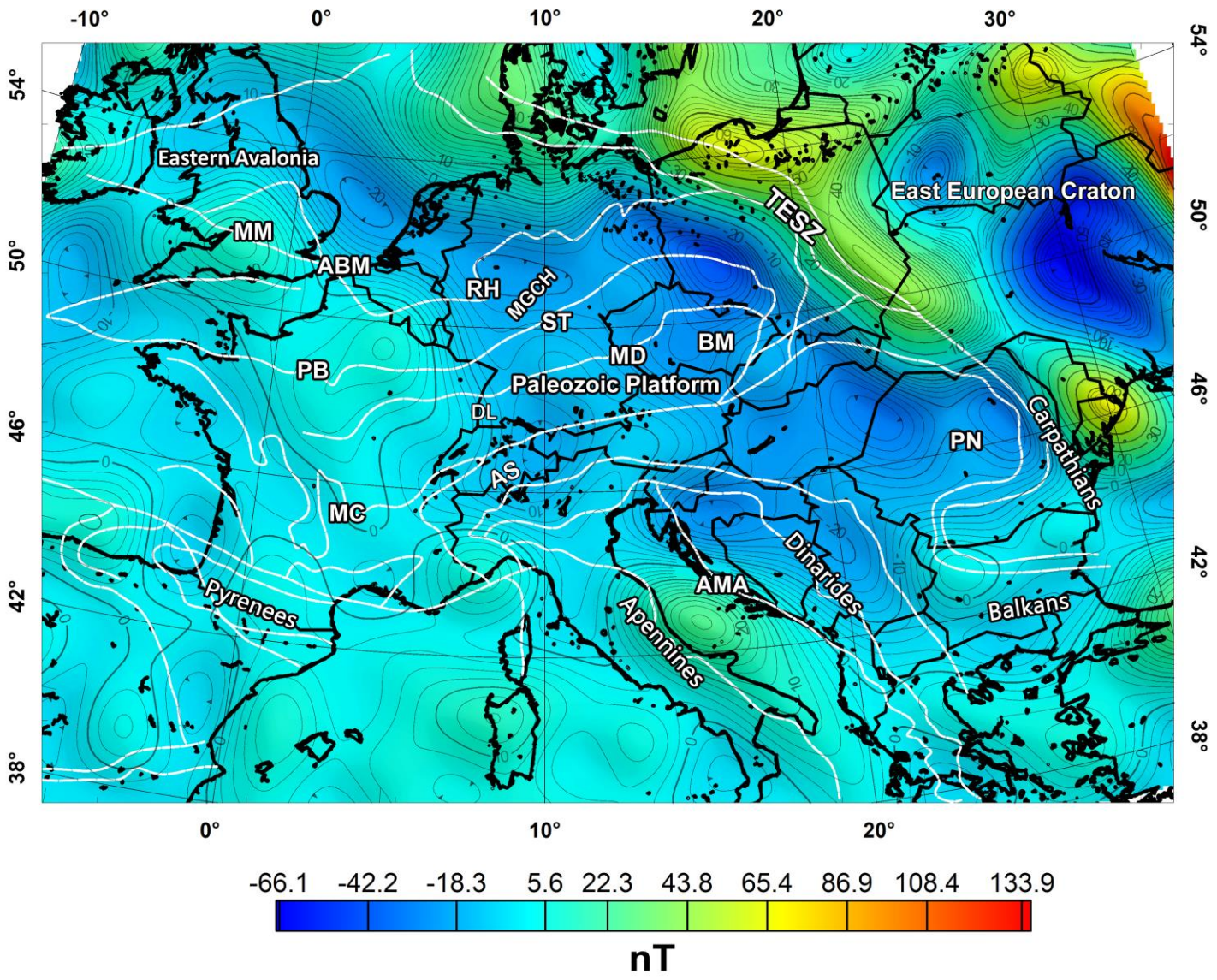
-10°
0°
10°
20°
30°
54°
50°
46°
42°
38°
Eastern Avalonia
MM
ABM
RH
MGCH
ST
TESZ
East European Craton
BM
MD
PB
Paleozoic Platform
DL
PN
Carpathians
AS
MC
Dinarides
AMA
Pyrenees
Apennines
Balkans
-66.1 -42.2 -18.3 5.6 22.3 43.8 65.4 86.9 108.4 133.9
nT

B

Figure 4.6 A) Aeromagnetic field upward continued at 100 km altitude; B) The satellite-derived MF7.

4.5 High altitude magnetic field in Europe

The character of the field does not substantially change even at higher altitudes, as shown in Figure 4.7A, where we show the magnetic field at 350 km altitude. It may be observed that, increasing the altitude, the regional-scale anomalies tend to expand and merge each other. The origin of these anomalies cannot be retrieved in local and small size crustal structures but in the average magnetic properties of whole continental units or in a merging of anomalies related to deep geological structures. In Figure 4.7, the aeromagnetic field is again compared with the map of the MF7 satellite model, which surely gives more weight in the representation of the regional magnetic trends, as it is based on high altitude satellite data. The main difference is found in the border of the map. In fact, as demonstrated in section 4.2, the extension of the upward continuation operator at 350 km altitude is around 346 km. By this, large areas in the marginal regions are visibly influenced by the border effect, e.g. above England, Tyrrhenian Sea and Eastern Europe. In particular, above Pyrenees mountains region, the strong magnetic low is even more intense with respect to the map at 100 km altitude, whereas the MF7 map shows a weak trend of value close to 0 nT. Moreover, the Pyrenees magnetic anomaly is merged to the NW with a trend of magnetic lows resulting from a huge border effect above England. Such differences may be the result of the border effect considerably enhanced in the aeromagnetic map at satellite altitudes.

So, at these elevations the MF7 model results more reliable in representing the large-scale anomalies and this map will be considered, instead of the aeromagnetic one, as it concerns the analysis of the European magnetic field at satellite altitude. Despite these differences, a good correlation between the maps may be found in the central part of Europe where the CEML is almost equivalent for both the aeromagnetic field and the MF7 model. At this altitude, the CEML has its maximum covering almost all the central-western European continent, with the peak placed above the Czech Republic.

The CEML anomaly has been analyzed many times in previous studies using high-altitude MAGSAT satellite data. Ravat et al. (1993) considered this anomaly as mainly due to the difference in crustal thickness and heat flow between the EEC and Paleozoic platforms in contact along the TESZ. Then, Taylor and Ravat (1995) carried out an alternative interpretation of the CEML, considering possible areas of dominant reverse magnetization of the Paleozoic crust: one representing the Paleozoic platform (with dip I=-50° and declination D=180°, i.e. with a reverse magnetization) and the other the Precambrian platform (with I=65° and D=0°, i.e. with a normal magnetization). The magnetization intensity was 3 A/m for both (Figure 4.8A).

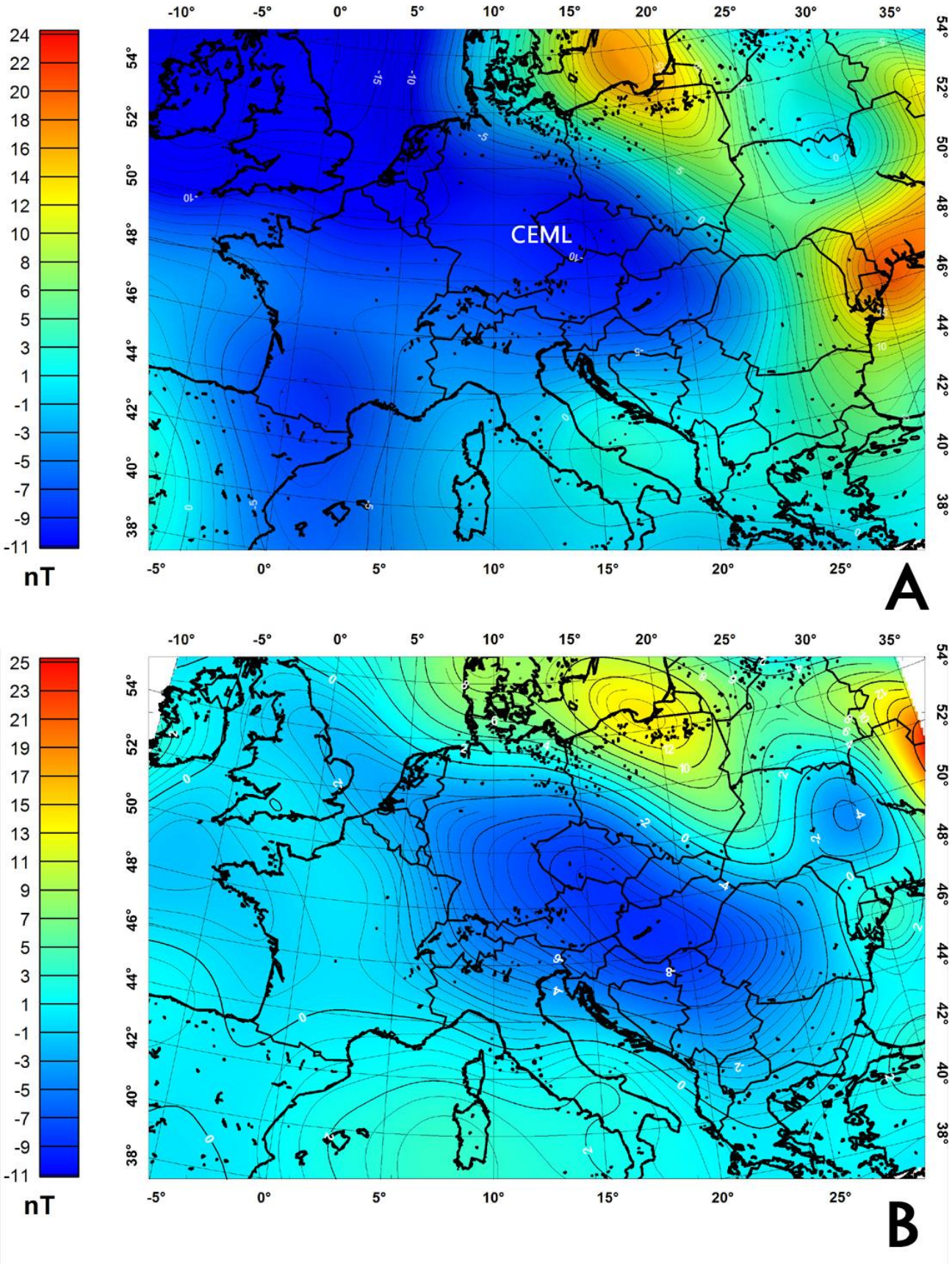

Figure 4.7 A) Map of the aeromagnetic data upward continued at 350 km; B) MF7 magnetic model map at 350 km altitude; CEML (Central European Magnetic Low).

These authors pointed out that the main origin of the CEML has to be assigned to a pattern of relatively small reversely magnetized sources in the upper-middle crust of the Paleozoic platform, whose anomaly signal merges at satellite altitude. The presence of reverse magnetization in central Europe was demonstrated by retrieving Permian quartz porphyries beneath the North German sedimentary basin, containing pyrrhotitic metasedimentary rocks having susceptibility values up to 2 x 10^{-3} cgs and *Q* ratio 100 (Henkel's, 1994). Further studies about Paleozoic metamorphic rocks indicated reversely magnetized sources in western Germany (Pucher, 1994) and studies on metasedimentary rocks pointed out a possible overprinting during the Permo-Carboniferous reverse superchron (Piper, 1987; Thominski et al., 1993). The presence of remanent magnetization in central Europe was also demonstrated by deep drillings in Germany, which pointed out also at great depths high values of the Koenigsberger ratio (*Q*) for both magnetite and pyrrhotite (e.g Pucher, 1994).

In addition to the Taylor and Ravat (1995) interpretation, Pucher and Wonik (1998) proposed an interpretation again based on the assumption of a reverse magnetization of the Paleozoic crust (Figure 4.8B). Note that in their model the CEML anomaly is entirely explained by the properties of the crust in Central Europe and it is not related to the EEC platform.

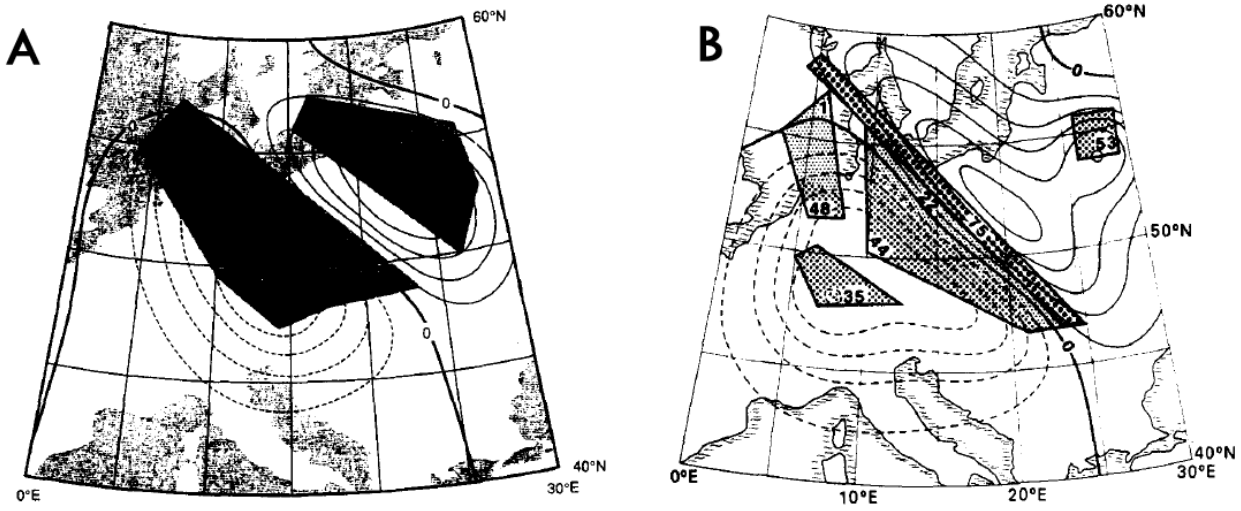

Figure 4.8 Magnetic model of the CEML of A) Taylor and Ravat (1995) and B) Pucher and Wonik (1998).

5

Analysis of the Total Gradient Modulus of the magnetic field in Europe

In this thesis, we contribute to the understanding of the main features of the magnetic field in Europe, by using a new approach based on three main aspects:

1) the use of a large scale aeromagnetic dataset, allowing a discussion and a relative comparison among the local and regional-scale magnetic anomalies with high accuracy, compared to the analysis based on only a high-altitude satellite dataset.

2) the use of techniques able to simplify the interpretation of the magnetic sources by reducing or suppressing the dipolar shape of the magnetic anomalies.

3) a multiscale approach for analyzing the scaling properties of the magnetic field in a multiscale set of data;

The first step in the interpretation of the main magnetic field features in Europe was carried out by computing the Total Gradient ($|\nabla T|$**)** of the aeromagnetic field at each altitude of observation. The use of this technique allows retrieving the contribution of sources generating local and regional scale anomalies and identifying the main magnetic properties of the European crust. By this, the CEML was interpreted by comparing the previous models with the $|\nabla T|$ model of deep sources distribution.

The typical dipolar shape of magnetic anomalies may sometimes complicate the interpretation of the magnetic field. The dipolar effect, due to the non-vertical directions of both the total magnetization and the inducing field, may be substantially removed by computing the total gradient maps of the total magnetic intensity. The resulting total gradient anomalies have the advantage of being spatially located directly over the source bodies. The removal of dipolar effects may also be

obtained by other methods, such as the reduction to the pole and the "pseudogravimetric" transformation (Baranov, 1957). These transformations, however, despite of their popularity, need the source total magnetization direction to be specified, which is generally unknown and is often assumed as being along the geomagnetic field inducing direction. For large regions of Europe such an assumption could be obviously incorrect.

Total gradient $|\nabla T|$ (Nabighian, 1972) is defined as:

$$|\nabla T| = \sqrt{\left(\frac{\partial T}{\partial x}\right)^2 + \left(\frac{\partial T}{\partial y}\right)^2 + \left(\frac{\partial T}{\partial z}\right)^2} \tag{23}$$

where $\partial T/\partial x$, $\partial T/\partial y$ and $\partial T/\partial z$ are the derivatives of the total magnetic field (T) with respect to the directions x, y, and z. The use of the total gradient intensity (also called 'modulus of the analytic signal') has been of great utility to interpret potential field data, helping to localize in a very simple way the edges of the sources and their horizontal position without specifying a priori information about source parameters (e.g. Roest, 1992; MacLeod, 1993). The most important property of this method is the reduction or suppression of the dipolar effects of the magnetic anomalies, similarly to the Reduction To the Pole (RTP) and the "pseudo-gravimetric" transformation (Baranov, 1957).

However, the advantage of the total gradient technique is to have an almost complete independence from the variation of magnetic inclination (I) and declination (D) (Nabighian, 1972) in the case of 2D fields (profiles). In the 3D case such independence has not been proven mathematically, but we can assume that it is only weakly dependent on the directions of T (Haney et al., 2003). Salem et al., (2002) pointed out that, in the 3D case, a variation in the horizontal location of the total gradient amplitudes may be observed by changing the direction of magnetization, with a maximum shift for magnetic inclination of 30°. Moreover, we know that the total gradient is based on the directional derivative of the potential field anomaly, so we must take care of the possible enhancement of noise, such as gridding artifact, errors like track corrugations and so on.

Further useful information about the source parameters may come from performing the Euler deconvolution of total gradient data, by which we may at the same time delineate with high detail the geological structures and estimate the source depth position (e.g., Keating and Pilkington, 2004). In figure 5.1 we show a simple example for a spherical source placed at x=50 km and y= 50 km. In the total gradient map, the bipolarity of the magnetic anomaly practically disappears and the

maximum of the amplitude is located above the source. In this case, a direction of magnetization typical at the European latitude was chosen for the source (I=60°, D=0° for both the induced and magnetization fields) and the N-S profile shows only a slight deviation between the exact source position and the magnetic anomaly high (Figure 5. 1). Now it is important to study the behavior of the total gradient in the case of strong remanent magnetization.

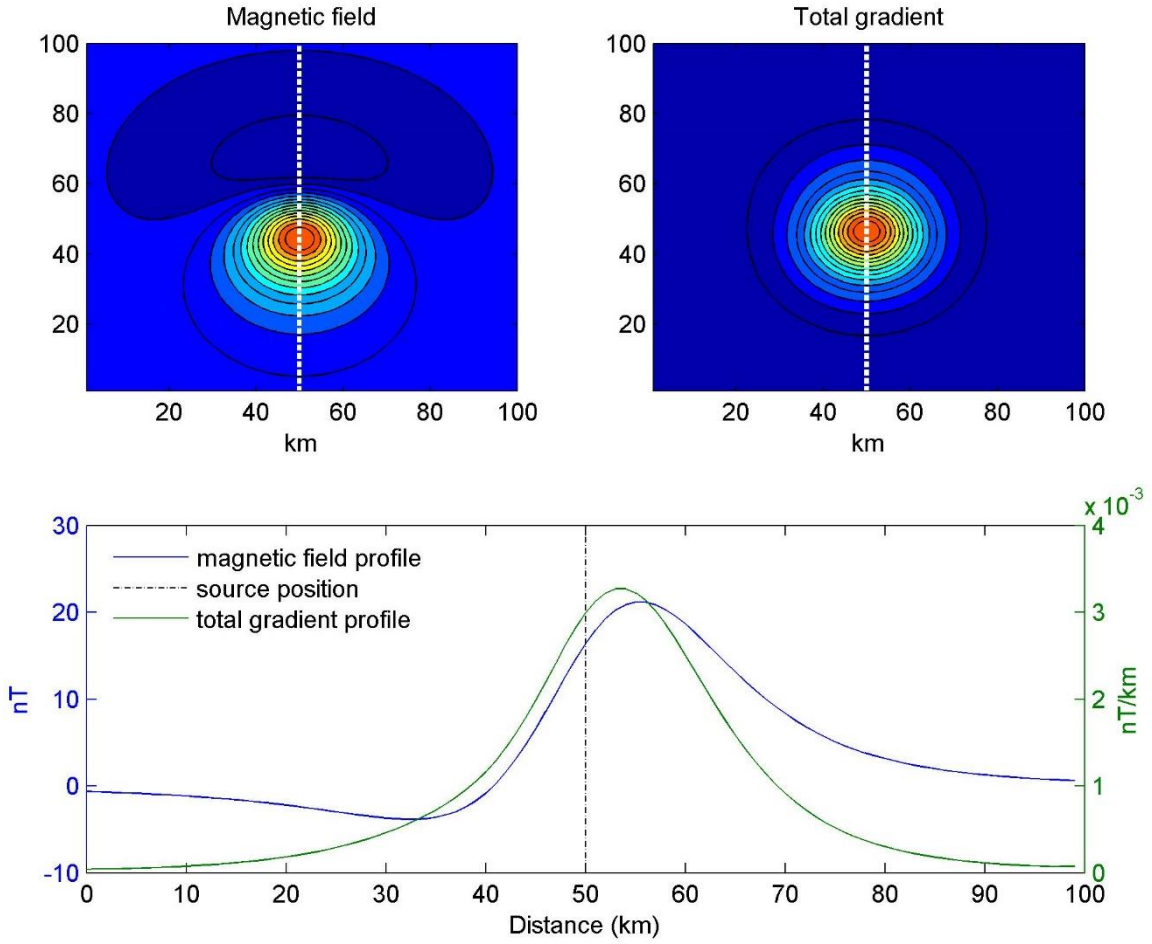

Figure 5. 1 Synthetic model of a spherical source (I=60°, D=0°) at x=50 km, y=50 km. T map (top left), $|\nabla T|$ map (top right) and comparison between T and $|\nabla T|$ profile (down).

5.1 Interpretation of total gradient data of reversely magnetized sources

In previous studies, several cases of different source distribution were modeled in order to verify the reliability of $|\nabla T|$ in complex magnetic environments (e.g. Roest et al., 1992; Roest and Pilkington, 1993; Salem et al., 2002; Shearer and Li, 2004). In this section we will focus our attention to the analysis of the total gradient results in case of sources with a strong remanent component of magnetization. This is because, as described in the previous chapter, this magnetic feature represents one of the main origin of regional-scale magnetic anomalies. Generally, the presence of reversely magnetized sources may represent a hard challenge to the inversion and to the quantitative interpretation of magnetic data (Shearer and Li, 2004). For this reason, in the last decades, some studies allowed defining useful methodologies and approaches able to retrieve the parameters of sources with strong remanent magnetization.

As described in the previous section, the total gradient is only weakly dependent on the direction of magnetization, so representing an advantageous method in detecting sources with different magnetic properties. In particular, Roest and Pilkington (1993) stressed this issue by comparing the total gradient and the pseudo-gravity horizontal derivative performed on synthetic models and real data of reversely magnetized sources. These authors pointed out the possibility of calculating the remanent magnetization parameters by simply observing the position of the total gradient maxima with respect to the magnetic field anomaly and horizontal derivative. This approach allows estimating and locating the sources with remanent magnetization within a complex geological environment.

In Figure 5.2 we consider a reverse magnetization for the same spherical source model of the last section. The parameters used for the total magnetization are D=30° and I= -10°, whereas the ambient magnetic field is calculated using I=60° and D=0°. Similarly to Figure 5.1, the total gradient map shows maximum amplitude located above the source with a slight shift towards the direction of the total magnetization. It may be observed that the $|\nabla T|$ maximum is fairly good coincident with the source position, but, with respect to the previous example, here the peak of $|\nabla T|$ is almost correspondent with the peak of the magnetic anomaly low. From these results we may point out easily the horizontal source location, despite the different directions of remanent and induced magnetization.

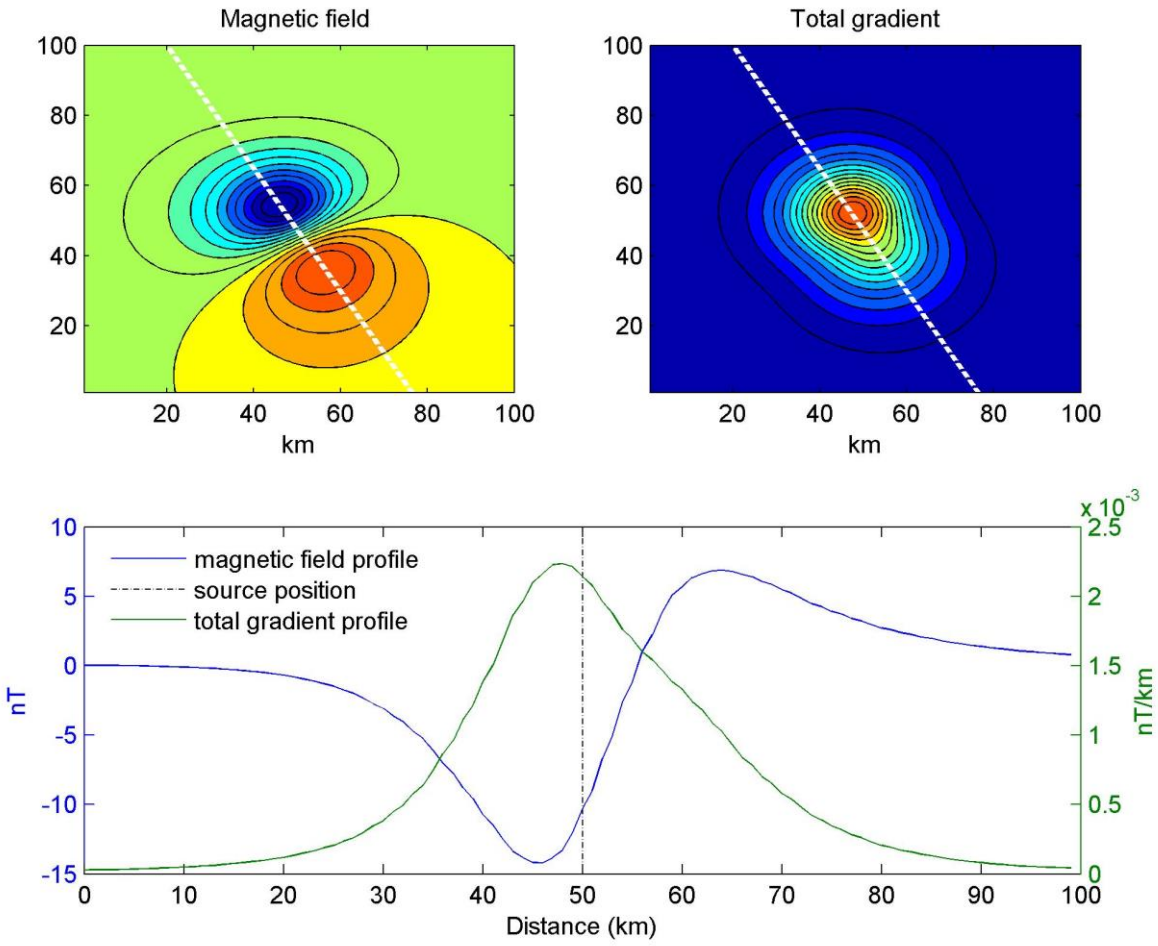

Figure 5. 2 Synthetic model of a spherical source reversely magnetized (*I*=-10°, *D*=30°) at x=50 km, y=50 km. *T* map (top left), $|\nabla T|$ map (top right) and comparison between *T* and $|\nabla T|$ profile (down).

Let now consider a more complex case in which both normally and reversely magnetized sources are considered in the same model, close to each other. The model is composed of three magnetic bodies: **B1** and **B2**, with normal magnetization (*I*= 65°, *D*=3°), and **B3**, reversely magnetized with *I*=-15° and *D*=230°. These parameters where chosen according to the results of paleomagnetic analysis in central Europe carried out by Pucher (1994) and used in the interpretation of the high altitude magnetic low (CEML) (Pucher and Wonik, 1998). In Figure 5.3A we show the magnetic field of this model. From this map we may note that B1 and B2 are well represented by two dipolar anomalies with the peaks of the magnetic low and high to the NE and SW, respectively.

The body B3, instead, is not well recognizable because its magnetic effect is hidden by the anomalies of the surrounding sources. The sole trace of the reversely magnetized source is the slight prolongation of the magnetic high of B2 towards the position of B3 and a weak increase in intensity of the magnetic low of B1 to the SW. We conclude that we may detect the reverse magnetization in such complex magnetic setting by only observing the magnetic field map.

In the following we will show how overcoming this difficulty by using the total gradient technique. The total gradient is shown in Figure 5.3B. In this map, as expected, the dipolar shape of the magnetic anomalies disappears and the maxima locate with high detail all over the sources generating the magnetic anomalies in Figure 5.3A. The reverse magnetized source B3 is here well distinguished from the other bodies regardless their direction of magnetization. For the sake of clarity, while for the magnetic field representation the lowest values ('blue' color) stand for the lows of the dipolar anomalies, in the total gradient figure they denote a non-magnetized zone. So, the total gradient maxima amplitudes are a direct proof of the presence of magnetized sources and vice-versa. These results allow considering the study of the total gradient map as a method to determine the magnetization, and so the presence of magnetic sources, in the area of analysis, at either local or regional scale. Moreover, being the total gradient very weakly dependent on the directions of the magnetic field, it allows retrieving with high detail also the sources characterized of strong remanent magnetization.

In the next section this approach will be applied to the interpretation of the magnetic anomalies over Europe. The total gradient maps are calculated at the same altitudes of the multiscale dataset in order to identify the main source contributions occurring at different crustal depth. As we will see in the next section, the total gradient results allow retrieving the origin of the regional-scale anomalies over central Europe by which it is possible to give a further suitable contribution to the interpretation of the high altitude magnetic low (CEML).

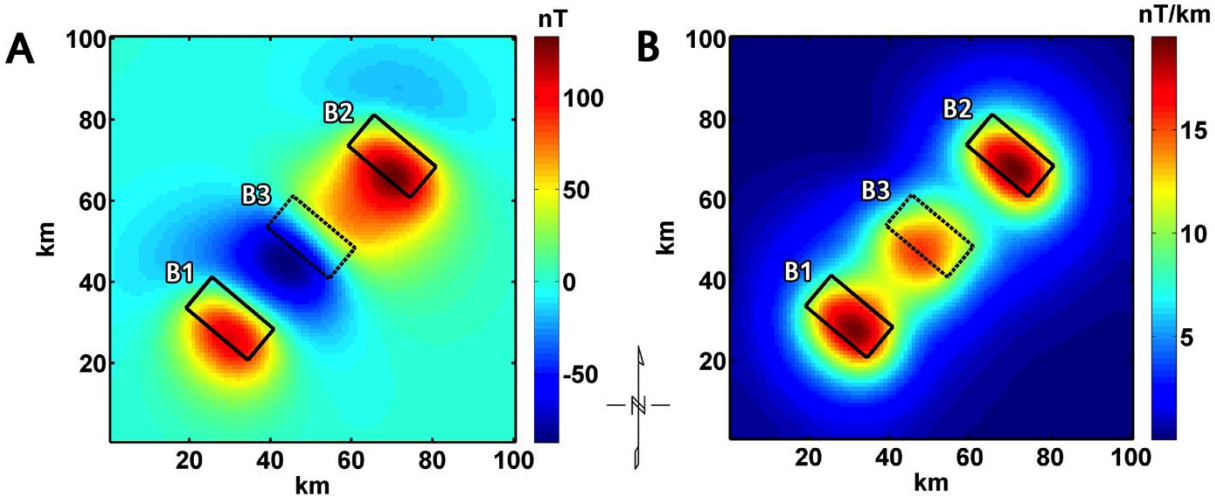

Figure 5. 3 Multi-source model with B1 and B2 normaly magnetized and B3 reversely magnetized. A) *T* map B) $|\nabla T|$ map.

5.2 Total gradient anomalies at low altitudes

In Figure 5.4 we present the shaded relief map of the total gradient at 5 km of altitude, where we can mainly see the contribution of shallow structures and high-magnetized crustal intrusions, which generate short-wavelength patterns of anomalies. The total gradient anomalies are represented in the map with a linear color distribution in order to give the correct weight to all the main magnetic features over the European continent. For this reason, the values > 15 nT/km may produce saturation in some areas and a merge of strong total gradient anomalies, such as above the north-eastern Europe, western Alps and Balkans. However, the purpose of this study is to analyze the most important magnetic structures at regional-scale over Europe, neglecting the sparse distribution of local anomalies, not giving a significant contribution to the continental representation of the magnetic field.

At large-scale, the most prominent feature in the map is a clear difference in magnetic properties of the Precambrian crust (EEC) with respect to the Paleozoic platform (PP). This is not surprising, since the same magnetic features have been observed in the low-altitude magnetic field map. The total gradient map above the EEC, indeed, confirms the irregular and intense distribution of short-wavelength patterns suggesting the presence of strong magnetized sources characterizing most of the upper crust. The total gradient amplitudes above the Precambrian crust of Poland and

eastern Romania are smooth due to a lower resolution of the dataset with respect to adjacent countries. Despite these differences, the main trend of $|\nabla T|$ in such territories agrees with the general total gradient representation above the EEC. These anomalies express tectonic features and intrusive bodies within the Precambrian basement that is covered by 1–2 km of sediments (Karaczun et al., 1978; Petecki et al., 2003). However, the $|\nabla T|$ anomalies change considerably moving towards SW. As already revealed by the magnetic field maps, the TESZ marks a sharp variation in magnetic intensity and source distribution. The $|\nabla T|$ results in central-western Europe show an opposite magnetic environment with respect to the EEC. Some well-defined and isolated anomalies are distributed over the Paleozoic platform within a general low magnetization area. Such low magnetization is revealed by the extended low intensities of the anomalies and, in particular, by the occurrence of large no magnetization areas (blue colored).

The main magnetic features in central Europe are arranged in readily apparent alignments above the principal magnetic structures as already described previously (Figure 5.4). Comparing the T map with the $|\nabla T|$ the main remarks are:

- Diffuse total gradient maxima coincide with the TESZ boundary, which interrupts the trend of the magnetic anomalies above the EEC. The relationship between such structure and the total gradient amplitudes are clearly represented in the map, where the trace of the TESZ is highlighted from the North Sea down to the Carpathians and northern Balkan.

- In central Variscan Europe, groups of $|\nabla T|$ maxima underline mainly the boundaries between crustal units and the presence of highly-magnetized magmatic rocks. The Saxothuringian zone is characterized by diffuse short-wavelength anomalies SW-NE trending, which strongly differs from the lower magnetization of the adjacent Rhenohercynian zone to the north and Moldanubian to the south. These $|\nabla T|$ anomalies define with high detail the position of the magnetic sources forming the Mid German Crystalline Rise (MGCR). Despite the common interpretation of the MGCR as a magmatic arc, formed above a south-dipping subduction zone in Upper Devonian and Carboniferous times, Oncken (1997) reinterpreted this geological structure proposing a more compound model characterized by two different crusts involved in geodynamic events during Carboniferous. However, the total gradient anomalies are well related to the presence of several granitoids and metamorphic rocks occurring within the whole Saxothuringian unit.

- The Rhenohercynian unit is lacking in significant magnetic features except for the total gradient maxima related to the young magmatic regions (Gabriel et al., 2011), where reverse magnetic anomalies are found; for instance the Soest magnetic anomalies, which are reversely polarized. Total gradient maxima in northern Europe are associated to the Caledonian basement and to deep relicts of the Scandinavian crust, formed during the collision between Baltica and Avalonia.

- The Moldanubian Zone, similarly to the Rhenohercynian, is characterized by a relatively weak magnetization. In the northern part, some weak pattern of maxima seems associated with the tectonic margin of the Saxothuringian zone. The main magnetic evidence occurs southwards at the margin coinciding with the Donau Line, representing a prolongation of the northern part of the Massif Central (Bosum and Wonik, 1991). These magnetic anomalies are probably associated with basic and ultrabasic rocks, which could be deep (Franke, 1989).

- In the north-western part of Europe (Eastern Avalonia) intense magnetic maxima occur above the Midland Microcraton (MM) in Southern England and continue down to the North Sea and Brabant Massif (BM), showing a very different magnetic environment with respect to the close Rhenohercynian Zone to the East. Strong $|\nabla T|$ anomalies of MM are mainly related to the outcrop of the Neoproterozoic basement and to local Carboniferous intrusions (Banka et al., 2002; Pharaoh and Gibbson, 1994). In Eastern England patterns of small magnetic anomalies are associated with calcalkaline magmatic rocks and to the southern metasedimentary rocks of the Brabant Massif in northern Belgium (Pharaoh et al., 1993; De Vos et al., 1993). Previous magnetic studies of the BM pointed out that this region might be considered as a 'microplate', highly different from the adjacent territories (Bosum and Wonik, 1991). Most of the total gradient anomalies are correlated with the outcropping Cambro-Ordovician basement, the crystalline basement and, in the eastern side, with young magmatic structures related to recent tectonic movements.

- The strong maximum of the Paris basin is one of the main magnetic features of the Armorican region, extending for more than 440 km from the English Channel to central France. Its interpretation is still not completely solved, but the origin may be attributed to

ophiolitic fragments (Millon, 1992) carried up to the shallow crust by Late Variscan faulting episodes (Autran et al., 1992).

- The Bohemian Massif region represents the main contribution of the Moldanubian zone in the western part of the Armorican terranes and the sources are well represented in the total gradient map by a pattern of maxima of short and long-wavelength covering the Czech Republic. Local magnetic anomalies are mainly associated to Miocene-Pleisotcene volcanic events, while the origin of regional-scale anomalies is attributed to the magnetized rocks of the deep basement (Švancara and Gnojek, 2000). The southeastern edge of the Saxothuringian zone is highlighted by a pattern of maxima related to deep structures and to Volcanoplutonic magmatic activity associated to the Variscan orogeny (Dallmeyer et al., 1995).
- In southern Europe, an extended pattern of strong maxima occurs above the Alpine system, associated with ophiolitic rocks and with a broad distortion of the lower crust; magnetic anomalies occurs also above the continental margins of the Tyrrhenian Sea, mainly correlated to crustal fractures of the deep geodynamic events (Rehault et al., 1987). According to Rota and Fichera (1987) the origin of the anomalies above the Apennines orogeny belt is due to the Paleozoic outcropping of the crystalline basement consisting in lower crustal granulites. In the Northern Adriatic Sea a wide and strong total gradient maximum is associated with the intense magnetic high described previously in the magnetic field map. Its origin is still not completely solved but a good correlation may be observed with the Dinarides belt front and with the occurrence of intrasedimentary batholitic formations (Speranza and Chiappini, 2002; Giori et al, 2007).
- In Eastern Europe, the most intense $|\nabla T|$ anomalies are displayed above the Balkan region and the Carpathians mountain chain. Most of the $|\nabla T|$ maxima are distributed in Bulgaria, where two main magnetic provinces are distinguished: the southern Bulgaria, interested by a pattern of small anomalies following the trend of the Balkan Mountains belt, and the northern foreland characterized by smoothed total gradient amplitudes. The short-wavelength anomalies are mainly associated with magmatic products formed during several volcanic events of different ages and characterizing most of the Balkan area, whereas the more smoothed amplitudes to the North are related to the magnetic basement beneath the Bulgarian foreland (Trifonova et al., 2009). Moving to the North, further $|\nabla T|$ maxima are retrieved above the Romanian region where the most prominent geological structure is the

Pannonian basin, a back arc basin formed during the complex evolution of the Carpathians-Alpine system (Horváth, 1993). The main magnetic features in this area are mostly connected to the Neogene-Quaternary volcanism and to the presence of pre-Neogene basic volcanic intrusions (Boccaletti et al., 1976). However, further interpretation of the regional magnetic trends above the Pannonian basin was carried out by Kis et al. (2011). The authors propose that xenolith and peridotite rocks formed in the deep crust-upper mantle and carried up into the shallow crust with strong remanent magnetization are the main source of reversely magnetized anomalies. Moreover, remanent magnetization was studied also in Slovakia and indentified as the main characteristic of several high-magnetization sources associated to Neogene-Quaternary volcanic rocks (Kubeš et al., 2010). These magnetic features occur in the central area of Slovakia and are well recognizable in the total gradient map by a diffuse patter of maxima SW-NE trending.

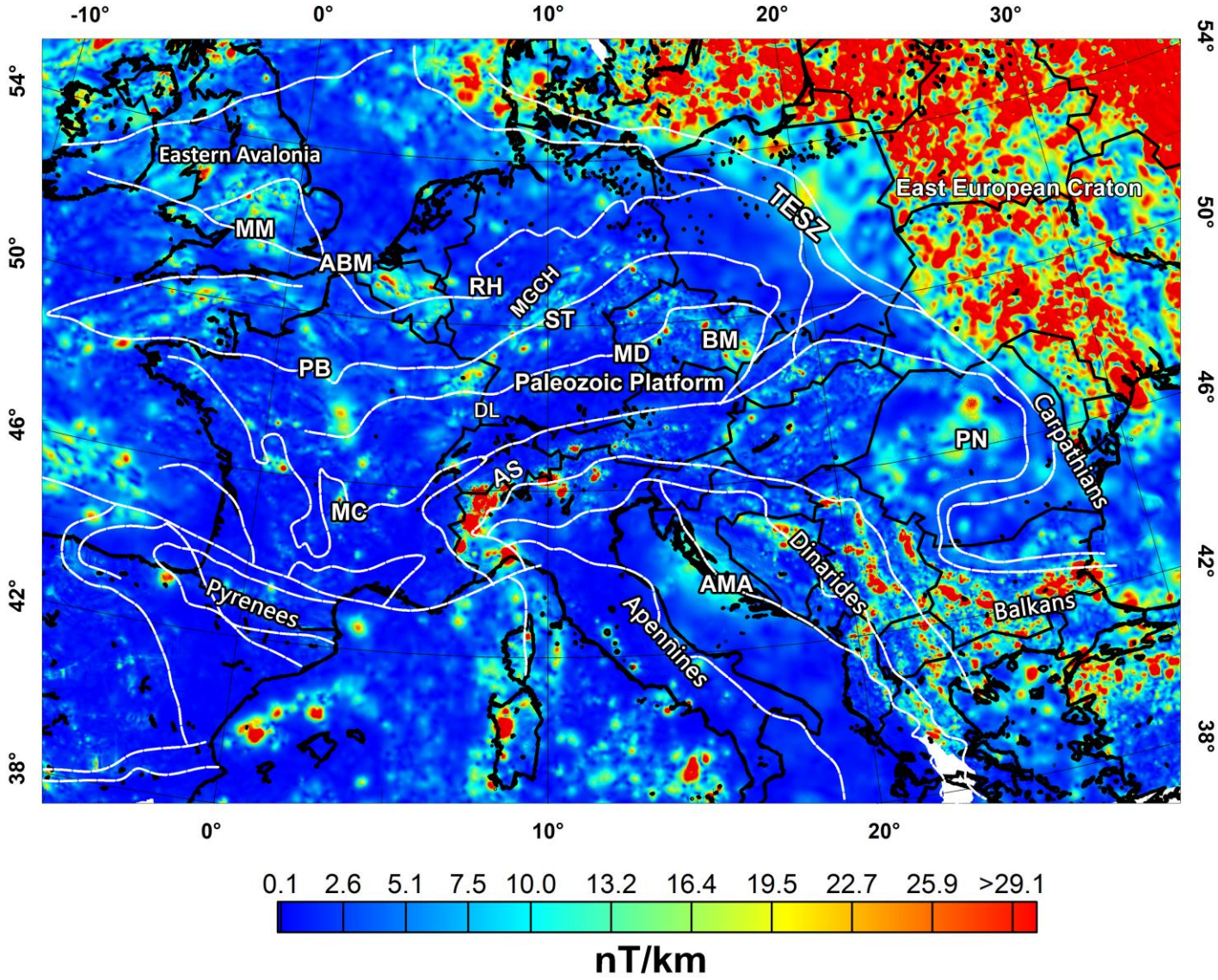

Figure 5. 4 Total gradient map of the aeromagnetic data at 5 km altitude. For abbreviations see Figure 4.5.

5.3 Total gradient anomalies at 100 km altitude

At 100 km altitude, the total gradient map is significantly different from Figure 5.5 and defined mainly by long-wavelength anomalies. The analysis of the signal maxima makes possible the identification of the major geological features of the continental Europe. Comparing the total gradient anomalies with the tectonic boundaries we may still observe fairly good correlations, in particular above the Carpathians and the TESZ region, since these geological boundaries involve the whole crust down to the Moho depth, as revealed by seismic surveys interpretations (e.g. Grad et al., 2009; Guterch and Grad, 2006). In some regions, many total gradient anomalies tend to join and it is difficult to discriminate between the local properties of specific magnetic areas. So, the interpretation of such anomalies must be carefully controlled by combining the results of further geophysical and petrological analyses. However, at high altitudes the total gradient anomalies are very useful thanks to their weak dependence on the direction of magnetization and provide a reliable representation of the large-scale magnetic properties of the crust.

The goal of this section is the distribution of the main magnetic sources in central Europe, which may be responsible for the high altitude magnetic low and for the apparent reverse polarization of such anomaly. The total gradient map at 100 km altitude is highly useful in this sense and the origin of the CEML may be identified by studying the location of the $|\nabla T|$ maxima in the areas surrounding the TESZ. A crucial step is comparing them with the magnetic anomalies in the *T* map at the same altitude. In particular, the total gradient is used here as a method to determine where remanent magnetization is actually contributing to the high altitude magnetic field, in comparison with what was suggested by previous studies.

The regional magnetic environment observed above the Precambrian crust (EEC), defined by the large patterns of total gradient maxima, is substantially opposite with respect to the anomaly field retrieved to the SW of TESZ. As already extensively described, the young crust of the Paleozoic platforms differs from the EEC for structural and physical properties, and such dissimilarities are clearly reflected in the representation of the magnetic anomalies over the European continent.

The strongest total gradient values, as expected, are concentrated above the EEC, suggesting the high magnetization of the whole Precambrian crust. Regardless of the anomalies displayed near the map margins, visibly influenced by upward continuation border effects, the total gradient maxima above the EEC are mostly located along the margins of the craton, whose origin is probably associated with the igneous mafic activity occurred along the margin with the Paleozoic orogenic belts (Bogdanova et al., 1996). Moreover, the outlines of the major $|\nabla T|$ maxima are in

good agreement with the edges of the different units composing the EEC. In the map we may recognize only the western territories of the EEC subdivided into the Fennoscandia unit, to the North, and the Sarmatia, to the South. The large-scale magnetic anomalies above the southern Fennoscandia, also observed at satellite altitude, were attributed to the local high crustal temperature and to variation in thickness (Hahn and Wonik, 1990; Pashkevich et al., 1993), while the total gradient amplitudes over Sarmatia suggest a more magnetized lithosphere and the increase of the Moho depth down to 60 km. Moreover, previous MAGSAT investigations over Sarmatia pointed out that further high-magnetized sources may occur also in the lower-crust and upper mantle (Pashkevich et al., 1993). In the eastern part of the map some strong $|\nabla T|$ maxima are probably correlated to the high-magnetic rocks of the Devonian Dniepr-Donets Aulacogen produced by Paleozoic deep mafic magmatism (Pashkevich et al., 1993).

The main characteristic in central Europe is the absence of significant total gradient anomalies except for the strong anomaly of the Adriatic Sea. Moreover, the patterns of small total gradient anomalies, representing the main small-scale magnetic features in different European regions (Figure 5.4), disappear at high altitude and are replaced by extended areas of blue color areas, suggesting that the middle-lower crust is characterized by a very low or absent magnetization, as demonstrated in the synthetic model in Figure 5.3. This particular behavior is discovered above most of central Europe region. These results are in good agreement with the representation of the magnetization distribution in Europe carried out by Nolte at al. (1992). Moreover, most of the total gradient anomalies are located to the NE, especially above the Poland region, and the maxima values occur exactly along the trace of the TESZ. So, as discussed before, this geological structure represents a visible boundary separating the scarcely magnetized crust of central Europe to the SW from the EEC.

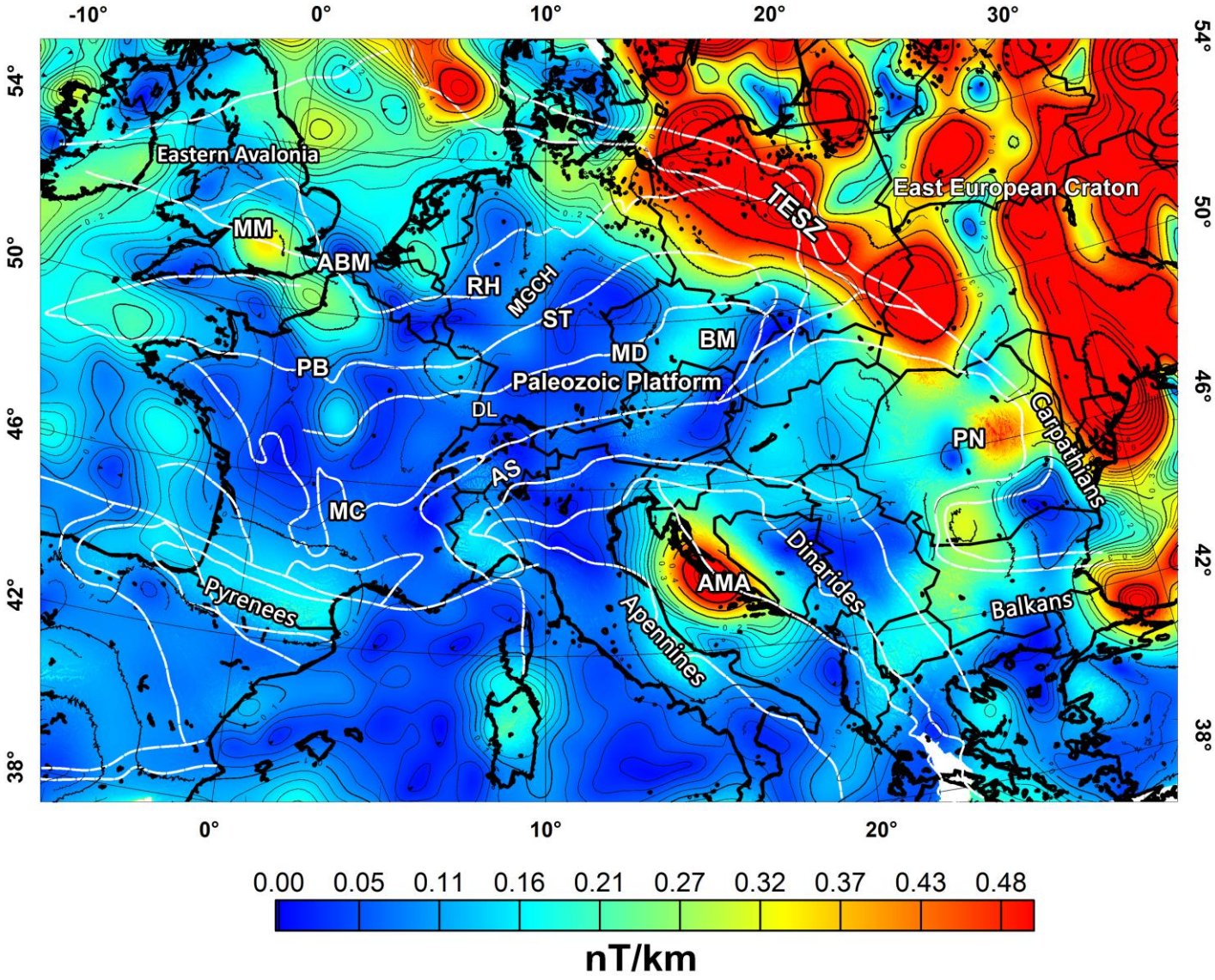

Figure 5. 5 Total gradient map of Europe at 100 km altitude.

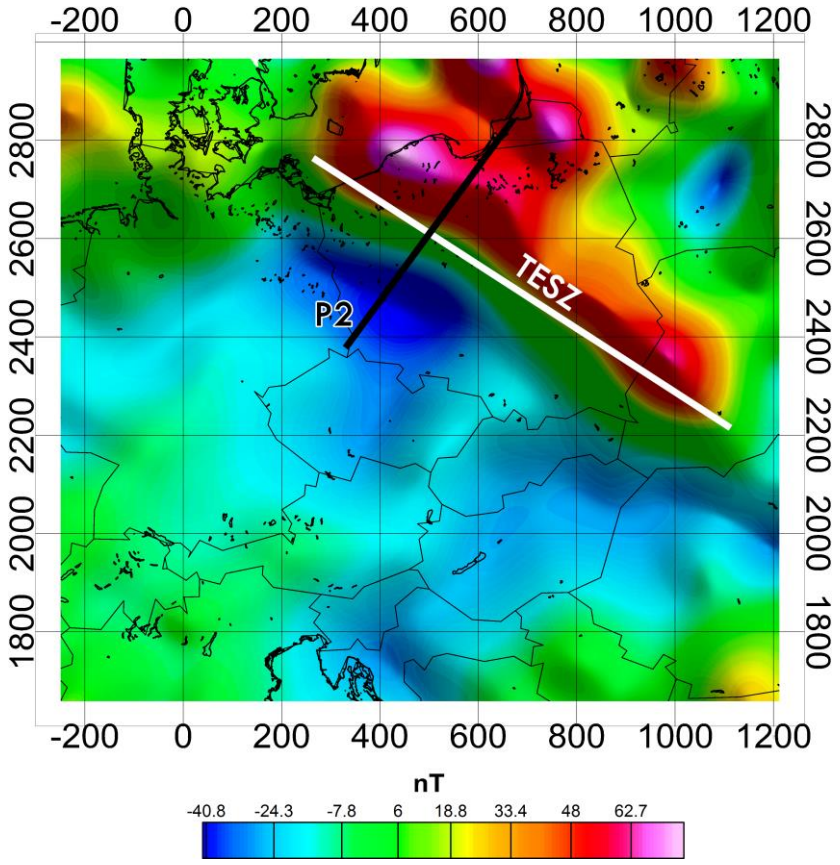

Figure 5.6 Trace of the profile P2 considered in to model of the TESZ area.

We identify such difference in the crustal magnetization as the main origin of the CEML, rather than a reversed polarization origin. To show that, we interpret the profile P2 at 100 km altitude (shown in Figure 5.6) in the TESZ area. Our 2D model (Figure 5.7) consists of two magnetic bodies in contact, simulating the Paleozoic Platform to the left (M1) and the East European Craton to the right (M2). The TESZ was estimated to be a 2-D structure with a strike length of 500 km and a 600 km along-profile length.

This model is certainly a simplification of the real geological setting of the crust, but it is useful to explain the high-altitude magnetic anomaly above the TESZ, as due to the juxtaposition of two platforms differing in thickness and magnetic properties. Even though susceptibility is expected to vary within the crust, being dependent on temperature and rock composition (Adnan et al., 1992; Hunt et al., 1995), we assumed that the main magnetic mineral is magnetite and average values of $10x10^{-3}$ (SI units) and $50x10^{-3}$ (SI units) susceptibility for M1 and M2, respectively. These values are consistent with magnetic susceptibility measurements of the crystalline basement, carried out in Poland by the Polish Geophysical Exploration Company (PPG), and compiled by Dabrowski (1971) and Grabowska et al. (2011). Due to the simplified model, more detailed studies (e.g., Williamson

et al., 2002; Grabowska and Bojdys, 2001; Grabowska et al., 2011), such as those regarding the highly-magnetized intrusion of the Lublin Graben, have not been take into account here.

Note also that the two main geological environments, M1 and M2, differ not only for crustal magnetization, but also for thickness and geothermal properties. As regarding the thickness, studies associating the main magnetic properties of this area to the crystalline basement (e.g. Grabowska and Bojdys, 2001) and many seismic surveys allowed defining its geometry (Środa et al., 2006). The Moho boundary (see Chapter 3.3) also shows an abrupt decrease in depth towards NE in correspondence with the TESZ (Guterch et al., 2006; Milano et al., 2016). Based on the above studies, we fixed the top of both magnetic blocks of our model (5 km for M1 and 3 km for M2) as corresponding to the shallow surface of the crystalline basement. As regards the bottom, we referred to the Moho depth, leading to depths of 30 km for M1 and 43 km for M2, respectively. Due to the low heat flow values in the TESZ area, (Majorowicz et al., 2003; Čermák and Bodri, 1995; Grabowska et al., 2011) we assumed that at the Moho the temperatures do not exceed 550-600°C. Finally, we considered the middle-lower crust normally magnetized with respect to the present-day geomagnetic field with I= 65° and D=3°.

In our model, the TESZ anomaly is interpreted through a contact between a thin and weakly magnetized crust to the SW with a thicker and more highly magnetized crust to the NE. The modeled magnetic profile (dashed line in Figure 5.7A) and the Total Gradient anomaly (Figure 5.7B) show a good agreement with the investigated anomalies. This suggests that the TESZ may be claimed as the main source contribution to the large-wavelength component of the central European magnetic field.

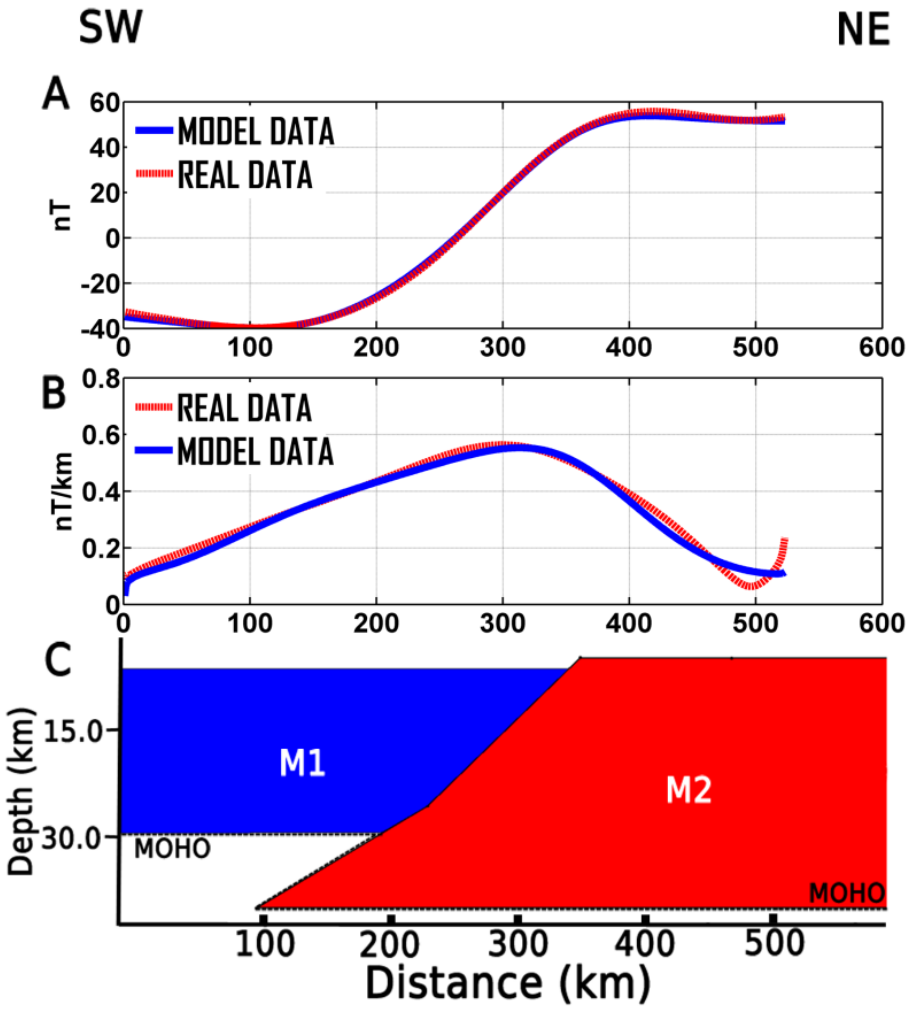

Figure 5.7 Simplified synthetic model of the TESZ: A) profiles of the magnetic field along P2 (in red) and the calculated magnetic anomaly (blue line); B) profiles of the total gradient observed (red line) and calculated (blue line); C) Representation of the model and source' geometries.

Regarding the Central Europe Magnetic Low, it cannot be assigned to only a single source (the TESZ boundary) but also to reversely magnetized contributions distributed all over central Europe, as already described in previous sections. In fact, sparse and weak total gradient amplitudes may be identified in different region of central Europe.

The interpretation of such anomalies may be carried out comparing the $|\nabla T|$ map (Figure 5.5) with the high-altitude map of the magnetic field (Figure 4.6 A). The first case is shown in figure 5.8 in which it is represented the magnetic field over the southern North Sea, Belgium and Netherlands. The main geological formations of the region are the Brabant Massif, Namur Basin and Ardennes Massif. Magnetic and paleomagnetic studies in Belgium (Garza and Zijderveld, 1996) described results about the late Paleozoic remagnetization and the reconstruction of the northward motion

during the Late Carboniferous. Paleomagnetic data collected in the area point out the reverse polarity of the magnetic rocks connected to regional remagnetization events coinciding with the tectonic and orogenic activity during Carboniferous times. The magnetic effect of such Paleozoic rocks is still clearly recognizable at high altitude where two strong magnetic lows occur above Belgium and Netherlands. Comparing the magnetic field map with the total gradient we observe that the magnetic lows become two maxima of the total gradient signal (Figure 5.8). Similar results were obtained in the model test of the previous section, where the magnetized source generates a magnetic low anomaly replaced by a maximum in the total gradient map. So, these results combined with the palaeomagnetic information allow interpreting these sources as characterized by a strong remanent component of magnetization of reversed polarity.

Similar remarks occur for the Bohemian Massif in Figure 5.8(2) Although palaeomagnetic analysis did not retrieve significant information about a reverse polarity in these area, we may observe a magnetic behavior similar to the Brabant Massif region. In fact, we may again observe a tight correlation in extension and shape between the intense magnetic low extending from the western Poland towards SW, covering most of the central Czech Republic, and the total gradient anomaly.

The third area considered in this study is the Pannonian basin, where an extended magnetic low, visible up to satellite altitudes, lies over Slovakia and Hungary. The Pannonian basin formed contemporary to the Tertiary evolution of the Carpathians and the Eastern Alps, related to a SW to W dipping subduction (Bielik et al., 2004). The origin of the magnetic anomaly was already studied by other authors, using mainly satellite data of the MAGSAT mission. Kis at al. (2011) interpreted the anomaly using a three-dimensional triangular model and considering a reverse magnetization of the source. The remanent magnetization is related to the exsolution of the hematite-ilmenite minerals found in the upper crust of the Pannonian Basin. The total gradient map once again shows a good correlation between the magnetic low anomaly and the position of the total gradient maxima.

The analysis of these well-defined anomalies in central Europe pointed out the presence of specific sources with a reverse polarity, producing strong magnetic anomaly even at high altitudes. Such sources seem to be the sole real and significant contributions to the magnetic field, probably linked to the middle-lower crust, within a general low magnetization of the Paleozoic platform.

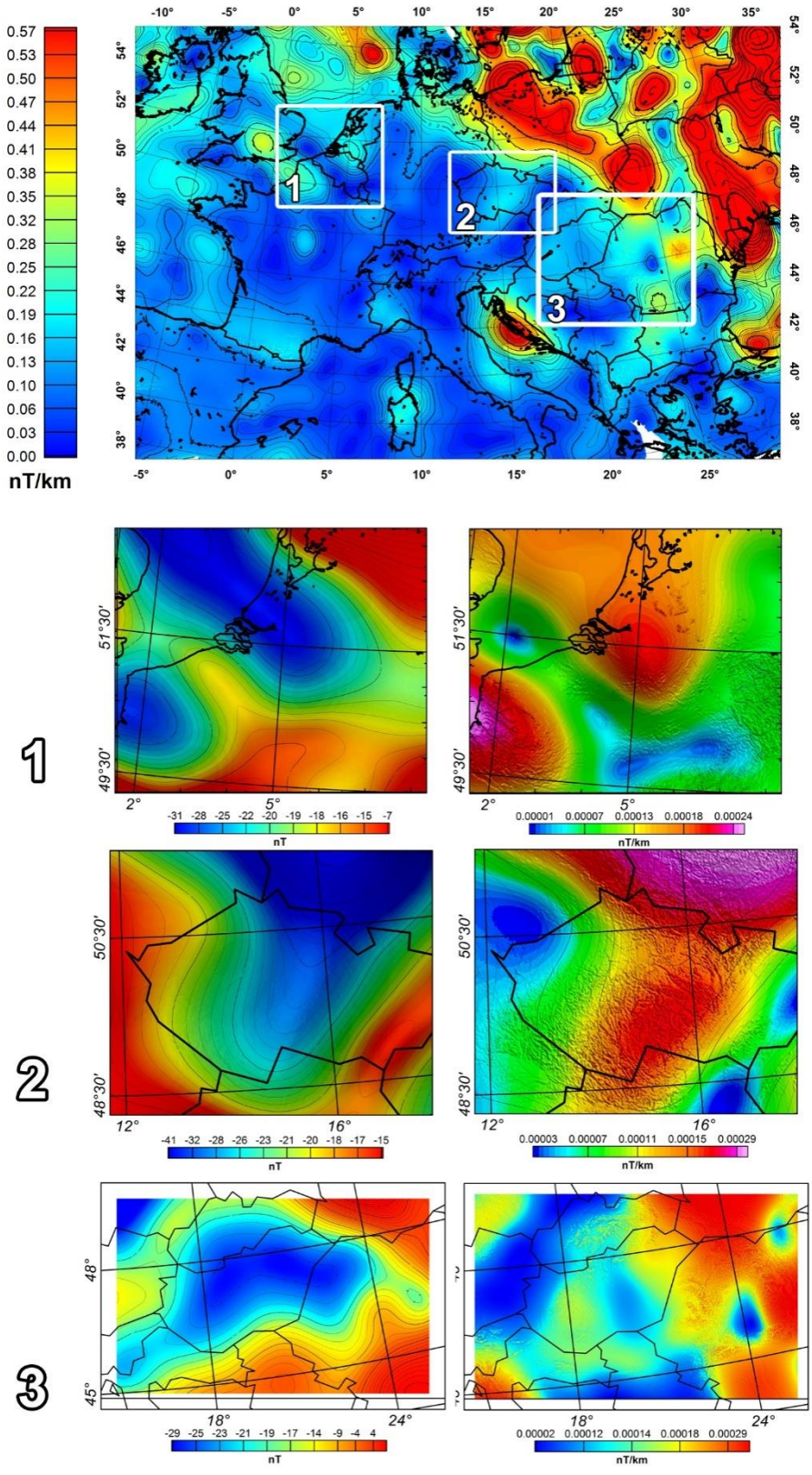

Figure 5. 8 Interpretation of the total gradient anomalies over the Anglo-Brabant Massif (1), Bohemian Massif (2) and Pannonian basin (3).

6

Multiscale Analysis of the aeromagnetic field in Europe

As indicated previously, the rationale for a multiscale approach is that, in general, there is no specific scale at which the potential fields can completely characterize the source. Scale invariance occurs only for homogeneous fields caused by ideal sources. For instance, the field of a uniformly magnetized sphere is homogeneous and it is scale-invariant: i.e., at each scale one may derive exactly the same source properties, which are the homogeneity degree and the depth to the center. Inhomogeneous fields are, however, the rule for real-world anomalies, and scale invariance can be assessed for these fields only in limited regions: very far or very close to the sources (Fedi, 2016). At intermediate scales, more refined inhomogeneous models must be assumed, as described in Fedi et al. (2015).

Whether the field could be better approximated by a homogeneous or inhomogeneous model, multiscale methods try to fill the gap of interpreting the data at only their measurement surface. To this end, various techniques may be used to interpret the field at more scales simultaneously, such as the Continuous Wavelet Transform (CWT) (e.g., Moreau et al., 1997; Sailhac and Gibert, 2003; Saracco et al., 2004; Fedi et al., 2010,), the Depth from EXtreme Points (DEXP) and the Multiridge analysis (Fedi, 2007; Fedi et al., 2009; Florio and Fedi, 2014). For all multiscale methods the scale is equivalent to the altitude of continuation.

As mentioned previously, the Multiridge geometric method (Fedi et al., 2009, Florio and Fedi, 2014) is based on the joining and concatenating of the extreme points (ridges) characterized as the zeros of the horizontal derivative of the field, the zeros of the vertical derivative of the field and the zeros of the potential field itself (Figure 2.1). In this way, the depth to the source is simply determined by the intersection of the ridges (Sailhac and Gilbert, 2003, Saracco et al., 2004; Fedi et

al., 2009), corresponding to the top of the source. This multiscale method has reduced sensitivity to noise compared to the Euler deconvolution approach because the short-wavelength noisy components are attenuated naturally in the upward continuation. Note that the number of ridges is variable and depends on the order of partial differentiation of the potential field data (Fedi et al., 2009, Figure 1).

The Multiridge analysis consists of three main steps: i) forming a Multiridge data set by upward continuation; ii) searching for the zeros of the horizontal derivative of the field, the zeros of the vertical derivative of the field and the zeros of the potential field itself at each altitude; iii) extrapolating the ridges down to the source region and identifying the source positions (singular points) as the zones where more ridges intersect each other; iv) selecting one or more ridges and applying Euler deconvolution or the scaling function method to the field values, in order to estimate the structural index and/or the depth to the source (Fedi et al. 2009).

In this work, the Multiridge method is used to model the deep sources beneath three specific European regions, where the magnetic anomalies contribute significantly to the magnetic field at each altitude of observation: the Bohemian massif area, the Adriatic plate and the Trans European Suture Zone region.

The retrieval of information of deep crustal sources is certainly a goal needing special attention because of the huge change in physical properties of rocks vs. depth (i.e. temperature, magnetic properties and grain size). To this end, Fedi (2007) and Fedi et al. (2009) have shown how multiscale methods (i.e. DEXP, Multiridge) are characterized by high stability and performance in interpreting anomaly fields generated by multiple sources. These methods, in fact, take advantage of the natural behavior of potential field data versus the altitude (Fedi, 2007).

The use of several orders of derivative allows the interference between the effects of different sources to be reduced and, thereby, allows obtaining a clear representation of source distributions with depth. In order to better clarify this concept, we test the performance of the Multiridge method by assuming a multi-layer model.

In Figure 6.1A we show the magnetic anomaly field generated by a two-source model at 1 km and 100 km altitude. By assuming the Curie isotherm corresponding to the Moho boundary, the blocks 1 and 2 have the top at 10 km and 8 km depth and the bottom at 30 km and 40 km depth, and magnetization of 1 A/m and 3 A/m, respectively. Only induced magnetization has been considered in this model, and the direction of the induced field is I=65° and D=2° (average values in central Europe).

As we will see later, this model is useful for interpreting the high-altitude magnetic anomaly over the TESZ. In Figure 6.1A we show the Multiridge section of the profile A-B crossing the contact line between the bodies 1 and 2. The ridges of the 1st derivative order of the magnetic field occur in the central part of the profile. When the field is inhomogeneous, these ridges are curved lines. In this case, according to Fedi et al. (2004) we can nevertheless distinguish two or more sets of scales, for each of them a segment of the ridges appears approximately straight. We refer to Martelet et al., (2001) and Fedi et al. (2004, Figures 3 and 8 of the paper) for more details. This behavior is clearly visible in the Multiridge section of the model, where two main slopes of the ridges are identifiable, suggesting the existence of multiple source contributions. The portions of ridges from 0 km to 15 km altitude, extrapolated down to the source region, correspond to the contact zone between the tops of the two blocks at 10 km depth; the portions of ridges up to 100 km altitude intersect each other instead at about 30 km depth, corresponding well with the strong change in thickness and magnetization between the lowest part of the two sources.

We now describe a more complex source distribution (model B, Fig. 6.1), where shallow bodies (blocks 3, 4 and 5) are added to the model, in addition to the deep blocks 1 and 2. In this case we test the ability of the Multiridge method to retrieve the deep sources despite the interference of shallower magnetic source signals. The geometry and magnetic parameters of blocks 1 and 2 and of the induced magnetic field have not been changed. The magnetization of the shallow bodies varies between 1 and 3 A/m and the maximum depth to the bottom is 8 km depth (see Figure 6.1 caption for details). Observing the magnetic field map at 100 km in model B, we note that the main source contribution is related to the deepest blocks 1 and 2 which generate a long-wavelength anomaly, similarly to the high-altitude anomaly of model A. The Multiridge section of the same profile A-B shows a set of ridges retrieving several singular points at different depths. The low-altitude parts of the ridges are fairly well correlated to the edges of the shallow bodies 3, 4 and 5; but even in the central part of the section, the contact between the tops of the blocks 1 and 2 is still well recognized.

Interesting results are retrieved at higher altitudes. Since the magnetic field is inhomogeneous, the depth positions of shallow sources can no longer be resolved by the ridges with the increase of altitude, as demonstrated by their confused trends and shapes. In the central part of the section the ridges are straight lines converging into the source region. The intersection of these ridges retrieves the correct depth position of the deep contact between the main blocks 1 and 2, similarly to the results obtained for the model A.

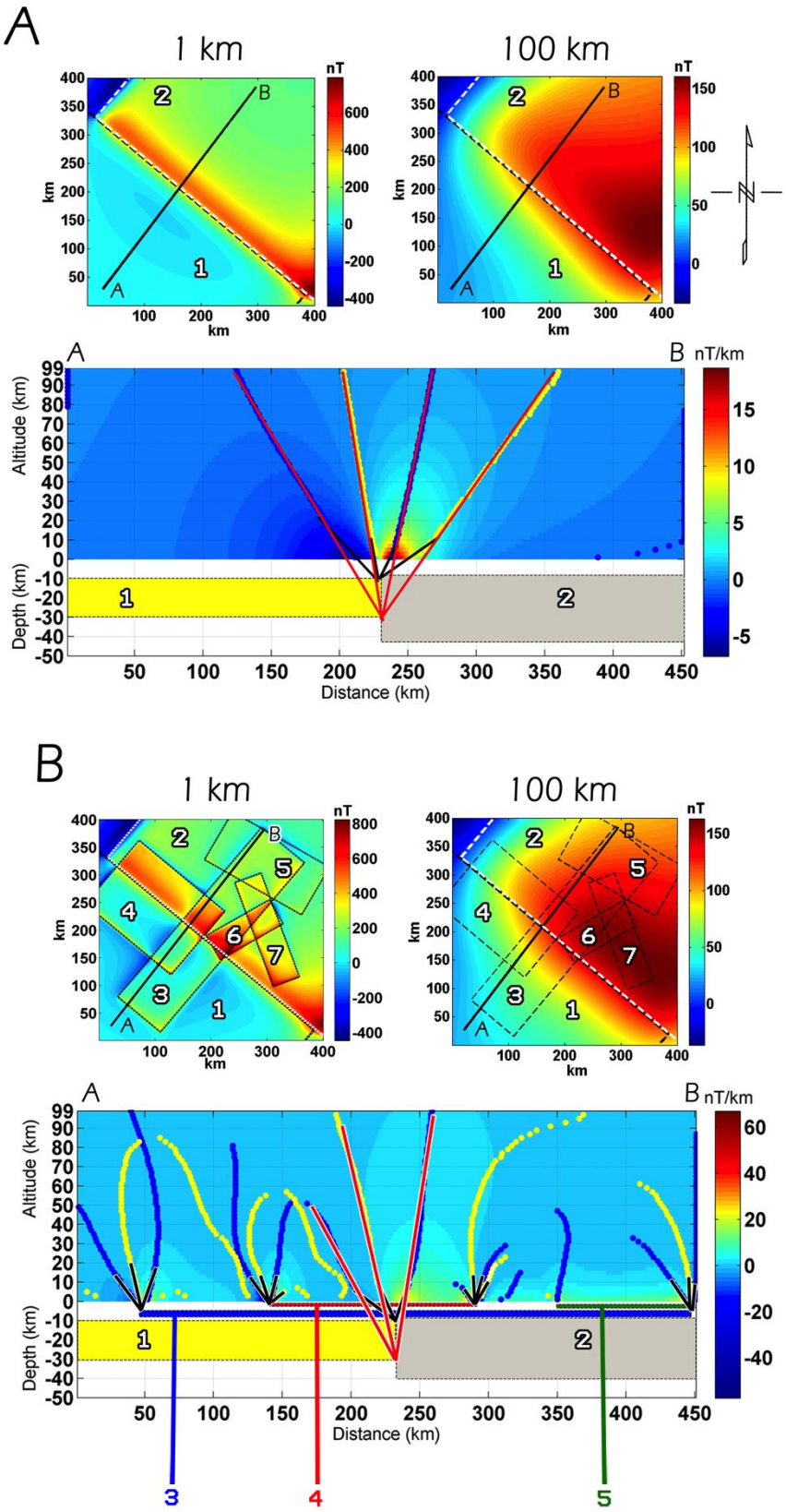

Figure 6. 1 Magnetic field of a two-source model at 1 km and 100 km altitude (up). The model blocks (1 and 2) have magnetization of 1 A/m and 3 A/m and 20 km and 35 km thickness, respectively. Multiridge analysis is performed along the profile A-B of the 1st order derivative of the magnetic field up to 100 km altitude (down). **B**: Magnetic field maps at 1 km and 100 km altitude of a multi-source model (up). Shallow sources have been considered, in addition to the main blocks 1 and 2. The shallowest

bodies have magnetization values ranging from 1 to 3 A/m and a maximum depth to the bottom of 8 km. Multiridge analysis is performed along the profile A-B of the 1st order derivative of the magnetic field (down). The main singular point positions of the several sources are well retrieved by the multiridge analysis, as shown for the limits of blocks 3, 4 and 5 and for the contact zones of blocks 1 and 2.

6.1 The Bohemian Massif magnetic anomalies

The first Multiridge analysis was performed above one of the main geological units of central Europe: the Bohemian Massif (Figure 6.2). The profile corresponds to the vertical geological section imaged by seismic profile CEL09 (Figure 5 in Hrubcová et al., 2005). We calculated the Multiridge section of the 2nd order derivative of the magnetic field up to 100 km altitude. We show in Figure 6.2, that this section is characterized by a high number of ridges with a good convergence toward singular points placed at different depths. We see that many ridges are not straight lines, indicating that the field is inhomogeneous and, as illustrated in the previous section, the deepest source depths are retrieved from the behavior of the ridges at higher altitude and vice versa for the shallow sources. In particular, the white straight lines in Figure 6.2 represent the position of the shallow sources, which are located in the upper 10 km depth range; the dark blue ridges intersect each other at the middle crustal level between 10 and 20 km depths; finally, the singular points detected from the high-altitude portions of the ridges (highlighted in red) closely match at 30-40 km depth. We can identify the main magnetic layers beneath the Bohemian Massif by connecting the singular points related to the same depth-range. By comparing the Multiridge section with the seismic data of profile CEL09 (Figure 6.2), we observe a good correspondence between the resolved magnetic interfaces and the main seismic reflectors. In particular, according to Hrubcová et al. (2005), the P-wave velocity distribution shows a relatively high Vp gradient in the upper crust of the Bohemian Massif (5.8 - 6.0 km/s), which is well correlated to the white magnetic boundary, matching the shallowest singular points. Then, in the middle crust, the blue lines are in a good agreement with the two main reflectors recognized by the seismic data with a velocity contrast of 0.15–0.3 km/s at 8–13 km and 17–20 km depths, respectively. Finally, the transition-zone between the crust and the upper-mantle has been identified in the central part, beneath the Moldanubian, at a maximum depth of 39 km with a gradual increase of the Vp velocity from 6.5 km/s at 19 km to 8.1 km/s above the Moho. In the NW, beneath the Saxothuringian and partly the Barrandian, the Moho has been inferred at the depth where a strong velocity gradient occurs vertically, from 6.9 to 7.5

km/s. In the SE, the same authors suggest that the lower crust/upper-mantle transition is a 17 km thick gradient zone, at 23–40 km depth, with Vp velocities ranging from 6.8 to 7.8 km/s. The red magnetic interface retrieved by the deepest singular points is fairly well coincident with the seismic-Moho boundary. Specifically, these deepest singular points correspond to areas of greater morphological curvature or abrupt changes in depth of the Moho.

Our ability to obtain geological information at great depths from the magnetic data is related to the low heat-flow found in the Bohemian massif area (30-60 mW/m2) (Čermák et al., 1991). In such conditions, the Curie isotherm is expected to be close to the depth of the Moho boundary, where the temperature ranges between 400 and 600° C (Čermák, 1975; Čermák et al., 1991); in this way the Moho could be a proxy for the bottom of the magnetic crustal layer (Corrado et al., 1979; Gasparini et al., 1981).

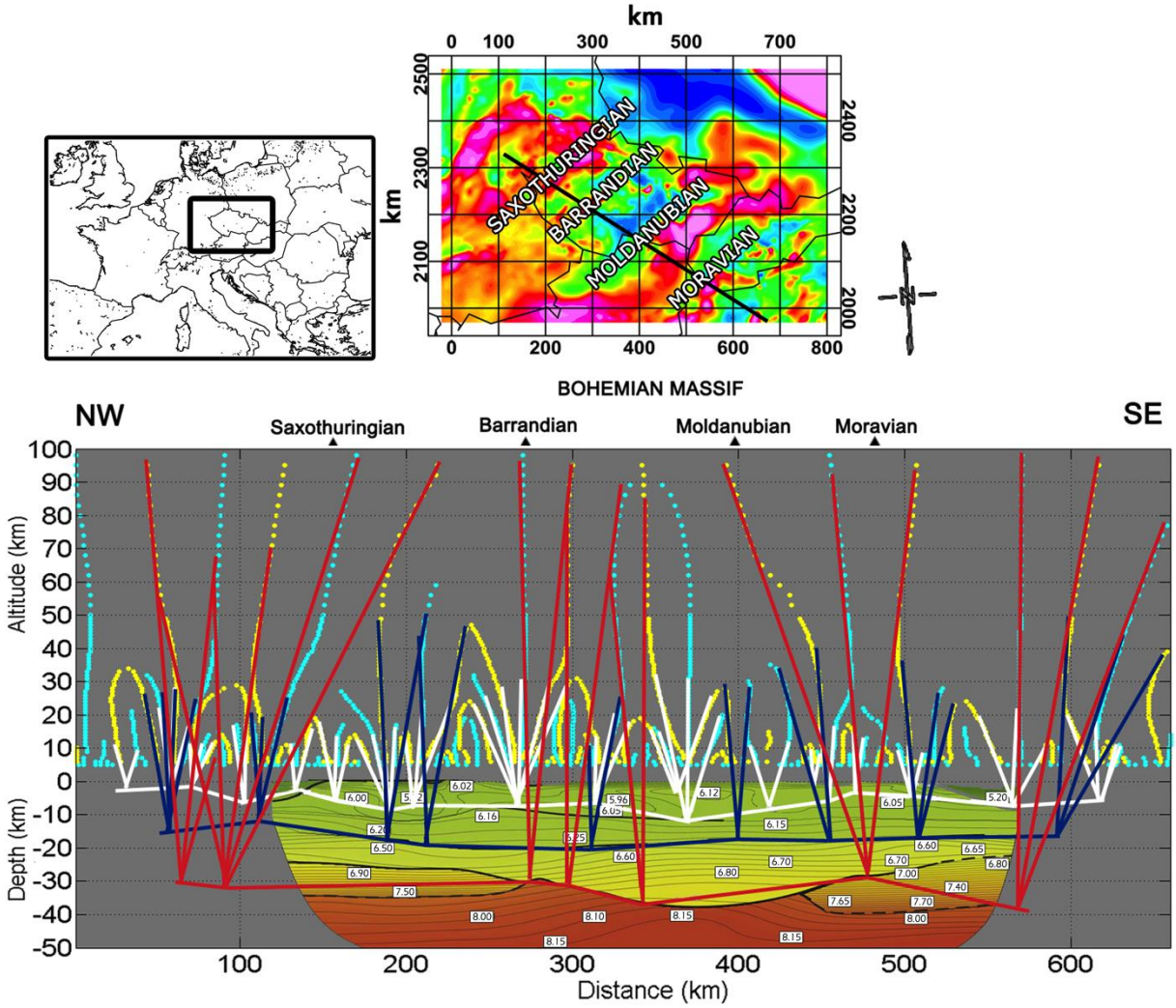

Figure 6. 2 Comparison between the multiridge section and the geological model of a seismic profile taken from

Hrubcová et al., 2005. The singular points occurring in the upper, middle and lower crust are retrieved by the white, blue and red straight lines, respectively.

6.2 The Adriatic magnetic anomalies

Similarly to the analysis of the Bohemian Massif magnetic field, the same approach is here used to study one of the most intense magnetic anomaly of southern Europe, the Adriatic magnetic anomaly, whose effect is clearly visible up to satellite altitudes. For this reason, we may expect that the long-wavelength component of such anomaly is mainly associated to deep magnetic sources beneath the Adria plate.

The complex geological setting of the Mediterranean area is not well constrained and remains controversial as regards the identification of the internal and external boundaries of the Adriatic plate (Battaglia, 2004; Pinter and Grenerczy, 2006). The geodynamic events of the Apennine (Carminati et al., 2003), Alpine (Kummerow et al. 2004) and Dinaric (Di Stefano et al., 2009) subductions allowed the formation of a foreland basin system in the northern portion of the Adriatic Sea, constituting the western, northern, and eastern margins (Cuffaro et al., 2010) (Figure 6.3 A). The presence of gabbroid intrusions, thermal cooling and generation of horsts and grabens have been explained by Middle Triassic extensional movements and consequent crustal thinning (Winterer and Bosellini, 1981; Bertotti et al., 1998; Pamic and Balen, 2005; Juracic et al., 2004). The Moho boundary beneath this region is around 30 km deep in central Adriatic and it deepens down to 38-40 km in the Croatian region (Figure 6.3 B). The crustal heat flow ranges between 30 and 40 mW m^{-2} (Scrocca et al., 2003).

In the last decade, previous studies pointed out the wide magnetic anomaly as due to uplift of the magnetic basement and the presence of volcanic and/or ophiolitic intrasediment sources (Giori et al., 2007; Mancinelli et al., 2015). Giori et al. (2007) carried out this interpretation by using an integrated dataset from Italian and Croatian national oil companies. However, this dataset was based exclusively on the grid of the Italian aeromagnetic surveys and, in part, of the offshore Croatian data coverage, so not resorting to a complete representation of the study area.

The EMMP data used in this work, provide instead a consistent advance in the representation and analysis of such important magnetic province. As already described previously, the Adria plate is mostly covered by an intense magnetic anomaly occurring between the central Adriatic Sea and

the coast of Croatia and presenting a NW-SE trend. We also showed that the strong Adriatic Magnetic Anomaly (AMA) is still clearly visible up to high altitudes (Figure 6.4), both in the upward continued aeromagnetic map and in the satellite-derived MF7 model map.

The aeromagnetic data were upward continued up to 20 km altitude and the multiscale analysis was performed along two profiles (P1, P2) crossing the Adriatic magnetic anomaly (Figure 6.4A). In Figure 6.5 the Multiridge section of the 3rd derivative order is presented allowing a reduction of the interference between the effects of different sources.

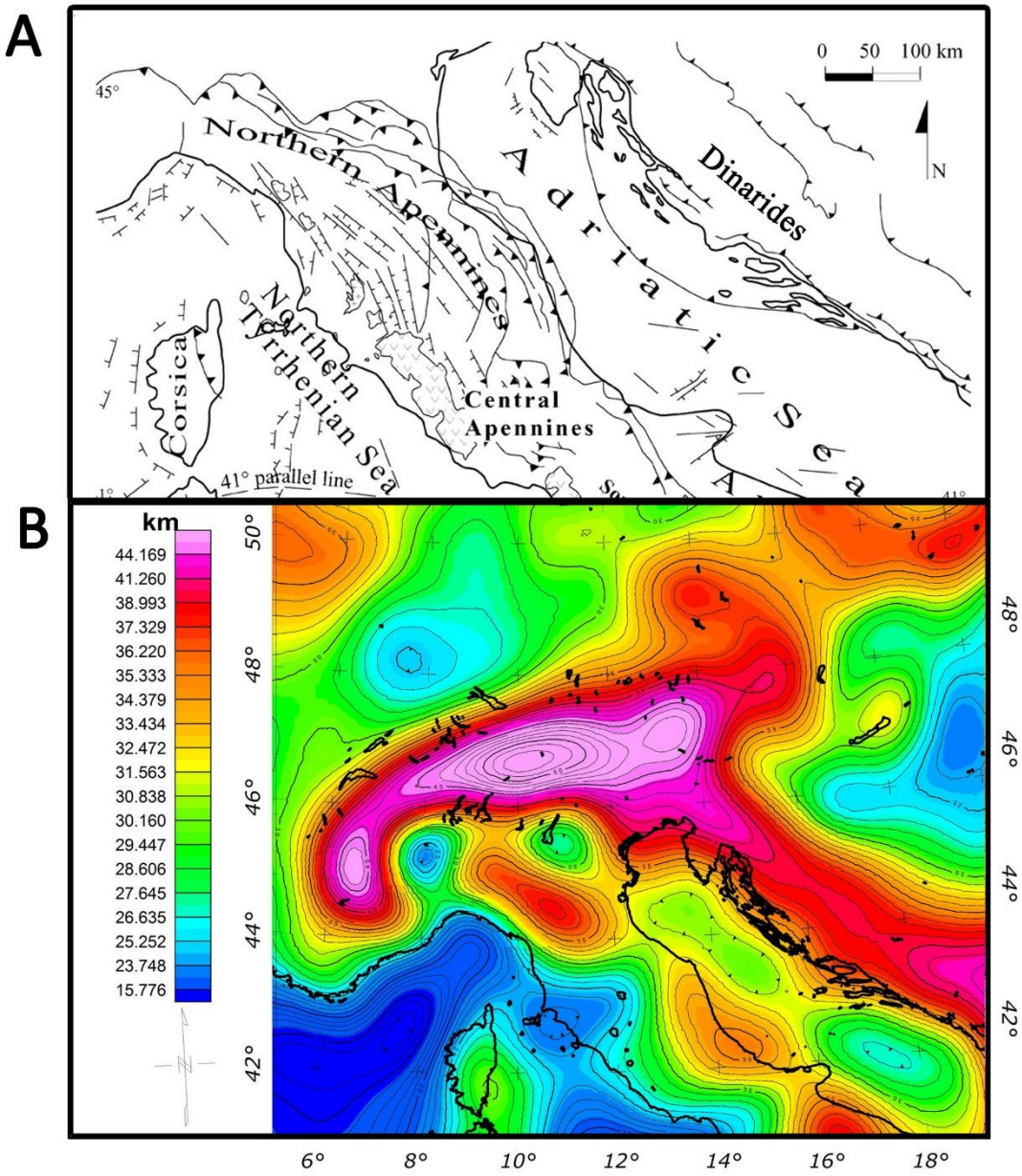

Figure 6. 3 A) Tectonic map Adriatic region (modified after Speranza et al., 2003); B) The Moho depth map above northern Italy (data from Grad et al., 2009).

As expected, the Multiridge section shows a high density of ridges converging at singular points, representing the depth position of the sources of the magnetic anomalies. Similarly to the Bohemian Massif analysis, a geometric approach was used, based on prolonging the ridges down to the source region. Only the high-altitude portion of the ridges was considered, in order to retrieve the depth estimate of the basement, which is supposed to be the main magnetic source of the regional-scale magnetic anomaly. The estimated depth values range between 5 and 14 km.

The nature of the singular magnetic sources can be evaluated by employing the 'scaling function' method along the ridges of the Multiridge sections. To this end, the homogeneity degree (n) was evaluated for most of the ridges and the estimated depth values are in good agreement with the depth of the singular points calculated by the geometric method (Figure 6.5). Our estimates for the homogeneity degree range between -3.3 and -3.5. So, considering that k=3, because we are using the 3rd order derivative of the magnetic field, the respective average structural index (equation 21) may be estimated as 0.4, a value which is typical of finite fault structures. These kinds of idealized models can be approximately adopted for explaining the most complex features of the morphology of an interface or a basement (for instance, Li, 2005).

The multiridge depths estimated for the profile P1 (Figure 6.6A) were then compared with the model of the magnetic basement carried out by Mancinelli et al. (2015). These authors performed a forward modeling relative to the observed gravity and magnetic anomalies. Based on surface observations of Triassic gabbroid rocks in the Croatian archipelago (Pamic and Balen, 2005; Juracic et al., 2004), these authors interpreted the potential field data as due to a gabbroid-rich basement. Giori et al. (2007), however the AMA was explained as a twofold effect, related both to the uplift of the magnetic basement towards the Croatia coast and to highly-magnetized intrasedimentary intrusions.

Our multiridge model is in good agreement with the progressive NE uplift of the magnetic basement described by Mancinelli et al. (2015). In particular, the singular points detected by the multiridge analysis seems to be well associated with the horst and graben structures formed during the extensional movements and crustal thinning of the Middle Triassic (Figure 6.6-6.7).

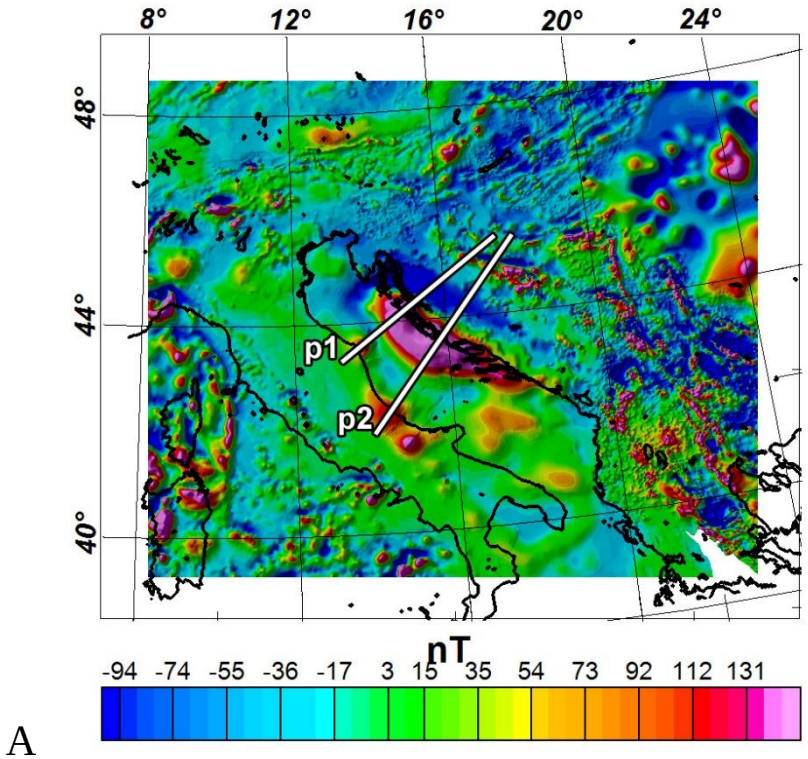

A

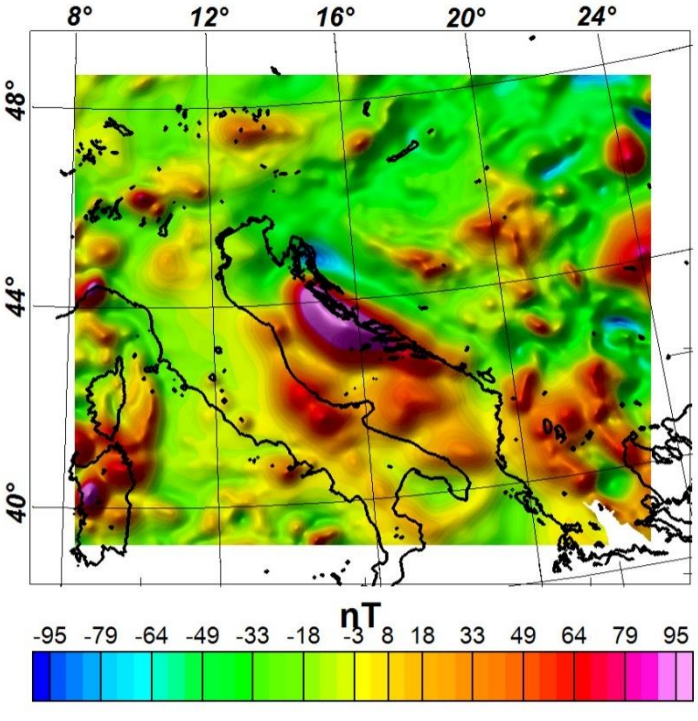

B

Figure 6. 4 Total magnetic field over the Adriatic plate at 5 km altitude (A) and 100 km altitude (B) and Multiridge profiles.

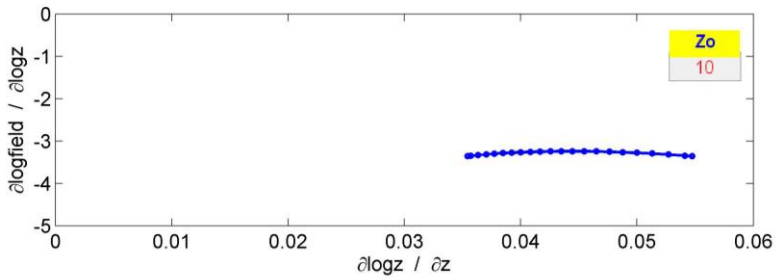

Figure 6.5 Estimation of the homogeneity degree by the use of the scaling function method

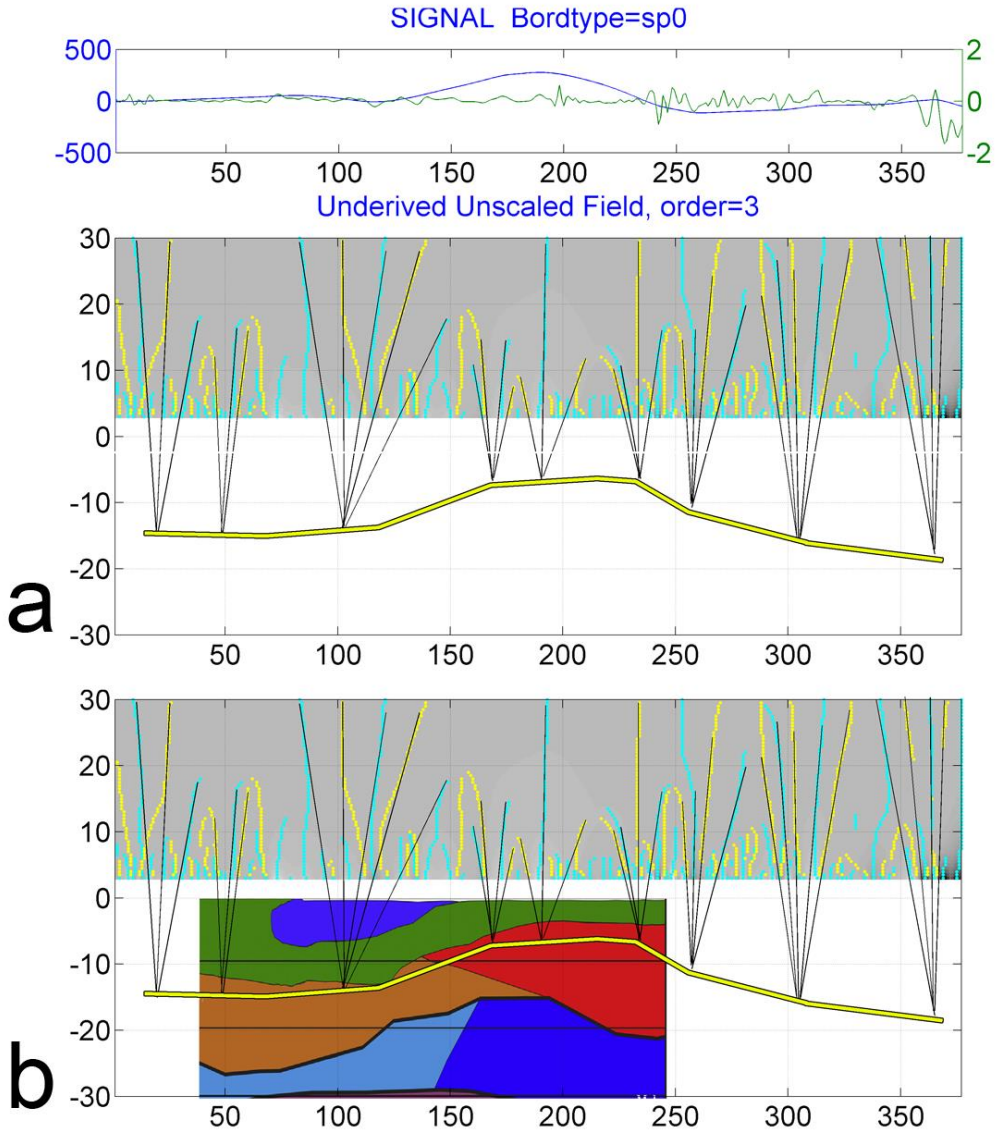

Figure 6. 6 Multiridge analysis of Profile 1 (a). The singular points retrieved are in good agreement with the depth to top of the magnetic basement model of Mancinelli et al. (2015) (b). A sharp uplift of the magnetic basement is shown by connecting the depth solution.

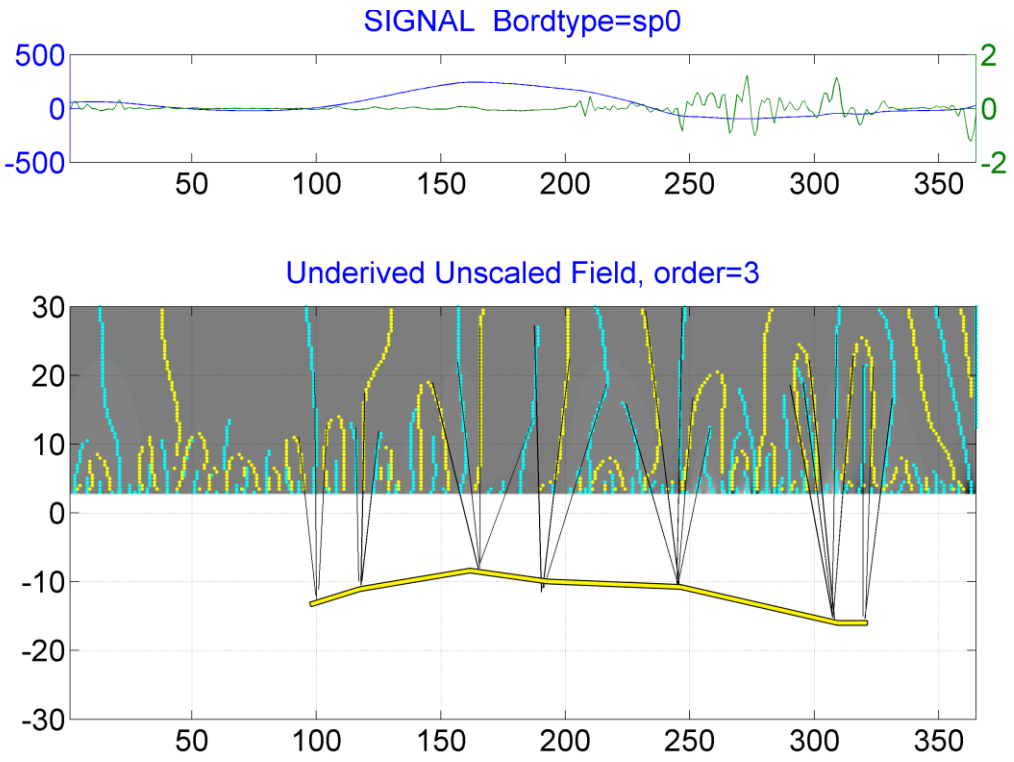

Figure 6. 7 Multiridge analysis of Profile 2. Similarly to Profile 1 the depth values retrieved suggest the uplift of the basement as the main source of the magnetic anomaly.

6.3 The magnetic field in the Trans European Suture Zone (TESZ) region

The Multiridge analysis was finally performed over the main geological structure of central Europe, which, as extensively described in previous sections, represents the main contribution to the regional-scale magnetic field up to satellite altitudes. The results of total gradient analysis pointed out that the TESZ, jointly with the occurrence of specific sources reversely magnetized within the Paleozoic crust, is the main cause of the CEML and its reverse dipolar shape, since it puts in contact the Paleozoic crust with the EEC differing in structural and magnetic properties.

Moreover, in several studies it was demonstrated how several crustal parameters change critically in the TESZ producing a sharp variation of the heat flow trend, the Curie temperature depth and Moho morphology.

The Multiridge analysis was performed by selecting a set of profiles crossing the TESZ magnetic anomaly (Figure 6.8), close to those analyzed by seismic surveys (Guterch and Grad,

2006). The geological interpretation of such seismic sections was used, once again, to check the depth values retrieved by the multiscale study and validate our results. In particular, the seismic sections are based on the POLONAISE '97 and CELEBRATION 2000 projects (Guterch et al., 1999; Guterch et al., 2003a), in which several seismic profiles were collected across the TESZ area, the southern Baltica and the northern front of the Carpathian Mountains. All the profiles were interpreted using modeling techniques by two- and three-dimensional seismic tomography and ray tracing (see Guterch and Grad (2006) for further details).

The Multiridge sections were produced from the multiscale field upward continued to 100 km, with a 1 km steps between 5 and 50 km altitude and at 3 km steps from 50 km to 100 km altitude. Figure 6.8 shows the six profiles considered in this study. As previously mentioned, Multiridge analysis is very stable and high-order derivatives may be used to the maximum allowed resolution without lowering the signal-to-noise ratio (Fedi et al., 2009; Florio and Fedi, 2014). In particular, according to Fedi et al. (2012), we can choose the appropriate order derivative of the field to give the clearest definition of the ridges and most consistent results. We studied the 1st order derivative for profile p1, the 2nd order derivative for profiles p2, p4, p6, and the 3rd order derivative for profiles p3 and p5. In Figure 6.9, we show the Multiridge sections of profile p1, p2, p3 and p5. As in the previous Multiridge analysis for the Bohemian Massif and Adriatic anomaly profiles, these ridges are affected by a curvature related to the transition from the effects of shallow structures to those of deep sources. Since this analysis aims at interpreting the deepest sources of the TESZ area, only the high-altitude portion of the ridges, from 50 km to 100 km was considered. These latter effects are dominant in the TESZ area, and by using the geometric approach, we can estimate (Figure 6.9) depth values corresponding to the deeper crust. Note that the depth values were obtained by calculating the best-fit straight lines to the ridges, in a least-square sense.

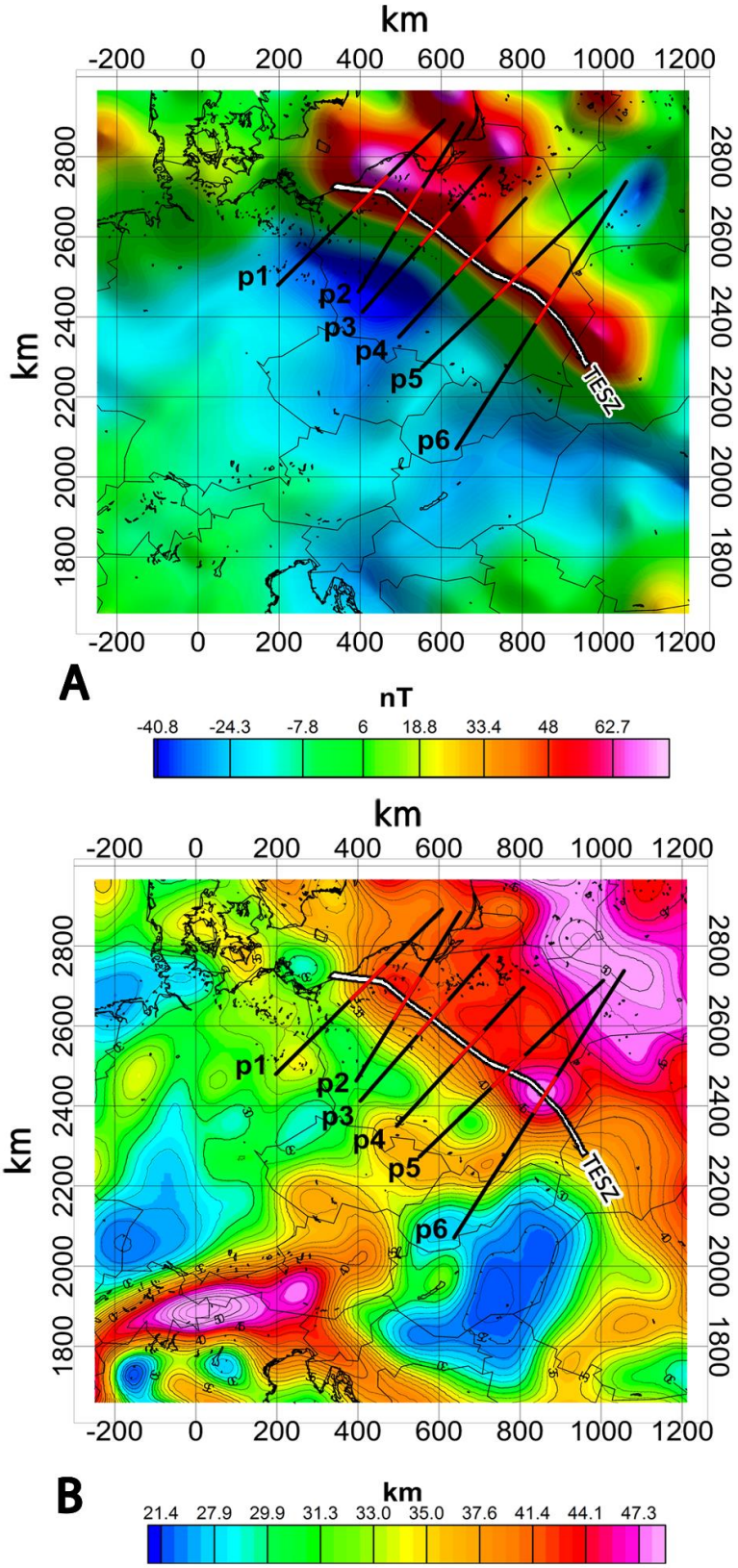

Figure 6. 8 A: Multiridge profiles crossing the magnetic anomaly of the TESZ. They were traced according to the position of the seismic surveys described in Guterch and Grad (2006). The portion crossing the TESZ magnetic anomaly is marked in red color; B: the map of the Moho depth in the area of study.

The depth results were obtained without using any kind of constraint (seismic or geological). Nevertheless, it is so worth considering the seismic profiles of the POLONAISE '97 and CELEBRATION 2000 projects (Guterch and Grad, 2006), and compare our results with the interpreted sections. In Figure 6.9, the Multiridge sections of the profiles p1, p2, p3 and p5 are compared with the seismic sections of Guterch and Grad (2006) identified as LT-7, LT-2, LT-4 and CEL01, respectively. Profiles p4 and p6 are not shown in Figure 6.9 because of the unavailability of seismic data.

It can be easily seen that the singular points obtained by the geometric method for the high-altitude sections of the dataset are positioned at great depths and, compared with the seismic interpretations, coincide closely with the TESZ area. The magnetic singularities are located at abrupt depth variations of the seismically defined Moho surface. The deepest solutions primarily occur where the Moho depth increases from the thinner crust of the Paleozoic Platform (to the SW) to the thicker Precambrian Platform (to the NE).

In order to identify the source-type, the homogeneity degree (n) was estimated using scaling function method. We evaluated n and z_0 along the ridges related to the TESZ anomaly on the previously considered profiles, and, using equation 21, we found N from 0.5 to 0.8, values typical for finite fault or sill structures. These kinds of idealized models can be approximately adopted for explaining the complex features of the morphology of an interface or a basement (e.g., Li, 2005). The depth values ranging from 40 km to 45 km confirm the depths estimated with the geometric method. This description of the Moho surface is in agreement with the geological model based on the seismic interpretation, where we recognize significant depth variations in the Moho boundary that demonstrate the transition from the thinner Paleozoic crust to the SW to the thicker Precambrian platform to the NE.

Let now bring together the Multiridge results for all the profiles of Figure 6.8 to give a picture of how the magnetic field can help to understand the complex structural nature of the TESZ and, specifically, to describe the transition from the thin SW crust to the thicker NE platform. This is shown in Figure 6.10, where the ridges of the profiles are plotted together in 3D representation to show the TESZ line and the morphology of the deepest crustal boundary detectable by these magnetic data. From the results the TESZ is represented as the deepest magnetic boundary within the crust; so if we assume the magnetite as the dominant magnetic mineral facies (e.g. Frost and Shive, 1986) it is expected to be representative of the depth of the Curie Point isotherm, namely 580 °C;

Finally, due to the low heat-flow in the area, the deep magnetic boundary appears to correspond well with the Mohorovičić discontinuity (e.g, Gasparini et al., 1981).

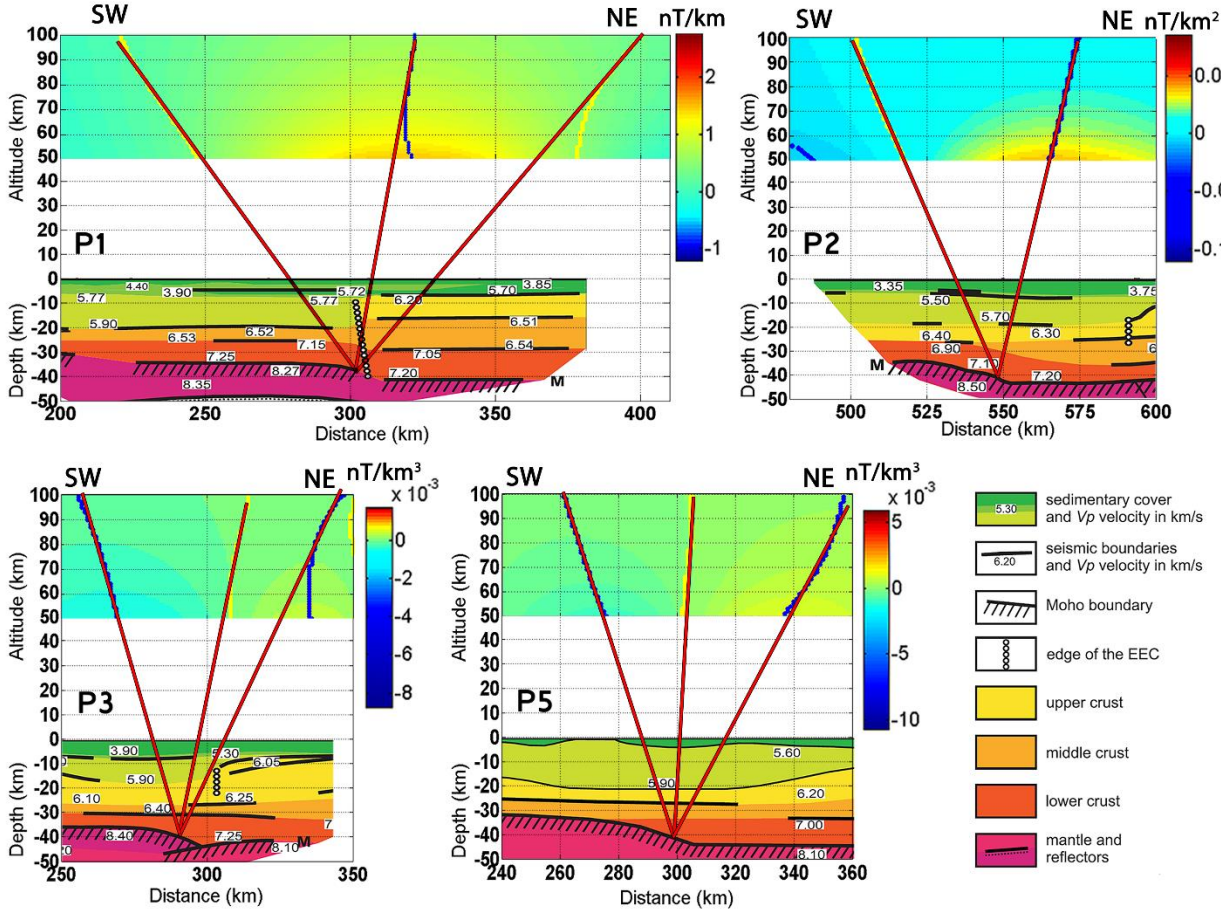

Figure 6. 9 Multiridge sections across TESZ and depth values estimation by the geometric approach. Multiridge sections are compared with corresponding geological models (modified after Guterch and Grad, 2006). Red straight lines are the best-fit linear regressions to the ridges and cross each other at the Moho interface.

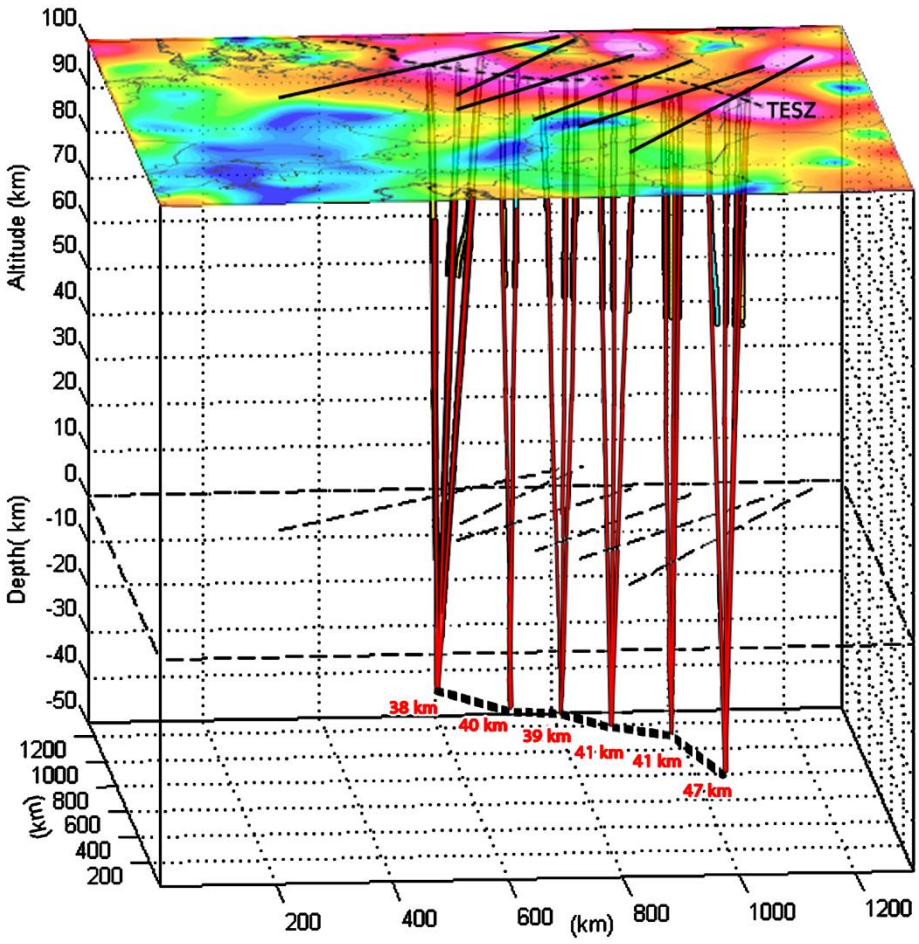

Figure 6. 10 A 3D representation of all multiridge profiles. The Moho configuration beneath the TESZ is shown by the dashed black line, defined by the singular points obtained from the high-altitude portion of the ridges shown in Figure 6.9.

7
Discussion and Conclusions

The present work was based on the application of multiscale methods to the aeromagnetic field of Europe. Our choice was justified by the complex and rich information linked to the field: at a single scale we cannot fully understand the whole content of the field, while analyzing the field at many altitudes may clarify its comprehension. Classical upward continuation is well known among potential field interpreters. It is mostly used to smooth the field, and for comparing surveys measured at different altitudes or with different instrumental platforms (aerial, marine, ground or satellite).

In the multiscale framework, upward continuation is instead just a tool to generate a multiscale 3D dataset, so allowing specific techniques to be used for a complete simultaneous analysis at many levels. Conjugating upward continuation with *n*-order field differentiation is the main essence for multiscale methods, which may be used for not losing resolution even at high altitudes, while preserving a stable behavior of the analyzed field.

Previous studies of the magnetic field in Europe were conducted or at a regional scale, at high altitudes (say 350 km), or at a local scale at low altitudes (say a few km). In this thesis we attempted to make the first study of the whole European area, conducted at both large and local scales.

One of the main results obtained in this research, is to have shown that high-resolution methods, such as the multiridge method, may provide accurate descriptions of complex areas, such as TESZ or ADRIA, being also well consistent with previous studies. In particular, we showed that multiscale methods of potential field data are able to reveal very useful information about the crustal features and may support and integrate the classical interpretation of seismic data regarding the Moho or other crustal structures.

This study may be divided in two main parts. The first part is related to a comparative study of the field at three altitudes: 5 km, 100 km and 350 km. It was made using the field itself and also the modulus of the total gradient of the aeromagnetic field. This last revealed to be a fundamental tool

to identify the areas characterized by a low-magnetized crust. This task cannot be made analyzing the aeromagnetic field, since the magnetic lows of the magnetic anomalies are not exclusively linked to low-magnetization areas, but strongly depend on the total magnetization of the sources, either normally or reversely polarized. The independence of the total gradient modulus from the directions of the inducing magnetic field and of the total magnetization vector appears clearly from the result of a simple test involving both normally and reversely magnetized sources. We found that the sources are clearly marked by maxima of the total gradient modulus, while magnetic field cannot help to obtain a similar information, due to the complex merging of the lows and highs of the several anomalies.

At high altitudes the long-wavelength magnetic anomalies are related to deeper crustal sources and to the regional-scale magnetic properties of the crust. The main magnetic anomaly at high altitudes is the extended magnetic low (CEML) covering most of central Europe and confining to the NE with the Trans European Suture Zone (TESZ). TESZ separates the Europe in two very different magnetic environments, characterized by a general magnetic low over the Paleozoic platform and a distribution of intense magnetic anomalies above the EEC. The maxima of the total gradient modulus of the aeromagnetic field delineate with high detail the TESZ fault line, marking out a magnetic boundary between two regions, which we interpreted as a contact area between the strong magnetized middle-lower crust of the EEC (to the NE) and the weakly magnetized Paleozoic platform (to the SW). The interpretation of a scarce crustal magnetization in central Europe, is well evident in the total gradient map, characterized by extended areas of low-amplitude values in the area of the CEML. Such hypothesis was also verified by a simple model of two extended blocks, differing in susceptibility and thickness.

However, the analysis of the total gradient intensity was also decisive to detect further magnetic sources in the CEML area, characterized by a reverse magnetization. In fact, maxima of the total gradient signal occurring in the areas of the Brabant Massif, of the Pannonian basin and of the Bohemian Massif, are located in correspondence with lows in the magnetic field, so clearly indicating the presence of sources with reverse magnetization and high *Q*-ratio. This is also in agreement with palaeomagnetic surveys, which have shown the presence of minerals, such as pyrrothite and magnetite, in metamorphic rocks and limestones of the Paleozoic formations.

The high-altitude magnetic low of Central Europe, so, can be interpreted as due to two different classes of sources:

• A weakly magnetized and thin crust in central Europe *versus* a strongly magnetized and thick crust at the EEC, bounded by the TESZ;

• The presence of rocks with a strong remanent component of magnetization characterizing some areas of the Paleozoic platform. This should give additional contribution to the CEML, especially in regard to its large extension in the central part of Europe.

The second part of the work was based on the use of multiscale methods, in order to carry out a quantitative interpretation of the magnetic anomalies over Europe, based on a simultaneous analysis of the data at many altitudes. We used, as main multiscale tool, the multiridge method, which allows retrieving information about the source depth and the structural index.

The multiridge analysis was performed in three specific regions:

- the Bohemian Massif, characterized by a complex pattern of short-wavelength magnetic anomalies, which vanish at high altitudes where long-wavelength anomalies take place. The local magnetic anomalies are mainly associated to Miocene-Pleisotcene volcanic structures and to volcano-plutonic magmatic activity associated to the Variscan orogeny. The origin of regional-scale anomalies was instead attributed to the magnetized rocks of a deep basement. Moreover, the Bohemian territory is structurally different from the general Paleozoic crust, presenting an anomalously large crustal thickness and, consequently, a lower heat flow with respect to the average flow of central Europe. The multiridge analysis was performed along the seismic profile CEL09 and its result shows that the independently-inferred magnetic interfaces agree well with those in the seismically-based geological section. Moreover, the magnetic interfaces continue laterally so extending the information related to the geological-seismic model. The magnetic interface retrieved by the deepest singular points is fairly well-coincident with the seismic-Moho boundary. In particular, the position of the ridges' intersection seems to correspond to specific areas of strong variation of the Moho morphology. The low heat flow of the region and the deep Curie depth suggest considering the Moho as the bottom of the magnetic crust in the area.

- The Adriatic magnetic anomaly, which represents the most intense magnetic evidence of southern Europe at satellite altitudes. A multiscale dataset was built by upward continuing the high-resolution grid data of the total magnetic field up to 20 km altitude. The Multiridge method was performed along two profiles crossing the magnetic anomaly. The reconstructed interface, which is in substantial agreement with that of previous magnetic

models, describes the pattern of the crystalline basement beneath the Adriatic magnetic anomaly. In particular, the magnetic anomaly is associated to a sharp uplift of the magnetic basement toward the Dinarides belt front.

- The TESZ structure, whose magnetic anomaly dominates the magnetic field and the total gradient signal in both the low and high altitude maps. The Multiridge method, applied along six profiles, allowed identifying a set of magnetic singular points, which clearly characterize the magnetic sources within the deep crust. This allowed drawing two main conclusions: a) the deepest magnetic interface in the crust closely corresponds to the seismic Moho discontinuity; b) the Moho is characterized by a complex morphology, with abrupt depth changes.

References

Adnan, J., A. de Sa, and W. O'Reilly, 1992.Simultaneous measurement of the variations in the magnetic susceptibility and remanence of materials in the temperature range 10-700øC and at elevated pressure (16-160M Pa),Meas. Sci. Technol., 3,289-295.

Ansorge, J., Blundell D. and Mueller St., 1992. Europe's lithosphere - seismic structure. In: "A Continent Revealed- the European Geotraverse," (D. Blundell et al., Eds.) Cambridge University Press p. 33.

Arisi Rota, F., and R. Fichera, 1987. Magnetic interpretation related to geo-magnetic provinces: The Italian case history, Tectonophysics, 138, 179 – 196.

Arkani-Hamed, J., Strangway, D.W., 1987. An interpretation of magnetic signatures of subduction zones detected by MAGSAT. Tectonophysics 133 (1–2), 45–55.

Arkani-Hamed, J., 1989. Thermoviscous remanent magnetization of oceanic lithosphere inferred from its thermal evolution, Journal of Geophysical Research 94, 17, 421-36.

Artemieva, IM and Meissner, R 2012, Crustal thickness controlled by plate tectonics: a review of crust-mantle interaction processes illustrated by European examples. Tectonophysics, vol 530-531, pp. 18-49. DOI: 10.1016/j.tecto.2011.12.037

Artemieva, I.M., Thybo, H., 2013. EUNAseis: A seismic model for Moho and crustal structure in Europe, Greenland, and the North Atlantic region. Tectonophysics 609, 97–153.

Autran, A., Chantraine, J., Lorenz, C., Mégnion, C., Weber, C., 1992. Conclusions générales. Forage Scientifique de Sancerre- Couy (Cher). Mém. GPF 3, 209– 212.

BABEL Working Group, 1993a. Deep seismic reflection/refraction interpretation of crustal structure along BABEL profiles A and B in the southern Baltic Sea. Geophys. J. Int. 112, 325–343.

Banka, D., Pharaoh, T.C. and Williamson, J.P. and TESZ Project Potential Field Core Group, 2002. Potential field imaging of Palaeozoic orogenic structures in northern and central Europe. Tectonophysics 360, 23-45.

Baranov V., 1957: A new method for interpretation of aeromagnetic maps: Pseudo gravimetric anomalies. Geophysics, 22, 359-383.

Baranov, W., 1976. Potential Fields and Their Transformations in Applied Geophysics, Gebruder-Borntraeger, Berlin.

Battaglia M., Murray M.H., Serpelloni E., and R. Bürgmann, 2004. The Adriatic region: an independent microplate within the Africa-Eurasia collision zone. Geophys.Res. Lett., 31(9), L09605, 10.1029/2004GL019723.

Beardsmore, G. R., and J. P. Cull, 2001. Crustal Heat Flow, Cambridge Univ. Press, Cambridge.

Belka, Z., Ahrendt, H., Franke, W. and Wemmer, K. 2000. The Baltica-Gondwana suture in Central Europe: evidence from K-Ar ages of detrital muscovites and biogeographical data, 87–102.

Beránek, B., and A. Dudek, 1972, The results of deep seismic sounding in Czechoslovakia, Z. Geophys., 38, 415–427.

Bertotti G, Picotti V, Cloetingh S, 1998. Lithospheric weakening during ‘‘retro-foreland’’ basin formation: tectonic evolution of the central South Alpine foredeep. Tectonics 17(1):131–142

Bielik, M., J. Séfara, J. Sotak, M. Kováč, V. Bezák, and D. Plašienka, 2004. The western Carpathians: Interaction of Hercynian and Alpine processes, Tectonophysics, 393, 63 – 86.

Blakely, R.J., 1996. Potential theory in gravity and magnetic applications. Cambridge Univ. Press, 441 p.

Blakely, R.J., Brocher, T.M., Wells, R.E., 2005. Subduction-zone magnetic anomalies and implications for hydrated forearc mantle. Geology 33 (6), 445–448.

Blundell, D., Freeman, R., and Mueller, S., 1992. (Eds.) A Continent Revealed – The European Geotraverse. European Science Foundation, Cambridge University Press, Cambridge, 287.

Boccaletti, M., Innocenti, F., Manetti, P., Mazzuoli, R., Motamed, A., Pasquare, G., Radicati di Brozolo, F., Amin Sobhani, E., 1976. Neogene and Quaternary volcanism of the Bijar Area (Western Iran), Bull. Volcanologique, 40-2, 121-133.

Bogdanova S.,Gorbatchev R.,Grad M., Janik T., Guterch A., Kozlovskaya E., Motuza G., Skridlaite G., Starostenko I., Taran L., and Eurobridge and Polonaise working Group, 2006. EUROBRIDGE: new insight into the geodynamic evolution of East European Craton, In Gee D.G.,Stephenson R.A (eds) European Lithosphere Dynamics. Geol.Soc.,London,Memoirs 32: 599-625.

Bostock, M.G., Hyndman, R.D., Rondenay, S., Peacock, S.M., 2002. An inverted continental Moho and serpentinization of the forearc mantle. Nature 417, 536–538.

Bosum, W. and Wonik, T., 1991. Magnetic anomaly pattern of Central Europe, Tectonophysics, 195, 43–64.

Brückl E., Bodoky T., Hegedûs E., Hrubcová P., Gosar A., Grad M., Guterch A., Hajnal Z., Keller G. R., Špičák A., Sumanovac F., Thybo H., Weber F. and ALP 2002 Working Group, 2003. ALP 2002 seismic experiment. Stud. Geoph. Geod., 47 (3): 671–679.

Cabanis, B., Thiéblemont, D., 1992. Géochemie des protolithes. Forage Scientifique de Sancerre-Couy (Cher). Mém. GPF 3, 123– 128.

Canny, J., 1986,Acomputational approach to edge detection: IEEE Transactions on Pattern Analysis and Machine Intelligence, 8, 679–698.

Carminati E, Doglioni C, Scrocca D, 2003. Apennines subduction-related subsidence of Venice. Geophys Res Lett 30. doi:10.1029/2003GL017001.

Čermák V., 1975. Temperature-depth profiles in Czechoslovakia and some adjacent areas derived from heat-flow measurements, deep seismic sounding and other geophysical data, Tectonophysics, Volume 26, Issue 1. Pages 103-119, ISSN 0040-1951, http://dx.doi.org/10.1016/0040-1951(75)90116-X.

Čermák, V. and Rybach, L. 1979. Terrestrial Heat Flow in Europe. Springer Berlin, Heidelberg and New York, 329 p Cermak, 1882. Crustal temperatures and mantle heat flow in Europe. Tectonophysics, 83, 123 -142.

Čermák, V., 1982. Regional pattern of the lithospheric thickness in Europe. In: V. Čermákand and R. Haenel (Editors), Geothermics and Geothermal Energy. Schweizerbart, Stuttgart, pp. 1- 10.

Čermák, V., and Bodri, L., 1986. 2D temperature modeling along five East-European geotraverses. J. Geodyn., 5, 133-163 pp.

Čermák, V., J. Šafanda, and A. Guterch, 1989. Deep temperature distribution along three profiles crossing the Teisseyre-Tornquist tectonic zone in Poland, Tectonophysics, 164, 151– 163.

Čermák V., Král M., Krešl M., Kubík J., Šafanda J., 1991. Heat flow, regional geophysics and lithosphere structure in Czechoslovakia and adjacent part of Central Europe. In Terrestrial heat flow and the lithosphere structure, edited by E. Hurtig and L. Rybach, Springer, Berlin, 133–165.

Čermák, V., 1993. Lithospheric thermal regimes in Europe, Phys. Earth Planet. Inter., 79, 179–193.

Čermák, V., and L. Bodri, 1995. Three-dimensional deep temperature modelling along the European geotraverse, Tectonophysics, 244 (1-3), 1-11.

Chadwick, R.A. and Pharaoh, T.C., 1998. The seismic reflection Moho beneath the United Kingdom and adjacent areas, Tectonophysics, 299, 255–279.

Chapman, D.S. and Pollack, H.N., 1975b. Global heat flow: a new look. Earth Planet. Sci. Lett., 28: 23-32.

Chiozzi, P., Matsushima, J., Okubo, Y., Pasquale, V., Verdoya, M., 2005. Curie-point depth from spectral analysis of magnetic data in central-southern Europe. Phys. Earth Planet. Inter. 152 (4), 267–276.

Christensen NI, Mooney WD. 1995. Seismic velocity structure and composition of the continental crust: a global view. J. Geophys. Res. 100(B6):9761–88.

Cocks, L.R.M., Fortey, R.A., 1982. Faunal evidence for oceanic separations in the Palaeozoic of Britain. J. Geol. Soc. (Lond.) 139, 465 – 478

Counil, J.-L.; Achache, J.; and Galdeano, A., 1989. Long-wavelength magnetic anomalies in the Caribbean: plate boundaries and allochthonous continental blocks," Journal of Geophysical Research 94, 7419-31

Cooper, G.R.J., 1997. Forward modeling of magnetic data. Computer and Geosciences, 23(10), 1125–1129.

Corrado. G., Rapolla, A., Gasparini, P. and Mantovani, M.S.M., 1979. Depth of Curie temperature from aeromagnetic anomalies in southeastern Minas Gerais, Brasil. rev. Bras. Geoc., 9, 33-38.

Cuffaro M., Riguzzi F., Scrocca D., Antonioli F., Carminati E., Livani M., Doglioni C., 2010. On the geodynamics of the northern Adriatic plate, Rend. Fis. Acc. Lincei 21 (Suppl. 1): S253–S279 DOI 10.1007/s12210-010-0098-9

Dallmeyer RD, Franke W, Weber K (eds), 1995. Pre-Permian Geology of Central and Eastern Europe. Springer-Verlag, Berlin, pp 1-611.

DEKORP Research Group, 1988. Results of the DEKORP 4/KTB Oberpfalz deep seismic reflection investigations. J Geophys 62: 69–101.

De Vos, W., Verniers, J., Herbosch, A., Vanguestaine, M., 1993. A new geological map of the Brabant Massif. Geol. Mag. 130, 605– 611.

Dąbrowski, A., 1971. Physical properties of the Podlasie Depression rocks, Geol. Quart. 15, 2, 441-463 (in Polish).

Di Stefano, R., E. Kissling, C. Chiarabba, A. Amato, and D. Giardini, 2009. Shallow subduction beneath Italy: Three-dimensional images of the Adriatic-European-Tyrrhenian lithosphere system based on high-quality P wave arrival times, J. Geophys. Res., 114, B05305, doi:10.1029/2008JB005641.

Enderle, U., K. Schuster, C. Prodehl, A. Schulze, and J. Bribach, 1998, The refraction seismic experiment GRANU95 in the Saxothuringian belt, southeastern Germany, Geophys. J. Int., 133, 245 – 259, doi:10.1046/j.1365-246X.1998.00462.x

EUROBRIDGE Seismic Working Group, 1999. P- and S-wave seismic velocity structure across the Fennoscandia-Sarmatia suture of the East European Craton beneath the EUROBRIDGE profile trough Lithuania and Belarus, Tectonophysics, 314(1–3), 193–218.

Farr, T. G., P. A. Rosen, E. Caro, R. Crippen, R. Duren, S. Hensley, M. Kobrick, M. Paller, E. Rodrigues, L. Roth, D. Seal, S. Shaffer, J. Shimada, J. Umland, M. Werner, M. Oskin, D. Burbank, D. Alsdorf, P. A. R. Tom G. Farr, Edward Caro, Robert Crippen, Riley Duren, Scott Hensley, M. P. Michael Kobrick, Ernesto Rodriguez. 2007. The Shuttle Radar Topography Mission, Rev. Geophys., 45, RG2004, doi:10.1029/2005RG000183.

Ferré, E.C., Friedman, S. A., Martin-Hernandez, F., Feinberg, J. M. , Till, J. L. et al.. 2014. Eight good reasons why the uppermost mantle could be magnetic. Tectonophysics, Elsevier, 624, pp.3-14.

Gebrande H, Bopp M, Neurieder P, Schmidt T ,1989. Crustal structure in the surroundings of the KTB drill site as derived from refraction and wide-angle seismic observations. In: Emmermann R, Wohlenberg J (eds) The continental deep drilling program (KTB). Springer, Berlin Heidelberg New York, pp 151–176.

Grabowska, T. and Bojdys, G., 2001. The border of the East-European Craton in south-eastern Poland based on gravity and magnetic data. Terra Nova 13, 92–98.

Grabowska T., Bojdys G., Bielik M., Csicsay K., 2011: Density and magnetic models of the lithosphere along CELEBRATION 2000 profile CEL01. Acta Geophysica, 59, 3, 526–560

Grosse, S., W. Conrad, H.J. Behr, e T. Heinrichs. Major gravity axis and anomalies in central Europe.*Freeman R, Giese P, Mueller St (eds) Proc 5th EGT Study Centre. Eur Sci Found, Strasbourg*, 1990: 35-146.

Ladislav Roth, David Seal, J. S. Scott Shaffer, Jeffrey Umland, Marian Werner, Michael Oskin, and a. D. A. Douglas Burbank, , 2007. The Shuttle radar topography mission, Reviews of Geophysics, 45(RG2004).

Fedi, M., and Rapolla, A., 1999. 3-D inversion of gravity and magnetic data wi dep resolution: Geophysics, 64, 452–460.

Fedi, M., Primiceri, R., Quarta, T., and Villani, A. V., 2004. Joint application of continuous and discrete wavelet transform on gravity data to identify shallow and deep sources. Geophysical Journal International, 156(1), 7–21. http://doi.org/10.1111/j.1365-246X.2004.02118.x

Fedi, M., 2007. DEXP: a fast method to determine the depth and the structural index of potential fields sources, Geophysics, 72(1), I1–I11, doi:10.1190/1.2399452.

Fedi, M., Florio, G. and Quarta, T., 2009. Multiridge analysis of potential fields: geometrical method and reduced Euler deconvolution, Geophysics, 74(4), L53–L65.

Fedi, M., Cella, F., Quarta, T. and Villani, A. V., 2010. 2D Continuous Wavelet Transform of potential fields due to extended source distributions, Appl. Comput. Harmon. Anal., 28, 320–337, doi:10.1016/j.acha.2010.03.002.

Fedi, M., and L. Cascone, 2011. Composite continuous wavelet transform of potential fields with different choices of analyzing wavelets, J. Geophys. Res., 116, B07104, doi:10.1029/2010JB007882.

Fedi, M., Florio, G. and Cascone, L., 2012. Multiscale analysis of potential fields by a ridge consistency criterion: the reconstruction of the Bishop basement. Geophysical Journal International, 188: 103–114. doi: 10.1111/j.1365-246X.2011.05259.x

Fedi M., Pilkington M., 2012. Understanding imaging methods for potential field data. geophysics 77(1), G13–G24.

Fedi M. and Florio G., 2013. Determination of the maximum-depth to potential field sources by a maximum structural index method. Journal Of Applied Geophysics, 88, 154–160, Doi: 10.1016/J.Jappgeo.2012.10.009.

Fedi M., Abbas M.A., 2013. A fast interpretation of self-potential data using the depth from extreme points method. geophysics, 78(2), E107–E116. DOI:10.1190/GEO2012-0074.1

Fedi, M., Florio, G., and Paoletti, V. 2015. MHODE: a local-homogeneity theory for improved source-parameter estimation of potential fields. Geophysical Journal International, 202(2), 887-900.

Fedi, M. 2016. Scaling Laws in Geophysics: Application to Potential Fields of Methods Based on the Laws of Self-similarity and Homogeneity. In Fractal Solutions for Understanding Complex Systems in Earth Sciences. Springer International Publishing, pp. 1-18.

Ferré, E.C., Friedman, S.A., Martín-Hernández, F., Feinberg, J.M., Till, J.L., Ionov, D.A., Conder, J.A., 2014. Eight good reasons why the uppermost mantle could be magnetic. Tectonophysics 624:3–14.

Finetti, I. R., 2005. Depth contour Map of the Moho discontinuity in the Central Mediterranean region from new CROP seismic data, in CROP Project, Deep Seismic Exploration of the Central Mediterranean and Italy, edited by I. R. Finetti, pp. 597– 606, Elsevier, New York.

Fletcher, K. M. U., Fairhead, J. D., Salem, A., Lei, K, Ayala And Cabanillas, P. L. M, 2011. Building a higher resolution magnetic database for Europe for resource evaluation. First Break, v29, pp. 96-1.

Florio G. and Fedi M., 2006. Euler deconvolution of vertical profiles of potential field data. 76th Annual International Meeting, SEG, Expanded Abstracts, 958–962.

Florio, G., Fedi, M. and Rapolla, A., 2009. Interpretation of regional aeromagnetic data by multiscale methods: the case of Southern Apennines

(Italy), Geophys. Prospect., 57, 479–489.

Florio, G. and Fedi, M., 2014. Multiridge Euler deconvolution. Geophysical Prospecting, 62: 333–351. doi: 10.1111/1365-2478.12078.

Franke, W., 1989. Tectonostratigraphic units in the Variscan belt of central Europe. Geol Soc. Am. Spec Pap. 230. 67-90.

Freeman R, Mueller St, 1990. (eds) Proc 6th EGT Worksh: Data compilation and synoptic interpretation. Eur Sci Found, Strasbourg, 457 pp.

Freeman R, Giese P, Mueller St, 1990. (eds) Proc 5th EGT Study Centre. Eur Sci Found, Strasbourg, 404 pp

Frost, B.R. and Shive, P.N., 1986. Magnetic mineralogy of the lower continental crust. J. Geophys. Res. 91(B6):6513–6521.

Gaál, G. and Gorbatschcv, R. 1987: An outline of the Precambrian evolution of the Baltic Shield. Precambrian Research 35, 15-52.

Gabriel, G., Vogel, D., Scheibe, R., Lindner, H., Pucher, R., Wonik, T. and Krawczyk, C. M., 2011. Anomalies of the Earth's total magnetic field in Germany – the first complete homogenous data set reveals new opportunities for multiscale geoscientific studies. Geophysical Journal International, 184: 1113–1118. doi: 10.1111/j.1365-246X.2010.04924.x

Gajewski D, Prodehl C, 1987. Seismic refraction investigation of the Black Forest. Tectonophysics 142: 27–48

Gasparini, P., Mantovani, M. S. M., Shukowsky, W., 1981. Interpretation of long wavelength anomalies, The Solution of the Inverse Problem in Geophysical Interpretation. R. Cassinis, 231–255, Plenum, New York.

Gebrande, H., M. Bopp, P. Neurieder, and T. Schmidt, 1989. Crustal structure in the surroundings of the KTB drill site as derived from refraction and wide-angle seismic observations, in The German Continental Deep Drilling Program (KTB), edited by R. Emmetmann and J. Wohlenberg, pp. 37-54, Springer-Verlag, New York.

Gibert, D., and Galdeano, A., 1985. A computer program to perform transformations of gravimetric and aeromagnetic survey. Comp. and Geosc., 11, 553–588.

Giese, P., and Pavlenkova, N.I., 1988. Structural maps of the Earth's crust in Europe. Izv. Akad. Nauk SSSR Fiz. Zemli 10, 3–14 (in Russian).

Giori, I., Caratori Tontini, F., Cocchi, L., Carmisciano, C., Bologna, C., Camorali, C.,Samarzija, J., Taylor, P., 2007. The Adriatic magnetic anomaly. In: EGM 2007International Workshop Innovation in EM, Grav and Mag Methods: A NewPerspective for Exploration Capri, Italy, 16–18 April.

Grabowska, T. and Bojdys, G., 2004. Preliminary density and magnetic models of the lithosphere along seismic profile P4 of the international project POLONAISE'97 in Poland, Geophys. Res. (Abstract), 6.

Grabowska, T., Bojdys, G., Bielik, M., Csicsay, K., 2011, Density and magnetic models of the lithosphere along CELEBRATION 2000 profile CEL01, Acta Geophysica, 59, 3, 526.

Grad M., Jensen S. L., Keller G. R., Guterch A., Thybo H., Janik T., Tiira T., Yliniemi J., Luosto U., Motuza G., Nasedkin V., Czubaw., Gaczyñski E., Oeroda P., Miller K. C., Wilde-Piórko M, Komminaho K., Jacyna J. and Korabliova L., 2003a. Crustal Structure of the Trans-European suture zone region along POLONAISE'97 seismic profile P4. J. Geoph. Res., 108 (B11).

Grad, M., A. Guterch, S. Mazur, G. R. Keller, A. Špičák, P. Hrubcová, and W. H. Geissler (2008), Lithospheric structure of the Bohemian Massif and adjacent Variscan belt in central Europe based on profile S01 from the SUDETES 2003 experiment, J. Geophys. Res., 113, B10304, doi:10.1029/2007JB005497.

Grad, M., Tiira, T., and Group, E. W., 2009. The Moho depth map of the European Plate, Geophys. J. Int., 176(1), 279–292.

Grosse S, Conrad W, Behr HJ, Heinrichs T, 1990. Major gravity axis and anomalies in central Europe. In: Freeman R, Giese P, Mueller St (eds) Proc 5th EGT Study Centre. Eur Sci Found, Strasbourg, pp 35–146

Guterch, A., Grad,M., Materzok, R., Perchuc, E., 1986. Deep structure of the Earth's crust in the contact zone of the Palaeozoic and Precambrian platforms in Poland (Tornquist–Teisseyre Zone). Tectonophysics 128 (3–4), 251–279.

Guterch, A., Grad, M., Thybo, H., Keller, G.R. and the POLONAISE WorkingGroup, 1999. POLONAISE'97—international seismic experiment between Precambrian and Variscan Europe in Poland, Tectonophysics, 314, 101–121.

Guterch A., Grad M., Keller G. R. And Celebration 2000 Organizing Committee, 2001. Seismologists Celebrate the New Millenium with an Experiment in Central Europe. Eos Trans. Am. Geophys. Union, 82 (45): 529, 534–535.

Guterch A., Grad M., Keller G. R., Posgay K., Vozár J., Špičák A., Brückl E., Hajnal Z., Thybo H., Selvi O. and Celebration 2000 Experimant Team, 2003a. CELEBRATION 2000 seismic experiment. Stud. Geoph. Geod., 47 (3): 659–669.

Guterch A., Grad M., Špičák A., Brückl E., Hegedûs E., Keller G. R., Thybo H. and CELEBRATION 2000, ALP 2002, SUDETES 2003 Working Groups, 2003b. An overview of recent seismic refraction experiments in Central Europe. Stud. Geoph. Geod., 47 (3): 651–657.

Guterch, A. and Grad, M., 2006. Lithospheric structure of the TESZ in Poland based on modern seismic experiments. Geological Quarterly, [S.l.], v. 50, n. 1, p.23-32, ISSN 1641-7291.

Hacker, B. R., P. B. Kelemen, and M. D. Behn, 2011. Differentiation of the continental crust by relamination, Earth Planet. Sci. Lett., 307, 501–516.

Hahn, A. and Wonik, T., 1990. Interpretation of aeromagnetic anomalies, in Proc. Sixth Workshop European Geotraverse (EGT): Data Compilations and Synoptic Interpretation, pp. 22.5-236, eds Freeman, R and Mueller, St., Strasbourg.

Haney, M., Johnston, C., Li, Y., and Nabighian, M., 2003. Envelopes of 2D and 3D magnetic data and their relationship to the analytic signal: 73rd Ann. Internat. Mtg., Soc, Expl. Geophys., Expanded Abstracts.

Harrison, C. G. A., and Carle, H. M., 1981. Intermediate wavelength magnetic anomalies over ocean magnetic anomalies over ocean basins, Journal of Geophysical Research 86, 11,585-99.

Hemant, K., and Maus, S. 2005. Geological modeling of the new CHAMP magnetic anomaly maps using a geographical information system technique, J. Geophys. Res., 110, B12103, doi:10.1029/2005JB003837.

Henkel, H., 1994. Standard diagrams of magnetic properties and density--a tool for understanding magnetic petrology. J. Appl. Geophys., 32: 43-53.

Hornby, P., F. Boschetti, and F. G. Horovitz, 1999, Analysis of potential field data in e wavelet domain: Geophysical Journal International, 137, 175–196.

Horváth, F., 1993. Towards a kinematic model for the formation of the Pannonian basin. Tectonophysics, 226, 333–357.

Horváth, G., F. Bada, P. Szafián, G. Tari, A. Adám, and S. Cloetingh, 2006. Formation and deformation of the Pannonian Basin: Constraints from observational data, in European Lithosphere Dynamics, Geol. Soc. Mem., vol. 32, edited by D. Gee and R. Stephenson, pp. 191– 206, Geol. Soc., London.

Hrubcová, P., Środa, P., Špičák, A., Guterch, A., Grad, M., Keller, G. R., Brueckl, E. and Thybo H., 2005. Crustal and uppermost mantle structure of the Bohemian Massif based on CELEBRATION 2000 data, J. Geophys. Res., 110, B11305, doi:10.1029/2004JB003080.

Hsu S.-K. 2002. Imaging magnetic sources using Euler's equation.Geophysical Prospecting 50, 15–25

Huang Y, Chubakov V, Mantovani F, Rudnick RL, McDonough WF. 2013. A reference Earth model for the heat-producing elements and associated geoneutrino flux. Geochem. Geophys. Geosyst. 14:2003–29

Hunt, C. P., Moskowitz, B. M. and Banerjee, S. K., 1995. Magnetic Properties of Rocks and Minerals, in Rock Physics and Phase Relations: A Handbook of Physical Constants (ed T. J. Ahrens), American Geophysical Union, Washington, D. C.. doi: 10.1029/RF003p0189.

Hurtig, E., Čermák, V., Haenel, R. and Zui, V.I. (Editors), 1992. Geothermal Atlas of Europe. Haack, Gotha.

Jacoby, L. L., 1991. A process dissociation framework: Separating automatic from intentional uses of memory. Journal of Memory and Language, 30, 513-541.

Janutyte, I. *et al*., 2014. Upper mantle structure around the Trans-European Suture Zone obtained by teleseismic tomography, Solid Earth Discussions,6(2), 1723–1763.

Jensen, S.L., Thybo, H., Polonaise'97 Working Group., 2002. Moho topography and lower crustal wide-angle reflectivity around the TESZ in southern Scandinavia and northeastern Europe. Tectonophysics 360 (1–4), 187–213.

Juracic M., Novosel A., Tibljas D. and Balen D., 2004. Jabuka shoal, a new location with igneous rocks in the Adriatic Sea. Geologia Croatica, 57/1, 81-85.

Karaczun, K., Karaczun, M., Bilin´ska, M., Uhrynowski, A., 1978. Magnetic Map of Poland; anomalies of vertical component ‘‘Z’’ of the geomagnetic field, 1:500000. Państw. Inst. Geol. Warszawa.

Keating, P. and Pilkington, M., 2004. Euler deconvolution of the analytic signal and its application to magnetic interpretation, Geophys. Prospect., 52, 165–182.

Kelly, A., R. W. England, and P. K. H. Maguire (2007), A crustal seismic velocity model for the UK, Ireland and surrounding seas, Geophys. J. Int., 171, 1172–1184.

Kis KI, Taylor PT, Wittmann G, Toronyi B, Puszta S. 2011. Inversion of magnetic measurements of the CHAMP satellite over the Pannonian Basin. J. Applied Geophysics 75: 412-418

Knapmeyer-Endrun, B., Krüger, F. and the PASSEQ Working Group, 2014. Moho depth across the Trans-European Suture Zone from P- and S-receiver functions. Geophys. J. Int. doi:10.1093/gji/ggu035.

Korja A, Heikkinen P., 2005. The Accretionary Svecofennian Orogen – insight from the BABEL profiles. Precambrian Res 136:241–268.

Królikowski, C., 2006. Crustal-scale complexity of the contact zone between the Palaeozoic Platform and the East-European Craton in the NW Poland. Geological Quarterly, 50, 33-42

Krs M., Krsova M., Pruner P. and Havlicek V., 1986. Paleomagnetism, palaeogeography and multi-component analysis of magnetisation of Ordovician rocks of the Barrandian in the Bohemian Massif. Sbornik Geologickych Ved, Uzita Geofyzika, 22: 9-48.

Kubeš P., Bezák V., Kucharič, L’., Filo M., Vozár J., Konečnỳ V., Kohút M., Gluch A., 2010. Magnetic field of the Western Carpathians (Slovakia): reflections on the structure of the crust. Geologica Carpathica, 61, 5, 437–447.

Kummerow J., Kind R., Oncken O., Giese P., Ryberg T., Wylegalla K., Scherbaum F., TRANSALP Working Group, 2004. A natural and controlled source seismic profile through the Eastern Alps: TRANSALP. Earth Planet. Sci. Lett.;225:115–129.

Landes, M., J. R. R. Ritter, P. W. Readman, and B. M. O’Reilly (2005), A review of the Irish crustal structure and signatures from the Caledonian and Variscan Orogenies, Terra Nova, 17, 111 –120.

Lanza, R. and Meloni, A., 2006. The Earth’s Magnetism - An Introduction for Geologists, Springer-Verlag Berlin Heidelberg.

Lee, W. H. K., and S. Uyeda, 1965. Review of heat flow data, in Terrestrial Heat Flow, edited by W. H. K. Lee, pp. 87– 190, A. G. U., Washington, D. C.

Lefort, J.P., Bardy, P., Poulpiquet, J., 1991. Interprétation des anomalies magnétiques reconnues en Marche occidentale et mer Celtique le long des profils SWAT. Mém. Soc. Géol. Fr. 159, 133– 134, 220 pp.

Li, X., 2005. Rejecting erroneous estimates in werner deconvolution: an inversion approach. SEG Technical Program Expanded Abstracts 2005. 676-679.

Luosto, U., 1991. Structure and dynamics of the Fennoscandian lithosphere, Report No. S-25, Inst. Seismology, Univ. Helsinki, pp. 43–49.

Lüschen E, Wenzel F, Sandmeier K-J, Menges D, Rühl Th, Stiller M, Janoth W, Keller F, Söllner W, Thomas R, Krohe A, Stenger R, Fuchs K, Wilhelm H, Eisbacher G, 1989. Near-vertical and wide-angle seismic surveys in the Schwarzwald. In: Emmermann R, Wohlenberg J (eds) The German Continental Deep Drilling Program (KTB). Springer, Berlin Heidelberg New York, pp 297–362.

Majorowicz, J. A., V. Čermák, J. Šafanda, P. Krzywiec, M. Wroblewska, A. Guterch, and M. Grad, 2003. Heat flow models across the Trans-European Suture Zone in the area of the POLONAISE '97 seismic experiment, Phys. Chem. Earth, 28, 375–391.

Majorowicz, J. and Wybraniec, S., 2011. New terrestrial heat flow map of Europe after regional paleoclimatic correction application, Int. J. Earth. Sci., 100, 881–887.

Mallat,A. and Hwang W.L., 1992. Singularity detection and processing with wavelets, IEEE Trans. Inform. Theory 38 (2) 617–643.

Mallat, S., and Zhong, S., 1992. Characterization of signals from multiscale edges. IEEE Transactions on Pattern Analysis and Machine Intelligence, 710–732.

Mancinelli, P., Pauselli, C., Minelli, G., Federico, C., 2015. Magnetic and gravimetric modeling of the central Adriatic regio. Journal of Geodynamics, Volume 89, September 2015, Pages 60-70, ISSN 0264-3707, http://dx.doi.org/10.1016/j.jog.2015.06.008.

Martelet, G., Sailhac, P., Moreau, F., and Diament, M. (2001). Characterization of geological boundaries using 1-D wavelet transform on gravity data: Theory and application to the Himalayas. Geophysics, 66(4), 1116.

Mastellone D., Fedi M., Ialongo S., Paoletti V., 2014: Volume upward continuation of potential fields from the minimum-length solution: an optimal tool for continuation through general surfaces. Journal of Applied Geophysics, 111, 346-355, DOI 10.1016/j.jappgeo.2014.10.020.

Maus S., F. Yin, H Luhr, C. Manoj, M. Rother, J. Rauberg, I. Michaelis, C. Stolle and R. D. Muller, 2008. Resolution of direction of oceanic magnetic lineations by the sixth-generation lithospheric magnetic field model from CHAMP satellite magnetic measurements. Geochemistry, Geophysics and Geosystems, 9, Q07021, doi:10.1029/2008GC001949

Maus, S., U. Barckhausen, H. Berkenbosch, N. Bournas, J. Brozena, V. Childers, F. Dostaler, J. D. Fairhead, C. Finn, R. R. B. von Frese, C. Gaina, S. Golynsky, R. Kucks, H. Lühr, P. Milligan, S. Mogren, D. Müller, O. Olesen, M. Pilkington, R. Saltus, B. Schreckenberger, E.Thébault, and F. Caratori Tontini, 2009. EMAG2: A 2–arc min resolution Earth Magnetic Anomaly Grid compiled from satellite, airborne, and marine magnetic measurements, Geochem. Geophys. Geosyst., 10, Q08005, doi:10.1029/2009GC002471.

Maus, S., 2010. An ellipsoidal harmonic representation of Earth's lithospheric magnetic field to degree and order 720. Geochem Geophys Geosyst 11(6):Q06015. doi:10.1029/2010GC003026).

McCann, T., 2008. The Geology of Central Europe, Precambrian and Palaeozoic, Mesozoic and Cenozoic. vol. 2, 748 pp., 1449 pp., vol. 1, Geol. Soc. of London, London.

McEnroe, S. A., F. Langenhorst, P. Robinson, G. D. Bromiley, and C. S. J. Shaw, 2004. What is magnetic in the lower crust?, Earth Planet. Sci. Lett., 226, 175–192, doi:10.1016/j.epsl.2004.07.020.

McGrath, P.H., 1991. Zero crossover—a FORTRAN program to determine the dip and extent of a geological boundary using horizontal derivatives of upward continued gravity data, Comput. Geosci., 17(7), 1017–1032.

MacLeod, I.N., Jones, K., and Dai,T. F., 1993. 3-D Analytic signal in the interpretation of total magnetic field data at low magnetic latitudes: Expl. Geophys., 24, 679–688.

Meissner, R., 1986. The continental crust – a geophysical approach, International Geophysics Series, Academic Press Inc., Orlando, 34, 426 pp.

Meissner, R., Wever, T. and Flueh, E.R., 1987. The Moho in Europe implications for crustal development, Ann. Geophys., 5B, 357–364.

Milano, M., M. Fedi, and J. D. Fairhead, 2016. The deep crust beneath the Trans-European Suture Zone from a multiscale magnetic model, J. Geophys. Res. Solid Earth, 121, 6276–6292, doi:10.1002/2016JB012955.

Millon, R., 1992. Formations magnétiques. Forage Scientifique de Sancerre-Couy (Cher). Me´m. GPF 3, 169–181.

Molina Garza, R. S., and J. D. A. Zijderveld, 1996. Paleomagnetism of Paleozoic strata, Brabant and Ardennes Massifs, Belgium: Implications of prefolding and postfolding Late Carboniferous secondary magnetizations for European apparent polar wander, J. Geophys. Res., 101, 15,799 – 15,818.

Mongelli, F., G. Zito, N. Ciaranfi, and P. Pieri, 1989. Interpretation of heat flow density of the Apennine chain, Italy, Tectonophysics, 164, 267–280.

Moreau, F., Gibert, D., Holschneider, M. and Saracco, G., 1997. Wavelet analysis of potential fields, Inverse Probl., 13, 165–178, doi:10.1088/ 0266-5611/13/1/013.

Mushayandebvu, M.F., van Driel P., Reid A.B. and Fairhead J.D., 2001. Magnetic source parameters of two-dimensional structures using extended Euler deconvolution. Geophysics, p. 814-823, doi:10.1190/1.1444971.

Nabighian, M. N., 1972. The analytic signal of two-dimensional magnetic bodies with polygonal cross-section: Its properties and use for automated anomaly interpretation: Geophysics, 37, 507-517.

Nabighian, M. N., and R. O. Hansen, 2001, Unification of Euler and Werner deconvolution in three dimensions via the generalized Hilbert transform: Geophysics, 66, 1805–1810, doi: 10.1190/1.1487122.

Nolet G. and Zielhuis A., 1994. Low S velocities under the Tornquist–Teisseyre zone: Evidence for water injection into the transition zone by subduction, J. geophys. Res. , 99, 15813–15820.

Olmsted, J.M.H., 1991. Advanced Calculus, Meredith, 706 p.

Oncken, O., 1997: Transformation of a magmatic arc and an orogenic root during oblique collision and it's consequences for the evolution of the European Variscides (Mid-German Crystalline Rise), Geologische Rundschau 86, pp. 2-20. DOI: 10.1007/s005310050118

Oppenheim, A.V. and Schafer, R.W., 1975. Discrete-Time Signal Processing. Prentice-Hall, Englewood Cliffs.

Pamic J. and Balen D., 2005. Interaction between PermoTriassic rifting, magmatism and initiation of the Adriatic Dinaric Carbonate platform (ADCP). Acta Geologica Hungarica, 48/2, 181-204.

Pashkevich, I.K., Markovsky, V.S., Orlyuk, M.I., Eliseeva, S.V., Mozgovaya, A.P. and Tarashchan, S.A., 1990. Magnetic Model for the Lithosphere of Europe. Naukova Dumka, Kiev, 165 pp. (in Russian).

Pashkevich, I.K., Orlyuk, M.I., Eliseeva, S.V. and Mozgovaya, A.P., 1993. Magnetic inhomogeneities of the continental Europe. In: A.V. Chekunov (Editor), The Lithosphere of Central and Eastern Europe. Naukova Dumka, Kiev, pp. 82-97 (in Russian).

Paul, M.K., Datta, S. and Banerjee, B., 1966. Direct interpretation of two dimensional structural faults from gravity data, Geophysics, 31, 940–948.

Paul, M.K. and Goodacre, A.K., 1984. The gravity profile and its role in positioning the edge of a two-dimensional faulted structure having an arbitrary vertical variation of density, Geophysics, 49, 1097–1104.

Pavlenkova, N.I., 1996. Crust and upper mantle structure in northern Eurasia from seismic data. Advances in Geophysics 37, 1–133.

Pavlis, N. K., S. A. Holmes, S. C. Kenyon, and J. K. Factor, 2012. The development and evaluation of the Earth Gravitational Model 2008 (EGM2008), J. Geophys. Res., 117, B04406, doi:10.1029/2011JB008916.

Pedersen, L.B., 1991. Relations between potential fields and some equivalent sources, Geophysics, 56, 961–971.

Petecki Z., Polechoñska O., Wybraniec S. and Cieoela E., 2003. Magnetic map of Poland at a scale of 1:500 000. Parts A and B on CD-rom. Pañstw. Inst. Geol. Warszawa.

Pharaoh, T.C., Brewer, T.S., Webb, P.C., 1993. Subduction-related magmatism of late Ordovician age in eastern England. Geol. Mag. 130, 647– 656.

Pharaoh, T.C., Gibbons, W., 1994. Precambrian rocks in England and Wales south of the Menai Strait Fault System, pp. 85–97. In: Gibbons, J.S., Harris, A.L. (Eds.), A revised correlation of Precambrian rocks in the British Isles. Geol. Soc. Lond., 110 pp.

Pharaoh, T.C., 1999. Palaeozoic terranes and their lithospheric boundaries within the Trans-European Suture Zone (TESZ): a review. Tectonophysics, 314 (1-3). 17-41. 10.1016/S0040-1951(99)00235-8.

Pinter, N. and Grenerczy, G., 2006. Recent advances in peri-Adriatic geodynamics and future research directions, edited by: Pinter, N., Springer Verlag, ISBN 1402042345, 1–20.

Piper, J.D.A., 1987. Palaeomagnetism and the Continental Crust. Open Univ. Press, Milton Keynes, 434 pp.

Plant, J.A., A. Whittaker, A. Demetriades, B. De Vivo, e J. Lexa , 1998. The Geological and Tectonic Framework of Europe. Eurogeosurveys, British Geological Survey.

Plewa, S., 1998. Map of heat flow in Poland, in Tectonic Atlas of Poland, edited by J. Znosko, plate 5, Pol. Geol. Inst., Warsaw.

Pucher, R., 1994. Pyrrohotite-induced aeromagnetic anomalies in western Germany. J. Appl. Geophys., 32: 32-42.

Pucher, R. and Wonik, T., 1998. A new interpretation of the MAGSAT anomalies of Central Europe. Phys. Chem. Earth, 23, 9-10: 981-985.

Radulescu, F., 1988. Seismic models of the crustal structure in Romania, Rev. Roum. Geol. Geophys. Geogr. Ser. Geophys., 32, 13–17.

Ravat, D.N., Hinze, W.J. and Taylor, P.T., 1993. European tectonic features obselwed by Magsat. Tectonophysics, 220: 157-173.

Reid, A. B., Allsop, J. M., Granser, H., Millet, A. J., and Somerton, I. W. 1990. Magnetic interpretation in three dimensions using Euler deconvolution: Geophysics, 55, 80–91.

Reid, A. B., FitzGerald, D., and Flanagan, G. 2005. Hybrid Euler magnetic basement estimation: Bishop 3D tests: 75thAnnual International Meeting, SEG, ExpandedAbstracts, 671–673.

Reynolds, R. L., Magnetic titanohematite minerals in uranium-bearing sandstones, U.S. Geol. Surv. Open File Rep., 77-355, 21 pp., 1977.

Robinson, P., R. Harrison, S. McEnroe, and R. Hargraves, 2002. Lamellar magnetism in the hematite-ilmenite series as an explanation for strong remanent magnetization, Nature, 418, 517–520, doi:10.1038/nature00942.

Roest,W. R., Verhoef, J., and Pilkington, M., 1992, Magnetic interpretation using 3-D analytic signal: Geophysics, 57, 116–125.

Roest, W. R. and Pilkington, M., 1993. Identifying remanent magnetization effects in magnetic data: Geophysics, 58, 653-659.

Rehault J.P., Moussat E., Fabbri A., 1987. Structural evolution of the Tyrrhenian back-arc basin. Mar. Geol., 74: 123-150.

Ridsdill-Smith, T.A., 2000. The application of the wavelet transform to the processing of aeromagnetic data [Ph.D. Thesis]: Perth, University of Western Australia, 173 p.

Rudnick, R.L., Goldstein, S.L., 1990. The Pb isotopic compositions of lower crustal xenoliths and the evolution of lower crustal Pb. Earth and Planetary Science Letters 98 (2), 192–207.

Rudnik, R. L., e D. M. Fountain., 1995. Nature and composition of the continental crust: a lower crustal perspective. Reviews of Geophysics, 33, 3 ,267-309.

Rudnick, R.L., Gao, S., 2003. Composition of the continental crust. In: Rudnick, R.L. (Ed.), The Crust. Treatise on Geochemistry. Elsevier-Pergamon, Oxford, pp. 1–64.

Rudnick, R.L. and Gao, S., 2014. The Composition of the Continental Crust, pp. 1-51, In: The Crust (2014), R.L. Rudnick, editor, Treatise on Geochemistry, Second Edition, Volume 4, (eds. H.D. Holland and K.K. Turekian), Elsevier-Pergamon, Oxford 805 p.

Sailhac, P., and D. Gibert, 2003, Identification of sources of potential fields with the continuous wavelet transform: Two dimensional wavelets and multipolar approximations: Journal of Geophysical Research, 108, doi: 10.1029/2002JB002021.

Salem, A., Ravat, D., Gamey, T. J., and Ushijima, K., 2002. Analytic signal approach and its applicability in environmental magnetic investigations, J. Appl. Geophys., 49, 231–244.

Salem A. and Ravat D. 2003. A combined analytic signal and Euler method (AN-EUL) for automatic interpretation of magnetic data. Geophysics 68, 1952–1961.

Saracco, G., Labazuy, P., Moreau, F., 2004. Localization of self-potential sources in volcano-electric effect with complex continuous wavelet transform and electrical tomography methods for an active volcano, Geophys. Res. Lett. 31 L12610, doi:10.1029/2004GL019554.

Sass, J.H., and Lachenbruch, A.H., 1979. The thermal regime of the Australian continental crust. In M.W. McElhinny (editor), The Earth - Its origin, structure and evolution. Academic Press.

Scarascia, S. and Cassinis, R., 1997. Crustal structures in the central-eastern Alpine sector: a revision of the available DSS data, Tectonophysics, 271, 157–188.

Scheck, M., U. Bayer, V. Otto, J. Lamarche, D. Banka, and T. Pharaoh, 2002. The Elbe Fault System in North Central Europe—a basement controlled zone of crustal weakness, Tectonophysics, 360, 281– 299.

Schellschmidt, R., Hurter, S., Förster, A., and Huenges, E.: Germany, in: Hurter, S., and Haenel, R. (Eds.), 2002. Atlas of Geothermal Resources in Europe, pp 32-35, plate 20-24, Office for Official Publications of the European Communities, Luxemburg.

Schmoll J, Bittner R, Dürbaum HJ, Heinrichs T, Meissner R, Reichert C, Rühl T, Wiederhold H, 1989. Oberpfalz deep seismic reflection survey and velocity studies. In: Emmermann R, Wohlenberg J (eds) The continental deep drilling program (KTB). Springer, Berlin Heidelberg New York, pp 99–149.

Scrocca D., Doglioni C., Innocenti F., et al., 2003. CROP Atlas: seismic reflection profiles of the Italian Crust. Mem. desc. Carta Geologica d'Italia.

Sen, G. and Jones, R.E., 1988. Exsolved silicate and oxide phases from clinopyroxenes in a single Hawaiian xenolith: Implications for oxidation state of the Hawaiian uppermantle. Geology 16 (1), 69–72.

Shearer, S. and Li, Y., 2004. 3D Inversion of magnetic total gradient data in the presence of remanent magnetization. SEG Technical Program Expanded Abstracts 2004: pp. 774-777.

Smith R.S., Thurston J.B., Dai T.-F. and MacLeod I.N. 1998. iSPITM – the improved source parameter imaging method. Geophysical Prospecting 46, 141–151.

Spector, A., Grant, F.S., 1970. Statistical models for interpreting aeromagnetic data. Geophysics 35, 293–302.

Speranza, F., and M. Chiappini, 2002. Thick-skinned tectonics in the external Apennines, Italy: New evidence from magnetic anomaly analysis, J. Geophys. Res., 107(B11), 2290, doi:10.1029/2000JB000027.

Środa, P., Czuba, W., Grad, M., Guterch, A., Tokarski, A.K., Janik, T., Rauch, M., Keller, G.R., Hegedüs, E., Vozár, J., and CELEBRATION 2000 Working Group, 2006. Crustal and upper mantle structure of the Western Carpathians from CELEBRATION 2000 profiles CEL01 and CEL04: seismic models and geological implications, Geophys. J. Int. 167, 2, 737-760, doi: 10.1111/j.1365-246X.2006.03104.x.

Stavrev, P. Y., 1997, Euler deconvolution using differential similarity transformations of gravity or magnetic anomalies: Geophysical Prospecting, 45, 207–246.

Steenland, N.C., 1968. On: "The geomagnetic gradiometer" by H. A. Slack, V. M. Lynch, and L. Langan (GEOPHYSICS, October 1967, p. 877–892). Geophysics, 33, 680–683.

Švancara J, Gnojek I, Hubatka F, Dědáček K, 2000. Geophysical field pattern in the west Bohemian geodynamic active area. Stud Geoph Geod 44: 307-326

Tait J., Schatz M., Bachtadse V. and Soffel H.C., 2000. Palaeomagnetism and Palaeozoic palaeogeography of Gondwana and European terranes. In Franke W., Haak V., Oncken O. and Tanner D. (Eds.), Orogenic Processes: Quantification and Modelling in the Variscan Belt. Geological Society, London: 21-34.

Taylor, P.T. and Ravat, D., 1995.An interpretation of the MAGSAT Anomalies of Central Europe, J. Appl. Geophys., 34, 83-91.

Tesauro, M., Kaban, M.K. and Cloetingh, S.A.P.L., 2008. EuCRUST-07: a new reference model for the European crust, Geophys. Res. Lett., 35, L05313, doi:10.1029/2007GL032244.

Thominski, H.P., Wohlenberg, J. and Bleil, U., 1993. The remagnetization of Devono-Carboniferous sediments from the Ardenno-Rhenish Massif. Tectonophysics, 225:411-431.

Thybo, H., A seismic velocity model along the EGT profile— fromthe North German Basin into the Baltic Shield. In: Freeman, R., Giese, P.,Muller, S.T. (Eds.), 1990. The European Geotraverse. Integrative Studies. European Science Foundation, Strasbourg, pp. 99–108.

Thybo, H., 1997. Geophysical characteristics of the Tornquist Fan area, northwest TESZ: indication of Late Carboniferous to Early Permian dextral transtension. Geol. Mag. 134, 597–606

Thybo, H., 2001. Crustal structure along the EGT profile across the Tornquist Fan interpreted from seismic, gravity and magnetic data. Tectonophysics, 334, 155-190.

Tomek Č., Dvořáková V. and Vrána S., 1997: Geological interpretation of the 9HR and 503M seismic profiles in Western Bohemia. In Geological model of western Bohemia related to the KTB borehole in Germany, eds. S.Vrana and V.Stedra, J.Geol.Sci., Prague, 47, 43-50.

Trench, A. and Torsvik, T.H. 1992. The closure of the Iapetus Ocean and Tornquist Sea: new palaeomagnetic constraints. Journal of the Geological Society, London, 148,423-425.

Trifonova, P., Zhelev, Z., Petrova, T., Bojadgieva, K., 2009. Curie point depth of Bulgarian territory infered from geomagnetic observations and its correlation with regional termal structure and seismicity. Tectonophysics 473, 362–374.

Vozár, J., F. Ebner, A. Vozárová, J. Haas, S. Kovács,M. Sudar,M. Bielik, and C. Péró (Eds.) (2010), Variscan and Alpine Terranes of the Circum-Pannonian Region, vol. 233, Geol. Inst., SAS, Bratislava.

Ziegler, P. A., 1990. Geological Atlas of Western and Central Europe, 554 pp., Shell Internationale Mattshappij B.V., The Hague, Netherlands.

Wasilewski, P.J., Thomas, H.H., Mayhew, M.A., 1979. The Moho as a magnetic boundary, Geophysical Research Letters, 6 (7), 541-544.

Wasilewski, P.J., Mayhew, M.A., 1992. The Moho as a magnetic boundary revisited. Geophys. Res. Lett. 19 (22), 2259–2262.

Wilde-Piórko, M., Świeczak, M., Grad, M., and Majdański, M., 2010. Integrated seismic model of the crust and upper mantle of the Trans-European Suture zone between the Precambrian craton and Phanerozoic terranes in Central Europe, Tectonophysics, 481, 108–115, doi:10.1016/j.tecto.2009.05.002.

Williamson, J.P., Pharaoh, T.C., Banka, D., Thybo, H., Laigle, M., Lee, M.K., 2002. Potential field modelling of the Baltica–Avalonia (Thor–Tornquist) suture beneath the southern North Sea, Tectonophysics, Volume 360, Issues 1–4, 20, Pages 47-60, ISSN 0040-1951, http://dx.doi.org/10.1016/S0040-1951(02)00346-3.

Winchester, J A. and The Pace Tmr Network Team, 2002. Palaeozoic amalgamation of Central Europe: new results from recent geological and geophysical investigations. Tectonophysics, 360, 5-2

Winterer L, Bosellini A, 1981. Subsidence and sedimentation on Jurassic passive continental margin, southern Alps Italy. AAPG Bull 65:394–421

Wüstefeld, A., Al-Harrasi, O., Verdon, J., Wookey, J. and Kendall, J.M., 2010. A strategy for automated analysis of passive microseismic data to image seismic anisotropy and fracture characteristics, Geophys. Prospect., 58, 755–773, doi:10.1111/j.1365-2478.2010.00891.x.

Wybraniec, S., Zhou, S., Thybo, H., Forsberg, R., Perchuc, E., Lee, M.K., Demianov, G.D., Strakhov, V.N., 1998. New map compiled of Europe's gravity field. EOS, Trans. Am. Geophys. Union 79 (37), 437–442.Wonik, T., Trippler, K., Geipel, H., Greinwald, S. and Pashkevitch, I., 2001. Magnetic anomaly map for Northern, Western, and Eastern Europe. Terra Nova, 13: 203–213. doi: 10.1046/j.1365-3121.2001.00341.x